

THE UNIVERSITY OF OKLAHOMA
GRADUATE COLLEGE

POLY(ETHYLENIMINE)-BASED ELECTROLYTES FOR BATTERIES AND FUEL
CELLS: SYNTHESIS, MODIFICATION AND CHARACTERIZATION

A DISSERTATION
SUBMITTED TO THE GRADUATE FACULTY
in partial fulfillment of the requirements of the
Degree of
DOCTOR OF PHILOSOPHY

By

FRANK ISAIAS YEPEZ CASTILLO
Norman, Oklahoma
2009

POLY(ETHYLENIMINE)-BASED ELECTROLYTES FOR BATTERIES AND FUEL
CELLS: SYNTHESIS, MODIFICATION AND CHARACTERIZATION

A DISSERTATION APPROVED FOR THE
DEPARTMENT OF CHEMISTRY AND BIOCHEMISTRY

BY

Daniel T. Glatzhofer

Roger Frech

Kenneth M. Nicholas

Charles V. Rice

David W. Schmidtke

Acknowledgements

I would like to thank those whom made it easier for me to complete this journey. First and foremost, I want to thank my wife, **Beatriz Ogando**. You encouraged me to come to graduate school when no one else thought it possible and you have been my strength in this process, I couldn't have done it without you.

Dr. Daniel T. Glatzhofer, I truly enjoyed working with you for the past five years. Your teaching style has inspired me to always do better. You never stopped working with your students and doing everything you could do to help us achieve our true potential. Thank you for all your patience and advice.

I want to thank **Dr. Roger Frech**, I considered myself fortunate for having the opportunity to collaborate with you and with your research group. I learned several valuable lessons from this experience. I would also like to express my gratitude to the rest of my advisory committee, **Dr. Kenneth Nicholas**, **Dr. Charles Rice** and **Dr. David Schmidtke** for their advice.

Dr. Mark Morvant, even though I didn't work with you in my research, I valued working with you as your T.A. I learned how much I love teaching while working with you. You have been a great influence in my academic career.

I would like to thank those whom I have met during this journey and that made it so much more interesting: **Guinevere Giffin**, I was lucky to get to work with you, I couldn't have asked for a better partner in our team efforts. Discussions

with you were always useful. **Rachel Mason**, our science discussions were great, but I will always be grateful to have in you someone to talk to about something else beside science. I'm honored to count you as one of my friends. **Heather and Bob Grimm**, you have become my family in the United States, you have been by my side in the good times, and most importantly, during the most difficult ones. Thank you.

I want to thank former and current members of Dr. Glatzhofer's research group: **Mike Erickson, Lieyu "Richard" Hu, Jiang Zhe, Matthew Meredith, Rahul Kadam, Sachin Chavan** and **Mohd Ismail**. I learned a lot from and with you. I'll always cherish the hours I spent working by your side.

I also would like to thank **Allison Fleshman** for all her mathematical wisdom. It was great to learn some math from you and be able to give it some physical sense. I hope I helped you learn a little organic chemistry along the way.

Finally, I would like to thank **Dr. Susan Nimmo, Carl Van Buskirk, Carol Jones**, and the rest of the staff in the Department of Chemistry and Biochemistry. Thank you for helping me along the way. You made everything easier for me to achieve my goals and do my best in this program. Thank you!

Table of Contents

Table of Contents	vi
List of Tables	ix
List of Figures	x
Abstract	xvi
Chapter 1. Introduction	1
1. Batteries	2
1.1. The electrochemical cell	4
1.2. Lithium ion batteries	6
1.3. Electrolytes	9
1.3.1. Liquid electrolytes	10
1.3.2. Gel electrolytes	11
1.3.3. Polymer electrolytes	12
a. Poly(ethylene oxide)	20
b. Poly(ethylenimine)	25
2. Fuel Cells	32
2.1. Hydrogen Proton Exchange Membrane Fuel Cells (PEMFCs)	34
References	37
Chapter 2: PEI-based electrolytes for lithium battery applications	43
1. Branched PEI-based electrolytes: Synthesis of branched poly(N-methylethylenimine), BPMEI	46
2. Linear PEI-based electrolytes: Synthesis of linear poly(N-ethylethylenimine), LPEEI, and linear poly(N-butylethylenimine), LPBEI	55
3. Conclusions	64
References	66
Chapter 3: Crosslinked LPEI·HCl-based membranes for hydrogen fuel cell applications: Structural characterization	68
1. Introduction	68

2. Structural characterization and determination of degree of crosslinking .	70
2.1. ¹ H NMR spectroscopy and degree of crosslinking.....	70
2.2. Ionic Conductivity.....	75
2.3. Vibrational Spectroscopy	78
3. Conclusions.....	84
References	85
Chapter 4: Crosslinked LPEI·HCl-based membranes for hydrogen fuel cell applications: Ionic conductivity studies	88
1. Background	89
2. Ionic conductivity studies.....	97
3. System optimization	105
4. Conclusions	111
References.....	112
Chapter 5: Crosslinked LPEI·HCl-based membranes: Hydrogen fuel cell application.....	114
1. Background	114
2. Fuel Cell Testing.....	118
3. Conclusions	131
References.....	132
Chapter 6: Future directions in poly(ethylenimine) research	134
References.....	138
Experimental Section.....	139
1. Polymer synthesis	139
2. Crosslinked LPEI·HCl based polymer electrolyte membranes	142
3. Techniques.....	143
3.1. Polymer electrolyte preparation	143
3.2. Vibrational spectroscopy.....	144
3.3. NMR spectroscopy	145
3.4. Differential scanning calorimetry.....	146

3.5. AC conductivity and impedance spectroscopy	147
3.6. MEA preparation and fuel cell tests	150
References.....	150

List of Tables

<i>Table 1.1.</i> Chemical structure of poly(siloxane)-based solid polymer electrolyte (SPE) materials	25
<i>Table 2.1.</i> Glass transition temperatures for BPEI, LPEI and their complexes with sodium and lithium triflate	44
<i>Table 2.2.</i> Glass transition temperatures, T_g (°C) of BPMEI and LPMEI and their lithium triflate complexes at various N:Li molar ratios	49
<i>Table 2.3.</i> Frequencies (cm^{-1}) in the $\delta_s(\text{CF}_3)$ region for BPMEI- LiSO_3CF_3 complexes. Relative intensities (%) are given next to frequency	52
<i>Table 2.4.</i> Frequencies (cm^{-1}) in the $\delta_s(\text{CF}_3)$ region for LPMEI- LiSO_3CF_3 complexes. Relative intensities (%) are given next to frequency	53
<i>Table 2.5.</i> Glass transition temperature (°C) of linear poly(<i>N</i> -methyl ethylenimine) (LPMEI), linear poly(<i>N</i> -ethylethylenimine) (LPEEI), and linear poly(<i>N</i> -butylethylenimine) (LPBEI), and LPMEI and LPEEI-based electrolytes	60

List of Figures

<i>Figure 1.1.</i> Estimated battery market in 2003 (\$ Billions of Dollars)	3
<i>Figure 1.2.</i> A schematic view of a Daniell cell.....	4
<i>Figure 1.3.</i> Schematic diagram of a lithium ion cell.....	8
<i>Figure 1.4.</i> Representation of cation motion in a polymer electrolyte	16
<i>Figure 1.5.</i> Structure of polymers considered as possible electrolytes for lithium ion batteries: (1) Poly(ethylene oxide), PEO, (2) Poly(bis(methoxyethoxyethoxy)phosphazene), MEEP, (3) Poly(ethylenimine), PEI	20
<i>Figure 1.6.</i> Schematic representation of a hydrogen fuel cell.....	33
<i>Figure 1.7.</i> Structure of (a) Nafion® and (b) Poly(benzimidazole)	35
<i>Figure 2.1.</i> ¹ H-NMR spectra of branched poly(ethylenimine) and branched poly(<i>N</i> -methylethylenimine) in methanol- <i>d</i> ₄	48
<i>Figure 2.2.</i> IR spectra of high <i>M</i> _w BPMEI and LPMEI and their complexes with lithium triflate (N:Li molar ratios 10:1 and 5:1) in the 735 – 1000 cm ⁻¹ region.....	51
<i>Figure 2.3.</i> IR spectra of high <i>M</i> _w BPMEI and LPMEI and their complexes with lithium triflate (N:Li molar ratios 10:1 and 5:1) in the 1000 - 1400 cm ⁻¹ region.....	52
<i>Figure 2.4.</i> Temperature-dependent conductivity data of BPMEI-LiSO ₃ CF ₃ and LPMEI-LiSO ₃ CF ₃	54
<i>Figure 2.5.</i> ¹ H-NMR spectrum of linear poly(<i>N</i> -ethylethylenimine), LPEEI, in CDCl ₃ (300.1 MHz ¹ H)	56
<i>Figure 2.6.</i> ¹ H-NMR spectrum of linear poly(<i>N</i> -butylethylenimine), LPBEI, in CD ₃ OD (400.0 MHz ¹ H)	58
<i>Figure 2.7.</i> ¹ H- ¹ H COSY spectrum of LPBEI in CD ₃ OD (400.0 MHz ¹ H)	59
<i>Figure 2.8.</i> Infrared absorbance spectra from 1000 to 1140 cm ⁻¹ of pure LPMEI and LPEEI and its complexes with different concentrations of LiSO ₃ CF ₃	61

<i>Figure 2.9.</i> Infrared absorbance spectra from 700 to 1000 cm^{-1} of pure LPMEI and LPEEI and its complexes with different concentrations of LiSO_3CF_3	62
<i>Figure 2.10.</i> Temperature-dependent infrared absorbance spectra from 1000 to 1140 cm^{-1} of a LPEEI- LiSO_3CF_3 complex (N:Li = 10:1). RT 1 is the initial spectrum at room temperature; RT2 and RT3 are the room temperature spectra after the first and second cycles of heating the sample up to 150°C and cooling, respectively.....	63
<i>Figure 3.1.</i> HR-MAS Solid State ^1H NMR spectra of crosslinked poly(ethylenimine) hydrochloride ($x\text{LPEI}\cdot\text{HCl}$) in water and solution ^1H NMR of linear poly(ethylenimine) hydrochloride in water- d_2 . The notation xlinker: 2N designates the number of crosslinker molecules added to the solution for every two PEI·HCl nitrogen atoms	71
<i>Figure 3.2.</i> Calibration curve for degree of crosslinking determined from NMR data: (\square) Solution ^1H NMR, (\blacklozenge) HR-MAS ^1H NMR	74
<i>Figure 3.3.</i> Log of conductivity as a function of degree of crosslinking. Degree of crosslinking as determined by: (\blacklozenge) HR-MAS ^1H NMR, (\square) estimation from the average calibration curve in Fig. 3.2.....	75
<i>Figure 3.4.</i> Concentration dependence of $\log \sigma$ (S/cm) for (a) $\text{BPEI}\cdot x\text{H}_2\text{SO}_4$ and (b) $\text{BPEI}\cdot x\text{H}_3\text{PO}_4$ at 300 K (\bullet) and 373 K (\circ)	77
<i>Figure 3.5.</i> Raman spectra of crosslinker stretching region. Crosslinked poly(ethylenimine)-hydrochloride, 3-(diethylamino)-acrolein (DMAA) and linear poly(ethylenimine)-hydrochloride ($\text{LPEI}\cdot\text{HCl}$) in water. The notation xlinker: 2N designates the number of crosslinker molecules added to the solution for every two PEI·HCl nitrogen atoms	79
<i>Figure 3.6.</i> Infrared spectra of crosslinker stretching region. Crosslinked	

poly(ethylenimine)-hydrochloride, 3-(diethylamino)-acrolein (DMAA) and linear poly(ethylenimine)-hydrochloride (LPEI·HCl). The notation xlinker: 2N designates the number of crosslinker molecules added to the solution for every two PEI·HCl nitrogen atoms	80
<i>Figure 3.7.</i> Raman spectra of lower frequency region. Crosslinked poly(ethylenimine)-hydrochloride and linear poly(ethylenimine)-hydrochloride (LPEI·HCl) in water. The notation xlinker: 2N designates the number of crosslinker molecules added to the solution for every two PEI·HCl nitrogen atoms	81
<i>Figure 3.8.</i> Infrared spectra of lower frequency region. Crosslinked poly(ethylenimine)-hydrochloride, and linear poly(ethylenimine)-hydrochloride (LPEI·HCl). The notation xlinker: 2N designates the number of crosslinker molecules added to the solution for every two PEI·HCl nitrogen atoms.....	83
<i>Figure 4.1.</i> Concentration dependence of $\log \sigma$ (S/cm) for BPEI·xH ₂ SO ₄ (a) and BPEI·xH ₃ PO ₄ (b) at 25°C (●) and 100°C (○)	89
<i>Figure 4.2.</i> Composition, x, dependence of proton conductivities of PEI:xH ₃ PO ₄ at 30, 60 and 100°C. Values for LPEI:xH ₂ SO ₄ are shown for comparison	90
<i>Figure 4.3.</i> Calibration curve for degree of crosslinking determined from NMR data: (□) Solution ¹ H NMR, (◆) HR-MAS ¹ H NMR	93
<i>Figure 4.4.</i> Conductivity dependence on temperature for samples with P:N molar ratio of 0.69 and different degrees of crosslinking. Data taken from ref. 10.....	95
<i>Figure 4.5.</i> Ionic conductivity of crosslinked linear poly(ethylenimine) hydrochloride with different phosphoric acid concentration, as a function of temperature; legend indicates the phosphorus to nitrogen (P:N) molar ratio and apparent energy of activation	

derived from the plot.....	96
<i>Figure 4.6.</i> Conductivity as a function of relative humidity for xLPEI·HCl/H ₃ PO ₄ membranes at 25°C with different phosphorus to nitrogen molar ratios, P:N. Both membranes have a degree of crosslinking of 0.84.....	99
<i>Figure 4.7.</i> Conductivity as a function of temperature for a crosslinked LPEI·HCl/H ₃ PO ₄ membrane with a 0.5 P:N molar ratio, and degree of crosslinking of 0.84, at different relative humidities.....	100
<i>Figure 4.8.</i> Conductivity as a function of relative humidity for xLPEI·HCl films with a degree of crosslinking of 0.84 and different phosphorus to nitrogen molar ratios. Measurements carried at 100°C.....	102
<i>Figure 4.9.</i> Conductivity at 100°C as a function of relative humidity for crosslinked LPEI·HCl membranes containing 2.0 P:N molar ratio. Samples had degrees of crosslinking varying from 0.46 to 0.84.....	103
<i>Figure 4.10.</i> Conductivity as a function of relative humidity for a crosslinked LPEI·HCl/H ₃ PO ₄ membrane with a degree of crosslinking of 0.84 and a 2.0 P:N molar ratio.....	104
<i>Figure 4.11.</i> WLF master curve for conductivity of crosslinked LPEI·HCl/H ₃ PO ₄ systems.....	105
<i>Figure 4.12.</i> Conductivity as a function of relative humidity for xLPEI·HCl membranes with a degree of crosslinking, DC, of 0.84, and different amounts of phosphoric acid. Samples were evaluated at 75, 90, 100 and 115°C.....	107
<i>Figure 4.13.</i> Conductivity as a function of relative humidity for xLPEI·HCl membranes with a degree of crosslinking, DC, of 0.46, and different amounts of phosphoric acid. Samples were evaluated at 75, 90, 100 and 115°C.....	108

<i>Figure 4.14.</i> Conductivity as a function of acid content for xLPEI·HCl membranes with a degree of crosslinking, DC, of 0.84, at 50% relative humidity. Samples were evaluated at 75, 90, 100 and 115°C.....	109
<i>Figure 4.15.</i> Conductivity as a function of acid content for xLPEI·HCl membranes with DC = 0.46 at 50% relative humidity. Samples were evaluated at 75, 90, 100 and 115°C	110
<i>Figure 4.16.</i> Conductivity as a function of relative humidity for a crosslinked LPEI·HCl/H ₃ PO ₄ membrane with a degree of crosslinking of 0.45 and a 1.5 P:N molar ratio.....	111
<i>Figure 5.1.</i> Typical cell potential vs. current density plot for a H ₂ /O ₂ PEMFC. Potential losses are indicated in the figure.....	116
<i>Figure 5.2.</i> Conductivity as a function of relative humidity for a crosslinked LPEI·HCl/H ₃ PO ₄ membrane with 2.0 P:N molar ratio and 0.66 degree of crosslinking.....	118
<i>Figure 5.3.</i> Schematic view of a typical MEA (as prepared). Diagram shows the different components of the MEA in their relative order.....	119
<i>Figure 5.4.</i> Diagram of a fuel cell setup including electrical and gas connections.....	120
<i>Figure 5.5.</i> Potential (V) vs. current density (mA/cm ²) curves for fuel cell operating at 30% relative humidity with an MEA containing a Nafion® 117 film	122
<i>Figure 5.6.</i> Power (mW) vs. current density (mA/cm ²) curves for fuel cell operating at 30% relative humidity with an MEA containing a Nafion® 117 film	123
<i>Figure 5.7.</i> Potential (V) vs. current density (mA/cm ²) curves for fuel cell operating at 30% relative humidity with an MEA containing a crosslinked LPEI·HCl / H ₃ PO ₄ film with 1.0 P:N molar ratio and a degree of crosslinking of 0.24.....	124

<i>Figure 5.8.</i> Power (mW) vs. current density (mA/cm ²) curves for fuel cell operating at 30% relative humidity with an MEA containing a crosslinked LPEI·HCl / H ₃ PO ₄ film with 1.0 P:N molar ratio and a degree of crosslinking of 0.24.....	125
<i>Figure 5.9.</i> Potential (V) vs. current density (mA/cm ²) curves for fuel cell operating at 30% relative humidity with an MEA containing a crosslinked LPEI·HCl / H ₃ PO ₄ film with 2.0 P:N molar ratio and a degree of crosslinking of 0.66.....	126
<i>Figure 5.10.</i> Power (mW) vs. current density (mA/cm ²) curves for fuel cell operating at 30% relative humidity with an MEA containing a crosslinked LPEI·HCl / H ₃ PO ₄ film with 2.0 P:N molar ratio and a degree of crosslinking of 0.66.....	127
<i>Figure 5.11.</i> Potential (V) vs. current density (mA/cm ²) curves for fuel cell operating at 30% relative humidity with an MEA containing a crosslinked LPEI·HCl / H ₃ PO ₄ film with 2.0 P:N molar ratio and a degree of crosslinking of 0.66.....	128
<i>Figure 5.12.</i> Power (mW) vs. current density (mA/cm ²) curves for fuel cell operating at 30% relative humidity with an MEA containing a crosslinked LPEI·HCl / H ₃ PO ₄ film with 2.0 P:N molar ratio and a degree of crosslinking of 0.66.....	129
<i>Figure 5.13.</i> Potential (V) vs. current density (mA/cm ²) curves for fuel cells operating at 90°C and 30% relative humidity with different MEAs	130
<i>Figure 5.14.</i> Power (mW) vs. current density (mA/cm ²) curves for fuel cells operating at 90°C and 30% relative humidity with different MEAs	130

Abstract

Poly(ethylenimine) (PEI) is an ion conducting polymer with great potential for applications in lithium batteries and proton exchange membrane fuel cells. Branched poly(ethylenimine) was *N*-methylated *via* an Eschweiler-Clarke reaction to produce branched poly(*N*-methylethylenimine), BPMEI. Novel alkylated linear poly(*N*-ethylethylenimine), LPEEI, and linear poly(*N*-butylethylenimine), LPBEI, were synthesized from linear poly(ethylenimine), LPEI, *via* reductive amination of aliphatic aldehydes. Differential scanning calorimetry was used to determine the glass transition temperature, T_g , of neat BPMEI ($T_g = -91^\circ\text{C}$), LPEEI ($T_g = -80^\circ\text{C}$) and LPBEI ($T_g = -50^\circ\text{C}$). T_g s of various *N*-alkylated PEI-lithium triflate complexes with different salt concentrations were determined. BPMEI exhibited a greater T_g change upon lithium triflate addition (from -91°C to 13°C) than that of LPMEI complexes (from -93°C to -14°C). It was found that LPEEI complexes showed higher T_g s at all salt concentrations than the corresponding LPMEI- LiSO_3CF_3 system. IR and Raman spectroscopy were used to study complexes of these polymers with lithium triflate for battery applications. Vibrational spectra of BPMEI- LiSO_3CF_3 complexes revealed that aggregate formation is not observed until salt concentration reaches 5:1 (N:Li molar ratio). Additionally, a decrease in the relative concentration of “free” ions, compared to equivalent linear systems, was observed. LPEEI’s spectra presented few changes upon salt addition, suggesting that salt addition causes less disruption of the local polymer microstructure than that observed in LPMEI systems in previous studies.

Linear poly(ethylenimine) hydrochloride, LPEI·HCl, was successfully crosslinked using malonaldehyde generated *in situ*, and the degree of crosslinking was determined from the ratio of crosslink to polymer backbone hydrogens obtained using ^1H NMR spectroscopy. The ionic conductivity was highest at intermediate degrees of crosslinking (*ca.* 0.45), approximately 1.0×10^{-3} S/cm at room temperature and 75% relative humidity. IR and Raman spectroscopy were used to characterize the crosslinked network. The presence of β -amino-ethenyliminium crosslink units was identified through a series of bands between 1570 and 1640 cm^{-1} . Ionic conductivity studies were performed on crosslinked LPEI·HCl as a function of relative humidity, degree of crosslinking, temperature and phosphoric acid content. Results showed that the dependence of the conductivity on these factors is complex and that it involves a drastic transition in which the conductivity increases by several orders of magnitude. The onset of this transition appeared to be related to the composition of the polymer membranes. Membranes with ionic conductivities as high as 0.16 S/cm at 130°C and 20% RH were obtained. Crosslinked LPEI·HCl/ H_3PO_4 -based membranes were used in membrane electrode assemblies, MEAs, for proton exchange membranes fuel cells. MEAs were tested at temperatures ranging from 60 to 130°C and 30% RH. Upon comparison, LPEI-based MEAs exhibited better performance than Nafion® 117-based MEAs tested under the same conditions. PEI-based MEAs with 2.0 P:N and 0.66 degree of crosslinking produced 0.30 mA/cm^2 at 0.38 V at 90°C and 30% RH. Nafion® 117-based MEAs produced 0.047 mA/cm^2 at 0.34 V under the same conditions.

Chapter 1: Introduction

In a time when oil prices reach record highs and attention is being paid to the effects of human activities on our environment, a revision of our energy technologies is needed. In 1998, global leaders created a protocol to reduce significantly the amount of green house gases (GHG) emitted in each of their countries.¹

The use of alternative energy sources and the implementation of new technologies that reduce the amount of GHG emissions while improving the efficiency of fuel consumption is key for the success of these types of initiatives. Companies such as General Motors,² Honda,³ and Toyota,⁴ have already introduced technologies that store energy produced by the engine in lithium ion batteries that can be used later to power the drive train of an electric motor. These companies have also started to work on prototypes that use hydrogen fuel cells to power vehicles.²⁻⁴

Additionally, the surge of portable devices that the electronic industry has developed in recent years has imposed new needs on the battery industry. The goal is to develop batteries that would supply the amount of energy required for the operation of devices for longer periods of time. Environmental concerns have also pushed forward the use and implementation of rechargeable battery technologies. Improvements in battery and fuel cells technologies are directly related to advances in the chemistry of their different components.

While fuel cells generate energy and batteries store it, both of them are electrochemical devices that take advantage of the energy released during a chemical reaction to power a process. In both of these devices an active material is oxidized in one of the electrodes and ions are produced while generating a current. In order for the electrochemical cell to work properly, the ions produced must travel to a second electrode.

The medium that allows ion transport from one electrode to the other is called an electrolyte. Regardless of the processes that take place at the electrodes, improving the ion movement through the electrolyte is key for the advancement of battery and fuel cell technologies and has received significant attention.

Poly(ethylenimine) is a versatile material that could be tailored to accommodate the needs not only of the battery industry, but also those of the emerging fuel cell industry. The research presented here focuses on those two significant aspects: *a*) the synthesis of functionalized poly(ethylenimine) materials to study their interactions with lithium salts; and *b*) the synthesis and characterization of poly(ethylenimine)-based systems that can be used as proton exchange membranes in polymer electrolyte membrane fuel cells (PEMFC).

A more detailed description of relevant aspects of lithium-polymer batteries and proton exchange membranes fuel cells is needed to fully comprehend the work presented in the following chapters and is given here.

1. Batteries

Winter and Brodd,⁵ defined batteries as self-contained units that store

chemical energy and convert it into electrical energy when needed to power different applications. There are two types of batteries: primary or non-rechargeable batteries and secondary or rechargeable batteries. Assembled in the charged state, primary batteries are intended to be used until the active material is completely exhausted; discharge is the primary process during the operation of these electrochemical devices. Secondary batteries, once discharged, can be restore to their charged state by an electric current flowing in the direction opposite to the electric current resulting from the discharge of the battery. Secondary batteries, also known as accumulators, are usually assembled in the discharged state, requiring users to charge the device before the battery can be discharged in a secondary process.⁵

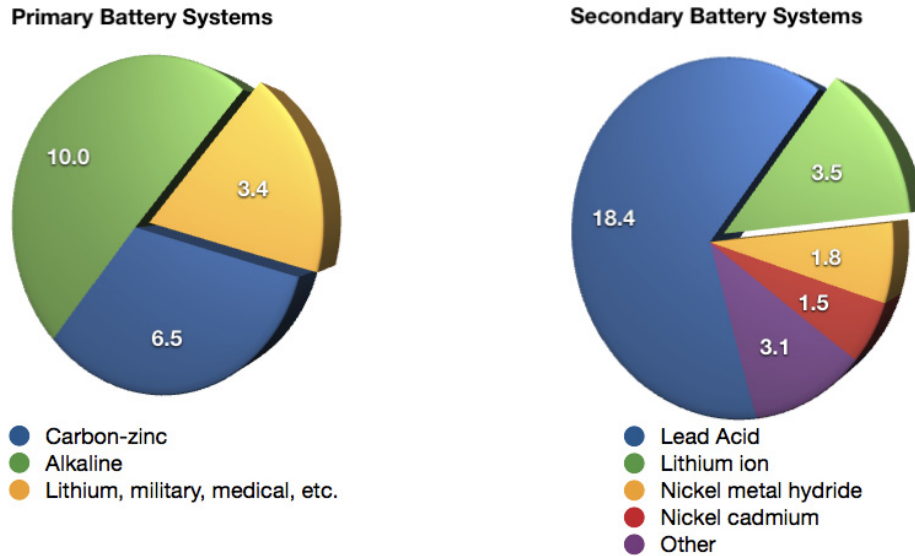


Figure 1.1. Estimated battery market in 2003 (\$ Billions of Dollars).⁵

In 2003, reports estimated that the value of the battery market was \$48.2 billion, with the rechargeable battery segment contributing over \$25 billion to the

total value (see Fig. 1.1). It is not surprising that a lot of effort is put into developing cheaper, more reliable and durable batteries.^{5,6}

1.1. The electrochemical cell

In order to understand the way a battery works it is useful to consider a simple voltaic cell, i.e. a Daniell cell, developed by John Frederic Daniell in 1836 (see Fig. 1.2).

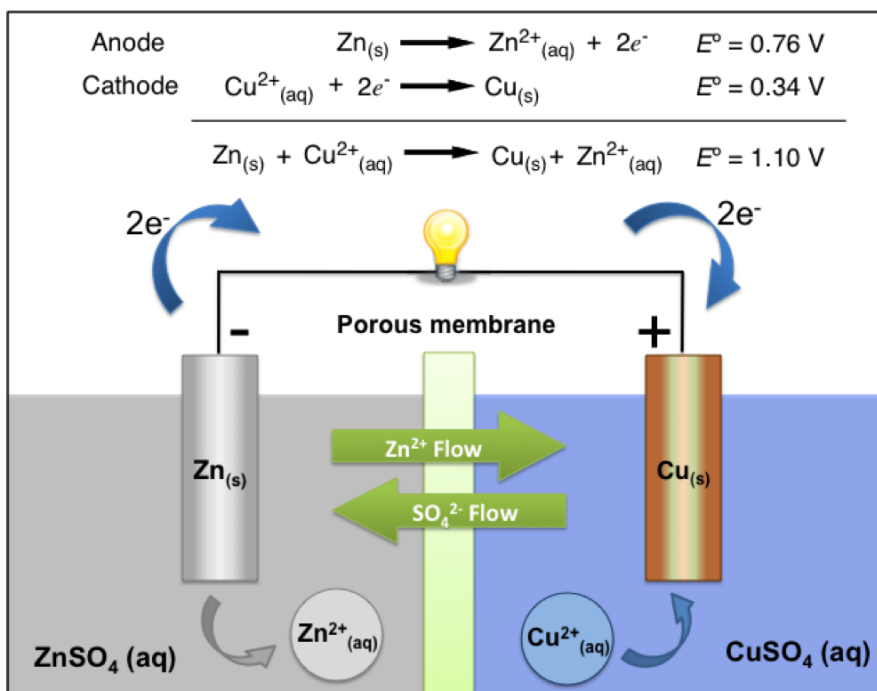


Figure 1.2. A schematic view of a Daniell cell.⁷

Fig. 1.2 shows a simple schematic view of a Daniell cell. This cell consists of a zinc electrode immersed into a zinc sulfate solution and a copper electrode immersed into a cupric sulfate solution. A porous membrane keeps both of these solutions separated. However, ion exchange is a possibility between both

solutions, as shown in Fig. 1.2 for Zn^{2+} and SO_4^{2-} . This ion exchange can hurt the performance of the electrochemical cell, e.g. the flow of Cu^{2+} into the ZnSO_4 solution, not shown, can result in Cu^0 plating out onto the zinc electrode, effectively stopping the flow of electrons through the circuitry.

When the cell is set up, the zinc of the electrode is oxidized into Zn^{2+} and the electrons are conducted through an external circuit into the copper electrode, where Cu^{2+} ions in solution get reduced and plate out as Cu^0 onto the surface of the electrode. The reducing zinc electrode is called the anode, while the oxidizing copper electrode is called the cathode. The solutions that allow the movement of ions between the anode and the cathode are called electrolytes.⁷ Most electrolytes are liquids with dissolved salts, acids or bases to make them ionic conductors.⁸

The actual design and materials used in cells have been improved significantly since batteries were first conceived. However, the functioning principles remain the same, with slight variations according to the specifics of any given system. A proper battery consists of a combination of cells connected in series or in parallel or both to achieve a certain voltage and current level.⁸

Batteries are classified as primary or secondary depending on their ability to receive electrical charge. Primary batteries are non-rechargeable. The redox reaction that allows the discharge is not efficiently reversible, making it unable to regenerate the active material to repeat a discharge cycle. Secondary batteries are rechargeable electrochemical devices in which the active material can be

regenerated by applying an electrical current of opposite polarity to that of the discharge current.⁹ This type of battery is widely used in portable consumer electronics, power tools, etc., due to its ability to deliver power beyond the capability of a primary battery and because of the reduced cost by being reusable.⁸

Active materials for batteries are selected to achieve the highest energy density possible. Lead-acid (1859), nickel-iron (1908), nickel-cadmium(1909) are some of the materials originally used in the development of secondary batteries, and the lead-acid battery is still widely used in automotive SLI (starting-lighting-ignition) battery applications, while the nickel-cadmium battery was later developed for widespread use in portable electronic devices and other applications.⁶

Newer secondary battery systems include the silver-zinc, the nickel-zinc, nickel-hydrogen, and lithium ion batteries. While the specific energy of nickel-cadmium batteries has not changed significantly in the last decade and was, as of 2002, at 35 Wh/kg, better performance has been obtained with other systems.

1.2. Lithium ion batteries

Lithium rechargeable batteries are batteries that have a lithium metal or lithium-alloy negative electrode which functions as the anode during discharge. Solid intercalation compounds, as well as soluble inorganic cathodes and polymeric materials can be used for the positive electrode, while aprotic liquid

organic electrolytes and solid polymer electrolytes can be used in these batteries. Polymer electrolytes are popular in the cell design due to their lower reactivity towards lithium, providing a safer battery.¹⁰

The safety concerns associated with the use of lithium metal as the anode material for rechargeable batteries arise from its reactivity with the electrolyte and the changes that the lithium metal electrode suffers after repetitive charge and discharge cycling.¹⁰ During recharge, lithium ions are electroplated onto the metallic lithium electrode, forming a “mossy and in some cases a dendritic deposit”,¹⁰ which has a larger surface area than that of the original film and increases its overall reactivity, thus rendering the battery thermally unstable. This has prompted government agencies and international organizations to regulate the shipment, use and disposal of rechargeable lithium batteries.¹⁰

Lithium ion batteries (LIB), first introduced by Sony in 1991, have an important safety advantage over their lithium counterparts, these batteries do not contain lithium in a metallic form,¹⁰ and since they were introduced they have captured over half of the sales value of the secondary battery consumer market, with a production capacity that was estimated to be 75 million/cells per month in 2001.^{5,6,11} This economic success is closely related to the great performance of lithium ion batteries. LIBs have a specific energies that range from 100 Wh/kg up to 175 Wh/kg at 20°C, higher than any other alkaline rechargeable battery in the market with the exception of lithium metal batteries.⁸ Additionally, LIBs offer longer cycle life, generally over 1000 cycles at 80% depth of discharge, and they

operate over a wide range of temperatures (-25°C to 45°C).⁶ Figure 3 shows a schematic illustration of a typical lithium ion battery.

As illustrated in Figure 1.3, typical commercial lithium ion cells have a carbon/graphite anode, a lithium-cobalt oxide cathode, and an organic electrolyte of lithium hexafluorophosphate (LiPF₆) solution in ethylene carbonate.⁵

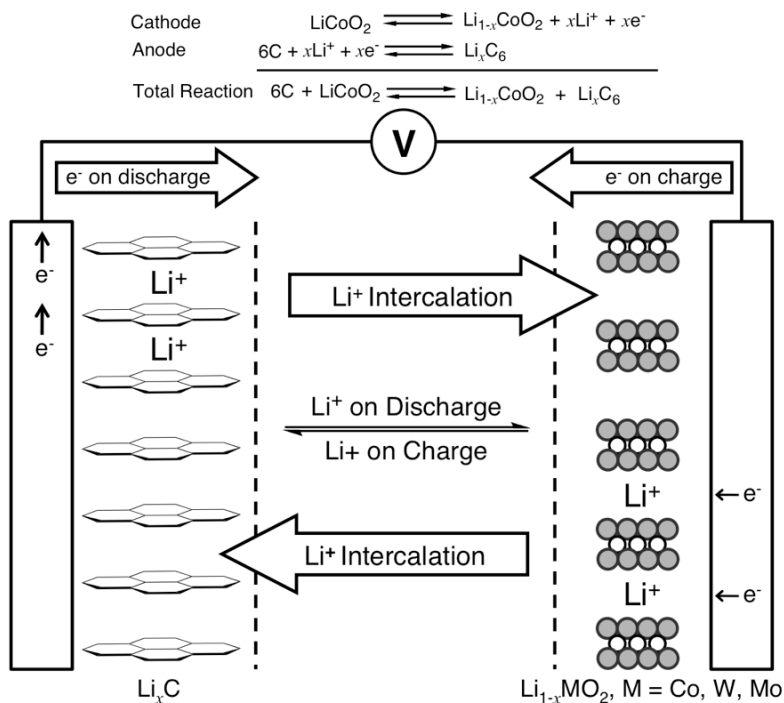


Figure 1.3. Schematic diagram of a lithium ion cell.^{12,13}

The cell operates by shuttling Li ions from one electrode to the other, with no electroplating involved.¹⁰ Solid solutions of lithium ions in some form of carbon are typically used as negative electrode in rechargeable LIBs.^{10,13,14} Lithium can be intercalated into graphitic carbon in ratios up to one lithium ion for six carbon atoms, giving a nominal composition of LiC_6 , with a theoretical maximum capacity

of 372 mAh/g. However, the values obtained for lithium cells are typically between 300 and 350 mAh/g.¹⁴

Rechargeable batteries that use lithium metal as the negative electrode have not been commercialized yet, mainly due to safety concerns. Lithium electrodes react with the electrolyte, forming a passivating film. The formation of this film during the charging and discharging cycles consumes fresh lithium and makes it necessary to include an excess of lithium in order to achieve a specific capacity. This process hinders the ability of the cell to achieve a 100% of its cycling efficiency.¹⁰

Other materials are also being studied to substitute for LiC_6 as the anode material. New materials could improve the ability to operate safely at higher current densities, reduce the capacity losses upon cycling, and lower the aspect ratio of the cells as well as lower costs.¹⁴ A variety of transition metal compounds with layered structures in which lithium can be intercalated and deintercalated during the operation cycles could be used as negative electrodes¹⁰: tin oxides (SnO_2) prepared by sol-gel methods and tin oxides doped with aluminum have been proposed. Compounds using tungsten and molybdenum oxides, such as Li_xWO_2 , Li_xMoO_2 , and Li_xTiS_2 have also been studied as possible anode materials.¹⁰

1.3. Electrolytes

Electrolytes provide a medium for ions to diffuse between the cathode and the

anode of an electrochemical cell.⁵ The flow rate of ions through the electrolytes, known as ionic conductivity, σ , limits the amount of current generated by a cell. The conductivity is a function of temperature and pressure as well as the density of carriers (n_i), their charge (q_i) and their mobility in the electrolyte (μ_i) as shown in Eq. 1.1.

$$\sigma(T,P) = \sum_j q_j n_j \mu_j \quad (1.1)$$

While the number of carriers is important for electron conductivity, in the case of ionic conductors, the mobility of the ions is extremely important.¹⁵

Electrolytes must have an ionic conductivity high enough to satisfy the current requirements for the cell ($> 10^{-3}$ S/cm from -40 to 90°C);¹⁰ they must be electrochemically stable within the redox potentials used during the operation of the cell (up to 5 V vs. lithium); they should be thermally stable at least up to 70°C and they should be compatible with other components in the cell as well.¹⁰

Lithium ion batteries have used four different types of electrolyte systems: liquid electrolytes, gel electrolytes, polymer electrolytes and ceramic electrolytes.¹² The typical activation energy of lithium ion conduction is in the range of 0.2 to 0.6 eV (5 to 18 kcal/mol).¹⁶

1.3.1. Liquid electrolytes

Organic carbonates have been used widely in the battery industry because they offer excellent stability, good safety properties and compatibility with

electrode materials.¹² Conventional organic liquid electrolytes show lithium ion conductivity of 10^{-2} S/cm at room temperature, which is between one and two orders of magnitude lower than that of aqueous electrolytes.^{10,12,16} Ethylene carbonate, propylene carbonate, dimethyl carbonate, diethyl carbonate and ethylmethyl carbonate are some of the most common solvents used for lithium ion rechargeable batteries. All of them exhibit dielectric constants that range from 3 to 90, and solvate lithium salts at high concentrations.¹² However, it is typical to find electrolyte formulations that use a mixture of two to four different solvents to enhance cell performance.¹²

Lithium hexafluorophosphate (LiPF_6) is currently the most common lithium salt used in lithium-ion batteries. LiPF_6 solutions provide high ionic conductivity, $>10^{-3}$ S/cm, high lithium ion transference numbers (~ 0.35), and acceptable safety properties.¹² Other lithium salts have been used in industry, i.e. LiClO_4 , LiAsF_6 , LiBF_4 . Organic lithium salts such as LiCF_3SO_3 (LiTf) and $\text{LiN}(\text{CF}_3\text{SO}_2)_2$ (LiTfsi) have also attracted a fair amount of attention from the battery industry.¹² Lithium bisperfluoroethanesulfonimide (LiTfsi) has received significant attention as it is more stable to water than LiPF_6 , making it easy to handle, can be easily dried, and it does not cause aluminum corrosion.¹²

1.3.2. Gel electrolytes

The first generation of Sony's lithium ion batteries used electrolyte solutions of lithium hexafluorophosphate in organic solvents such as ethylene carbonate.⁵

However, the use of these solutions has given rise to a major problem: electrolyte leakage. This has pushed scientists to find ways to immobilize the electrolyte inside the battery to reduce leakage.

Gelled polymer electrolytes have been used in Sony's second generation of lithium ion batteries. Gel electrolytes are made by impregnation of organic liquid electrolytes and lithium salts into a host polymer matrix.¹⁶ Electrolyte solutions normally consist of a solvent mixture such as ethylene carbonate and propylene carbonate, while the polymer matrix consists of materials such as poly(acrylonitrile), poly(vinylidene fluoride), or block copolymers of poly(vinylidene fluoride) and poly(hexafluoropropylene).^{5,16} The activation energy for lithium conduction in gel electrolytes is around 0.2 eV, which is comparable to that of organic liquid electrolytes. The ionic conductivity of these systems depends on the weight ratio of host polymer / organic liquid electrolyte. Increasing the amount of liquid electrolyte on the formulation increases the ionic conductivity, but it also raises safety problems.¹⁶

1.3.3. Polymer electrolytes

While liquid electrolytes exhibit high ionic conductivities and maintain constant contacts with the electrodes, they also introduce disadvantages that engineers have to consider when designing electrochemical cells. When using liquid electrolytes, electrochemical cells have to be designed so that the electrodes are separated; this is accomplished by the inclusion of a separator that does this

mechanically. Liquid electrolytes have also the potential to leak out of the cell, creating an additional problem.

An all-solid-state electrochemical cell appeals to the battery industry because it would eliminate the need for a separator and eradicate the leakage issue. However, solid state ion conductor materials, such as crystalline lithium super ionic conductors LISICONS (*e.g.* $\text{Li}_{3.4}\text{Si}_{0.4}\text{V}_{0.6}\text{O}_4$),¹⁷ and glass electrolytes, like $0.7\text{Li}_2\text{S}-0.3\text{P}_2\text{S}_5$,¹⁸ are hard and brittle, making it difficult to maintain good contact with intercalating electrodes during cycling, due to the volume changes of the electrodes during this process.¹⁸

Polymer electrolytes offer unique physical properties that make them the ideal alternative to other solid and liquid electrolytes. Polymers electrolytes are rigid enough on a macroscopic level that they can be used in the construction of all-solid-state batteries and function as ion conductor and mechanical separator between the electrodes, while being flexible enough, due to their viscoelastic properties, to adjust to the volume changes of the intercalating electrodes during operation.¹⁸

Several reviews on this topic reveal that for polymer electrolytes to be considered a competitive alternative to their liquid counterparts they should exhibit comparable ionic conductivities; low electronic conductivity, to avoid internal short circuits; good mechanical properties; chemical, thermal and electrochemical stability, the electrolyte should be inert while in contact with the electrodes at the operation temperature and should not get reduced or oxidized

at the potentials used while the cell is functioning.¹⁸⁻²⁰

High molecular weight amorphous polymers have the ability to behave as a solid at a macroscopic level, while maintaining large segmental motions of chain backbones at temperatures above their glass transition temperatures, T_g .^{15,18,21} The glass transition is a second order transition. T_g indicates the temperature at which, upon cooling of a polymer liquid, the molecular motions become so slow that an equilibrium packing of the molecules cannot be attained.²¹ At the glass transition temperature, the non-ordered chains of polymers become capable of large segmental movement. Suddenly, the polymer chains are free to rotate and translate, giving the polymer higher degrees of freedom and increasing the tendency of the material to flow.²² The physical entanglements present in high molecular weight amorphous polymers, or the crystalline domains in semi-crystalline polymers prevent the material from flowing. Thus, these materials may be classified as solids.^{18,23}

It is because of this rubbery state that polymers electrolytes are attractive for battery applications,²³ and a great amount of research has been carried out on polymer-salt systems, particularly on poly(ethylene oxide)-lithium salts systems, to gain a better understanding of the fundamental mechanisms that are responsible for the properties of these complex systems.¹⁸

As mentioned before, the ionic conductivity (Eq. 1.1) is a function of the mobility of the ions in the system. While the ions in crystalline solid electrolytes move through defects in the crystal structure of the material, polymer-salt

systems exhibit a different behavior. Ions in polymer-salt complexes move through a mechanism similar to that of low molecular weight analogues, with the exception that, in this case, the polymer itself functions as the solvent and it cannot move in a macroscopic sense.¹⁸

The salt has to dissolve in the polymer for these systems to work properly. This occurs if an overall reduction of the Gibbs free energy of the polymer-salt system is achieved upon mixing, $\Delta G < 0$.^{18,19}

$$\Delta G = \Delta H - T\Delta S \quad (1.2)$$

Since ΔG , as shown in Eq. 1.2, depends on the enthalpy and entropy of the system, we need to consider how these two properties change when dissolving a salt. A positive change in entropy can be expected due to the disordering of the ions from the crystalline lattice of the solid salt, while a negative contribution to entropy will result from the relative ordering and stiffening of the polymer chains as they coordinate to ions.^{18,19} Enthalpy changes will be the result of the combination of several processes. There is a positive enthalpy change due to the lattice energy of the salt, as well as a negative change in enthalpy caused by the solvation of cations by the appropriate atoms in the polymer chains. Additionally, favorable electrostatic interactions between ions also decrease the enthalpy of the system.^{18,19}

While in hydrogen bonding systems both cations and anions are solvated by the solvent, this is not the case in polymer-salt systems.¹⁸ It is found that, as in aprotic liquids, the ion-ion interactions in polymer-salt systems are strong enough

to cause the formation of ion pairs or larger ion clusters in solution,¹⁹ which also can have a significant effect on the conductivity of the polymer-salt complex.

Polymer electrolytes exhibit a complex mechanism of ionic conduction. While there are some similarities to the way ions move in liquid electrolytes, ion mobility in ‘dry’ polymer electrolytes is decoupled from the macroscopic viscosity of the system and depends strongly on the ability of the polymer to move at a microscopic level; hence the importance of the rubbery state of the polymer for the conductivity.^{18,19,23}

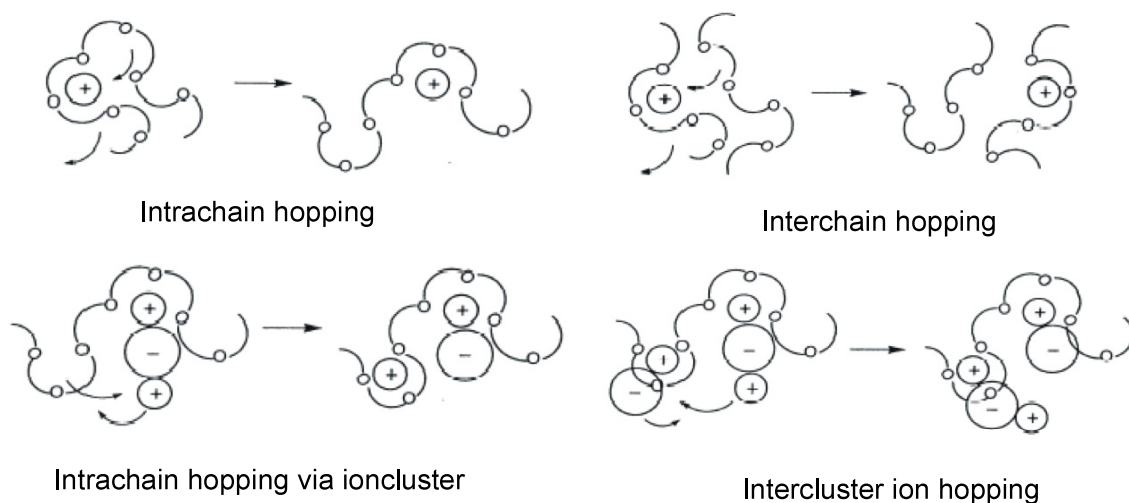


Figure 1.4. Representation of cation motion in a polymer electrolyte.¹⁸

Ions dissolved in amorphous polymers, or in the amorphous domains of semi-crystalline polymers, move through a semi-random motion of short segments of polymer chain. For poly(ethylene oxide), a “crank-shaft torsional motion” (see fig. 1.4),^{18,20} around the C–C and C–O bonds would be responsible for the ability of the polymer chain to wrap itself around the ions, to then unwrap itself, breaking

coordination to the ions and facilitating the movement of the ion to another site.¹⁸ Ions effectively dissociate from their polymer coordinating sites during this ion-hopping mechanism. Thus, the ion-polymer interactions have to be strong enough to promote salt dissolution, while being weak enough to allow ion mobility.¹⁹

The Williams-Landel-Ferry (WLF) equation can be used to describe a number of relaxation and transport processes in amorphous systems in the vicinity of the glass transition temperature and can be represented in the following form (eq. 1.3), where η is the viscosity at temperature T , T_s is the reference temperature, η_s is the viscosity at the reference temperature and C_1 and C_2 are constants that can be determined experimentally.¹⁹

Bruce and Gray,¹⁹ explain that the conductivity of polymer-salt systems can be expressed in terms of the WLF equation. It is possible to combine the Stokes-Einstein equation for the diffusion coefficient, D , with eq. 1.3. The resulting expression can then be combined with the Nernst-Einstein relationship (eq. 1.4), where q is the charge and assuming full dissociation of the salt in the polymer and k is the Boltzmann constant, to obtain eq. 1.5.

$$\log \left[\frac{\eta(T)}{\eta(T_s)} \right] = - \frac{C_1(T - T_s)}{(C_2 + T - T_s)} \quad (1.3)$$

$$\mu = qD/kT \quad (1.4)$$

$$\log \left[\frac{\sigma(T)}{\sigma(T_s)} \right] = -\frac{C_1(T - T_s)}{(C_2 + T - T_s)} \quad (1.5)$$

The WLF equation, as well as the related Vogel-Tamman-Fulcher (VTF) equation (1.6), can be used to accurately represent the variations of the ionic conductivity of amorphous polymer-salt systems with temperature.¹⁸⁻²⁰ This suggests that thermal motion above the reference temperature, and in particular above T_g , contributes to relaxation and transport processes, which is consistent with the ionic conduction mechanism previously described. However, deviations of the models from experimental data can still be obtained.¹⁹

$$\sigma = \sigma_0 \exp \left[\frac{-B}{(T - T_0)} \right] \quad (1.6)$$

It has been argued that these deviations correspond to the effects of other mechanisms at play at a microscopic level, in the polymer electrolyte, that are not considered in these equations. It has been proposed that solid ionic conductors could be characterized by the comparison of a structural relaxation time, τ_s , and a conductivity relaxation time, τ_σ .¹⁹ This model assumes that while the transport mechanism of cations in polymers, such as poly(ethylene oxide), is closely related to structural relaxation processes, the movement of the counter ion relies on a different transport process.

$$R_\tau = \frac{\tau_s}{\tau_\sigma} \quad (1.7)$$

Studies of the behavior of the ratio R_τ , defined in eq. 1.7, showed that, in polymer electrolytes, the structural and conductivity relaxations are very closely related, resulting in R_τ values close to 1. As the concentration of the salt in the polymer is increased, this ratio is found to be of the order of 0.1.¹⁹ This information suggests that even though there might be structural relaxation through segmental motions, these are not enough to permit the ions to move, which increases the conductivity relaxation time, decreasing R_τ . This may be caused by strong interionic interactions that result in ion immobilization or coulomb drag.¹⁹ This observation led Ratner and co-workers,^{19,24} to propose that while the cations move through the electrolyte by breaking and making of coordinate bonds, anion movement is dominated by hopping from an occupied site to a void (free space) large enough to contain the ion.¹⁹ This model is known as the dynamic bond percolation (DBP) theory.

The DBP theory incorporates elements that start to account for the effects that ion association may have on the ion transport mechanisms that govern the performance of polymer electrolytes, but it still fails to account for the possible coulombic interactions between moving ions.¹⁹

Ion-ion interactions can lead to ion association and the number and size of these clusters present in the polymer-salt complex affect the mobility, concentration and charge of the charge carriers that are responsible for the ionic conductivity of the material. Given the importance of ion association, several studies have dedicated a lot of effort to try to understand not only how the

polymer electrolyte coordinates to the metal cation (e.g. lithium), but also how to identify the different ionic species present in the polymer complex and try to correlate this information with the ionic conductivity of the different systems studied.²⁵⁻³⁹

Poly(ethylene oxide) (PEO), **1**, poly (bis(methoxyethoxyethoxy)phosphazene) (MEEP), **2**, and poly(ethylenimine) (PEI), **3**, are just a few of the polymers considered as electrolytes for batteries applications.

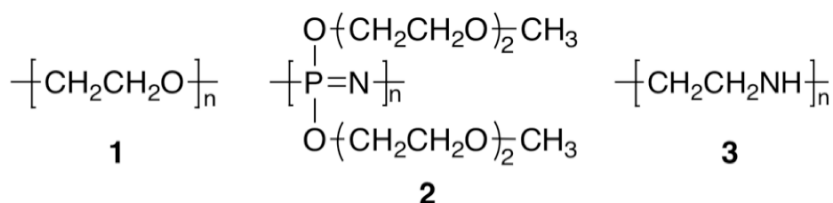


Figure 1.5. Structure of polymers considered as possible electrolytes for lithium ion batteries: (1) Poly(ethylene oxide), PEO, (2) Poly(bis(methoxyethoxyethoxy)phosphazene), MEEP, (3) Poly(ethylenimine), PEI

a. Poly(ethylene oxide)

A vast number of studies on polymer electrolytes have focused on poly(ethylene oxide), PEO, which polymer-salt systems constitute the first examples of “dry solid” polymer electrolytes.⁴⁰

The pioneer work of Wright on PEO complexes with sodium and potassium thiocyanate and sodium iodate^{34,41,42} brought attention to these materials and

their potential use in batteries but it would not be until 1978 when these materials were used as separators in lithium batteries.⁴⁰

PEO has been considered a very good matrix for lithium ion conduction due to its low glass transition temperature, T_g , and its ability to form complexes with alkali cations.²³

High molecular weight poly(ethylene oxide) is highly crystalline and studies have shown conductivity values of the order of 10^{-8} S/cm at ambient temperature, therefore limiting its applications to batteries that can operate at temperatures that range between 60°C and 100°C, where the ionic conductivity of the system can reach values of 10^{-4} S/cm.^{10,23,30,40}

Studies have shown that PEO forms stoichiometric crystalline complexes with alkali metal salts.^{26-29,43} Berthier and co-workers proposed that the ionic motion responsible for the conductivity in PEO-LiCF₃SO₃ and PEO-NaI systems takes place in the amorphous phase of the polymer and not in the crystalline phase.^{43,44}

The degree of dissociation of salts in the polymer host has been a concern to several research groups,^{44,45} and different methods have been developed in an attempt to elucidate the nature of the species, types of ions pairs and/or charge aggregates, involved in the conductivity mechanism for these materials.²⁵

Petersen and co-workers studied the ion-ion interactions in poly(propylene glycol) – lithium triflate complexes, PPG – LiCF₃SO₃.³⁴ They decided to investigate the ν_1 symmetric stretching mode of the SO₃⁻ group of the CF₃SO₃⁻ anion. This study was able to assign each of the bands observed in the Raman

spectra: “free” ion modes, which are not influenced by a change of cation, show at 1033.5 cm^{-1} ; ion pairs show at 1043 cm^{-1} , these are modes that are influenced by a change of cation; and higher degree multiplets or aggregate species show at 1053 cm^{-1} .³⁴ Petersen also observed the variation of the speciation in the PPG- LiCF_3SO_3 complexes with temperature.

Other studies by Frech *et al.* pointed out that in PEO systems the use of the symmetric stretching mode of the SO_3^- group, $\nu_s(\text{SO}_3^-)$, can be difficult due to the appearance of a PEO band in that particular region.⁴⁶⁻⁴⁸ However, ion-ion interactions can also be studied using the symmetric deformation mode of the CF_3 group of the triflate ion, $\delta_s(\text{CF}_3)$.⁴⁶⁻⁴⁸ The $\delta_s(\text{CF}_3)$ mode is particularly sensitive to the shifting of the electron density between the CF_3 and the SO_3^- in the triflate ion. Assignments in this region were made following the same reasoning used to assign the bands observed for the $\nu_s(\text{SO}_3^-)$ mode, for which the assignments were based on the observation that only one of the bands, 1032 cm^{-1} , is cation independent while the other two bands centered at 1042 and 1052 cm^{-1} are not. The multiple bands at around 752 , 757 , and 762 cm^{-1} in the $\delta_s(\text{CF}_3)$ spectral region are assigned to the “free” ions, ion pairs, and aggregates of triflate, respectively.⁴⁷⁻⁴⁹ Throughout these studies, evidence showed that the ionic speciation depends on the chain length of PEO, the concentration of salt and the temperature of the system.^{28,34,46-49}

In a more recent study,²⁸ Frech and coworkers showed that in the poly(ethylene oxide)₃: LiCF_3SO_3 complex, in which there is a Li^+ cation for each

three PEO repeat units, the amorphous phase has a short-range structure similar to that of the crystalline phase by looking at the variation of the symmetric stretching mode, $\nu_s(\text{SO}_3)$, with temperature. The symmetric deformation mode, $\delta_s(\text{CF}_3)$, was used to determine the variation in ion association with temperature. It was found that there is a single band at 760 cm^{-1} , assigned to the aggregate species, that does not change with temperature until the onset of the melting point is reached, at which point it shifts to 763 cm^{-1} , corresponding to a $[\text{Li}_2\text{CF}_3\text{SO}_3]^+$ species and giving some evidence to support the existence of a short-range order in the amorphous phase.²⁸

The investigation of the variations of the $\delta_s(\text{CF}_3)$ mode under various conditions to try to elucidate the ionic association in polymer salt systems can also be used with other polymer systems. This technique has been used in poly(ethylenimine)-based electrolyte systems for battery applications and in some of the studies reported in chapter 2 of this dissertation.

Fundamental studies conducted on PEO-based systems indicate that poly(ethylene oxide) forms a crystalline phase with lithium triflate, in which there is one lithium cation for every three PEO repeat units. The Li^+ cations are located within the PEO helix and is coordinated by three PEO oxygens and one oxygen from each two different CF_3SO_3^- groups located outside the helix. Each of these CF_3SO_3^- anions bridges between two different Li^+ ions.^{27,50} It has been reported that for certain dilute salt concentrations, the ionic association in PEO- LiCF_3SO_3 complexes changes over time.²⁷ IR spectroscopy shows that a band at around

760 cm^{-1} corresponding to aggregate species increases over time due to the formation of 3:1 O:Li crystalline domains.²⁷ This study, along with others focused on the elucidation of the phase diagram of PEO-LiCF₃SO₃ systems,^{27,29,44} led researchers to the consideration of alternative polymer-salt electrolyte systems. These alternative systems would be purposely designed to increase the fraction of amorphous domains in the materials to effectively increase the ionic conductivity. Polymer electrolyte materials were developed through two different approaches: *i*) by functionalizing amorphous, flexible polymers with PEO-like branches, like poly(bis(methoxyethoxyethoxy) phosphazene)-based systems (MEEP),^{31,51} ; and *ii*) by synthesizing polymers with backbone structures similar to that of PEO but with a different cation-coordinating heteroatom, such as linear poly(ethylenimine).^{39,52-54}

Poly(bis(methoxyethoxyethoxy)phosphazene), MEEP, was the first polymer material reported with a different molecular architecture based on comb-like polymers with solvating short branches.^{44,51} Poly(phosphazene)s are characterized by glass transition temperatures around -80°C ,⁵⁵ and the ionic conductivity of [LiCF₃SO₃]_{0.25}:MEEP complexes is between one and three orders of magnitude higher than that of PEO systems.⁵¹

A similar approach has been used with poly(dimethylsiloxane), PDMS. Short PEO segments have been incorporated into the PDMS chain, forming a linear copolymer in compound 4 (see Table 1.1). LiClO₄ complexes with this copolymer exhibit low T_g and, with a salt concentration of 0.4:1 Li:O, a conductivity of

1.6×10^{-4} S/cm at room temperature.⁵⁵ Comb-branched polymer architectures are also possible with poly(siloxane) backbones, as seen in compounds 5 and 6 in Table 1.1.⁵⁵

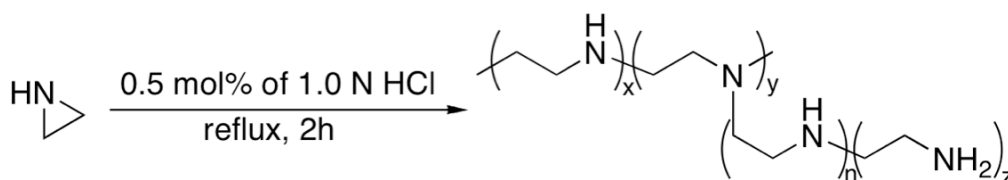
Table 1.1. Chemical structure of poly(siloxane)-based solid polymer electrolyte (SPE) materials

Compound	Molecular Structure	Reference
4	$\left[\begin{array}{c} \text{CH}_3 \\ \\ \text{Si}-\text{O}-(\text{CH}_2\text{CH}_2\text{O})_4 \\ \\ \text{CH}_3 \end{array} \right]_n$	56
5	$\begin{array}{c} \text{CH}_3 \\ \\ \left[\text{Si}-\text{O} \right]_n \\ \\ \text{O}-(\text{CH}_2\text{CH}_2\text{O})_{12}-\text{CH}_3 \end{array}$	57
6	$\begin{array}{c} \text{CH}_3 \\ \\ \left[\text{Si}-\text{O} \right]_n \\ \\ \text{CH}_2\text{CH}_2\text{CH}_2\text{O}-(\text{CH}_2\text{CH}_2\text{O})_{12}-\text{CH}_3 \end{array}$	58

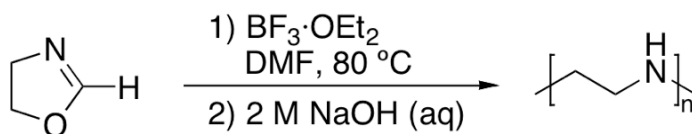
b. Poly(ethylenimine)

PEI is the nitrogen homologue of PEO. Its repeat unit is the result of substituting the oxygen atom with an amine (NH) group. PEI has an advantage over poly(ethylene oxide) in that it is a synthetically versatile polymer; it can be easily functionalized through reactions on the amine groups in the polymer's backbone. PEI can be synthesized, as shown in Scheme 1.1, by cationic ring opening polymerization of aziridine, but this reaction renders a highly branched polymer.^{59,60}

Saegusa and coworkers first presented a synthesis for linear poly(ethylenimine) (LPEI) through alkaline hydrolysis of poly(*N*-formylethylenimine) obtained from isomerization polymerization of unsubstituted 2-oxazoline using trifluoroborane as initiator in dimethylformamide at 80°C. As illustrated in Scheme 1.2, the resulting poly(*N*-formylethylenimine) is later hydrolyzed under basic conditions.⁵²

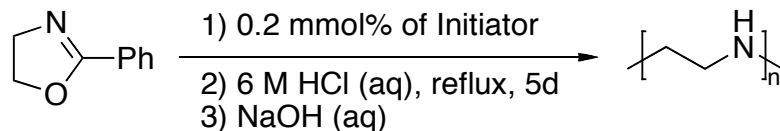


Scheme 1.1^{59,60}



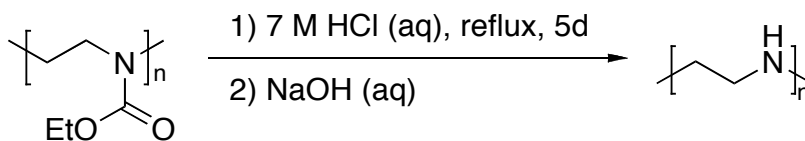
Scheme 1.2⁵²

Scheme 1.3 shows a somewhat different strategy to synthesize linear PEI, reported by Tanaka *et al.* in 1983.⁵⁴ LPEI is synthesized through the ring opening polymerization of 2-phenyl-2-oxazoline (POX) using dimethylsulfate (DMSF) or 2-phenyl-2-oxazolinium toluene sulfonate (POX·Tos) as initiator (0.2 mmol%). Acid hydrolysis can be used to effectively cleave the *N*-benzoyl group to obtain LPEI.⁵⁴



Scheme 1.3⁵⁴

Similarly, York *et al.* reported a synthesis of LPEI by acidic hydrolysis of commercially available poly(2-ethyl-2-ethyloxazoline), as shown in scheme 1.4.³⁹



Scheme 1.4³⁹

The potential of PEI as an electrolyte for alkali metal ions has been recognized by several studies.^{51,61-66}

Chiang *et al.* reported that LPEI dissolves sodium iodide and forms a high melting point crystalline complex when 0.3 moles of NaI per mol of repeat unit are used. The dc conductivity measured on samples containing 0.1 moles of NaI per mol of repeat unit was 5×10^{-6} S/cm at 75 °C, which was lower than the conductivity of comparable PEO systems under similar conditions.⁶¹ Even though these results were disappointing, fundamental research on PEI can improve that molecular level understanding of the different elements that control the ionic conductivity of a material.

Further studies presented by Chiang and coworkers also showed that lithium

salts, in a mole repeat unit per mole of salt ratio of 10:1, would also interact with LPEI in such a way that they could hinder crystallization of the pure polymer when cooled at a 20°C/min rate; conductivity values for the different lithium salt complexes were also reported.⁶² Harris *et al.* published data on LPEI-sodium triflate complexes with repeat unit to salt ratios ranging from 6:1 to 4:1. The conductivity values for these systems at 40 °C were around 2.4×10^{-7} S/cm for the 6:1 complex and 5.6×10^{-8} S/cm for the 4:1 complex.⁶⁴ When sodium triflate complexes of linear and branched PEI are compared, the branched polymer-salt complex, with a repeat unit to salt molar ratio of 20:1, shows a conductivity of 2×10^{-6} S/cm at 40°C.⁶³

This work encouraged others to study the conductivity behavior of branched PEI and lithium triflate; this system achieves conductivity values as high as 10^{-6} S/cm at room temperature for a 20:1 N:Li molar ratio.⁶⁵ Even though these values are still low when compared to systems like MEEP that show conductivities on the order of 10^{-5} S.cm⁻¹ with salt concentrations as low as 24:1 O:Li molar ratio.⁵¹ The low conductivity of LPEI – based systems has been blamed on the crystallinity of the system and the extensive hydrogen bonding that takes place.³⁰ Early attempts to improve the conductivity of PEI based systems included the study of poly(*N*-acetyl-ethylenimine), partially quaternized LPEI with ethyl and butyl groups, as well as crosslinking of the polymer with 1,2,7,8-diepoxyoctane.⁶⁶ Even though the chemical functionalizations were successful in hindering crystal formation in the polymer, they did not provide a

significant improvement on the conductivity of the polymer. In part, these early attempts ignored the potential role of hydrogen bonding in the conductivity behavior of LPEI-based systems, and the formation of ethyl or butyl quaternary ammonium cations on the polymer chain might decrease the ability of the nitrogen atom to coordinate the lithium cation, which would cause the conductivity to decrease, even though the polymer-salt complexes are amorphous.

A lot of research on LPEI-based polyelectrolyte systems has been done at the University of Oklahoma. The focus of this work has been on two aspects: improving the ionic conductivity and physical properties of PEI-based materials through functionalization of LPEI, as well as increase the fundamental understanding of these systems by evaluating particular systems.

Erickson *et al.* cyanoethylated LPEI to form poly(*N*-(2-cyanoethyl)ethylenimine), PCEEI, and studied the ionic association and conductivity of this polymer upon addition of lithium triflate.⁶⁷ The resulting polymer exhibited a T_g of -36°C , which is considerably lower than that of poly(acrylonitrile), PAN (*ca.* 80°C).⁶⁸ It was shown that the ionic conductivity of this system is mostly independent of salt concentration in the range studied, and that it has a conductivity value on the order of 10^{-8} S/cm at room temperature.⁶⁹ The variation of conductivity with temperature showed also that PCEEI electrolytes can reach conductivity values of 1.45×10^{-5} S/cm at 60°C , with a 10:1 N:Li molar ratio. This behavior is very different from PAN electrolytes with an

equivalent salt concentration, e.g. 10^{-9} S/cm above 100°C for salt concentration of 12:1 N:Li molar ratio.⁶⁸ When compared to poly(acrylonitrile)- LiCF_3SO_3 systems, it was noted that PCEI systems have a higher “free” ion concentration over the range of salt concentrations used.⁶⁹

Improvements on the ionic conductivity of linear PEI were made by attaching a PEO-like side chain to the nitrogen site, to form a polymer similar to MEEP.³⁸ Snow *et al.* have reported the synthesis of such polymer. Linear poly(*N*-(2-(2-methoxyethoxy)ethyl)ethylenimine) or LPEI-G2 can be synthesized by a reductive alkylation of LPEI using 2-(2-methoxyethoxy)acetic acid and sodium borohydride as reported in the literature.³⁸ Spectroscopic studies revealed that “free” ions are present in the polymer matrix and that these constitute the majority (nearly 50%) of the species responsible for the $\nu_s(\text{SO}_3)$ and $\delta_s(\text{CF}_3)$ bands observed.³⁸ Even though the amount of “free” ions in the electrolyte decreases with an increase in salt concentration, it remains a significant contributor at a salt concentration of 5:1 O:Li molar ratio.³⁸ The appearance of new bands in the polymer fingerprint region upon addition of salt suggests that the local conformation of LPEI-G2 changes due to interactions with lithium triflate. Additionally, spectroscopic evidence indicates that the primary coordination sites for lithium ions are the oxygen atoms on side chains rather than the nitrogen atoms on the LPEI-G2 backbone. LPEI-G2 exhibits a conductivity of 5×10^{-6} S/cm at room temperature for samples containing a lithium triflate concentration of 20:1 O:Li molar ratio, which is closer to the benchmark for solid polymer

electrolytes imposed by MEEP at comparable conditions.³⁸

Hu *et al.* reported the synthesis of branched poly(*N*-allylethylenimine), BPAEI.⁷⁰ The allyl side chains can be used to crosslink the polymer and improve its physical properties. BPEI's T_g changes dramatically with the addition of lithium triflate, from approximately -50°C with no salt to around 50°C with a N:Li molar ratio of 4:1; the T_g of the material decreases as a result of the allylation reaction and was found to be dependent on the amount of initiator used and it increases with the concentration of lithium salt.⁷⁰ AC conductivity measurements of an optimized sample (20:1 N:Li molar ratio and 60:1 N:initiator molar ratio) were reported. The conductivity achieved ranges from 1×10^{-8} S/cm at room temperature to 1×10^{-5} S/cm at 80°C .⁷⁰ While crosslinking the system did not improve the ionic conductivity of the system, it is a good strategy to improve the physical properties of polymer electrolyte system.

N-Alkylation of LPEI, avoiding the formation of quaternary salts, could be a good strategy to reduce or eliminate the hydrogen bonding in the system and therefore, improve the conductivity. A Clarke-Eschweiler reductive methylation of low molecular weight linear poly(ethylenimine) was first reported by Tanaka *et al.* in 1978.⁵³ This method reacted the polyamine with formic acid in excess and formaldehyde to produce linear poly(*N*-methylethylenimine), LPMEI.⁵³ Tanaka and co-workers later reported the synthesis of high molecular weight LPMEI,⁵⁴ and studied the thermal ionic conductivity behavior of LPEI and LPMEI systems with LiClO_4 and LiCF_3SO_3 .⁷¹ More recently, Sanders *et al.* reported a

comparative spectroscopic study of LPMEI systems containing lithium and sodium triflate.³⁷ Novel *N*-alkylated PEIs have been synthesized and studies of their lithium triflate complexes will be reported in Chapter 2 of this dissertation.

In addition to their potential application as solid electrolytes in lithium ion batteries, some polymeric materials have also been proposed as proton conductors for hydrogen fuel cell applications. PEI-based materials have been recognized as a potential proton conductors.⁷²⁻⁷⁵ It was thought that using a basic polymer, such as PEI, in combination with a mineral acid, i.e. phosphoric acid, would provide a more “understandable” proton pool than poly(vinyl alcohol) or poly(ethylene oxide) based systems.⁷⁵ Characterization and ionic conductivity studies on crosslinked PEI-H₃PO₄ based systems originally proposed by Glatzhofer and co-workers,⁷⁶ will be presented in chapter 3 of this dissertation.

2. Fuel Cells

Fuel cells are electrochemical devices that, like batteries, consist of an electrolyte in contact with an anode and a cathode. Fuel cells differ from batteries in that the active material or fuel is not an integral part of the cell.

Fig. 1.6 shows a schematic view of a proton exchange membrane fuel cell (PEMFC). As shown in the figure, hydrogen is fed into the anode where a catalyst oxidizes hydrogen to generate two H⁺ and 2e⁻, producing a current. Protons must flow from the anode through the electrolyte to the cathode, where they would participate in the reduction of oxygen by a catalytic reaction,

producing water. A continuous fuel flow into the electrochemical cell from an external source is needed to ensure the constant generation of electricity.^{6,77} Similar to batteries, fuel cells can be constructed in a modular fashion, connecting them in series to achieve the potential needed for a certain application.⁷⁷

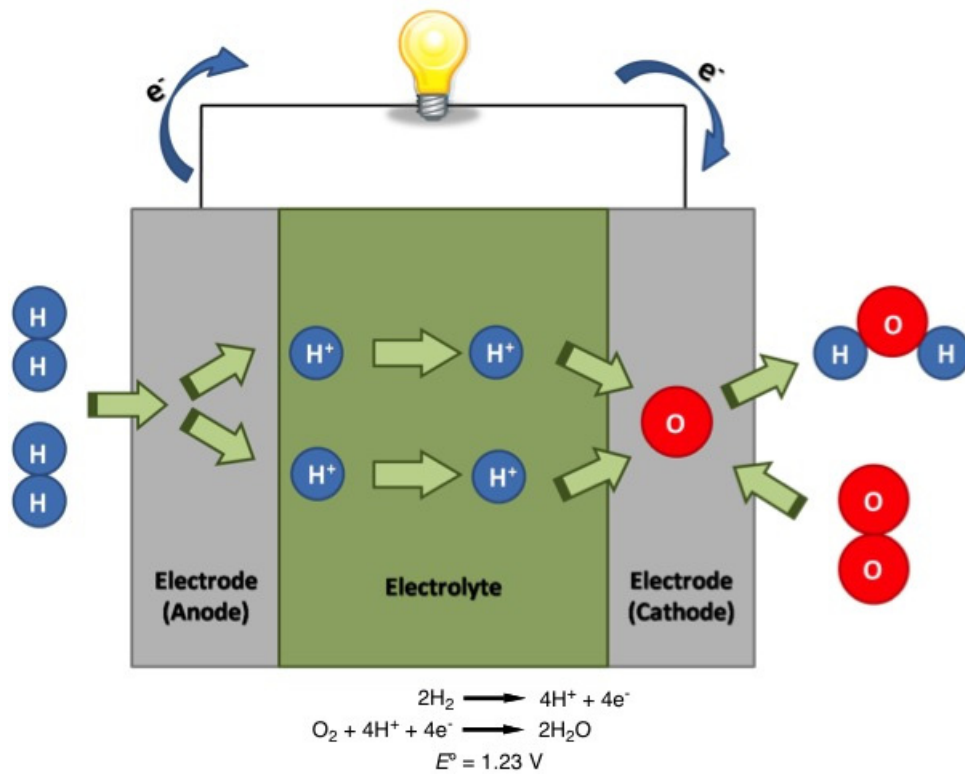


Figure 1.6. Schematic representation of a hydrogen fuel cell

Fuel cell technology is attractive because it is not subjected to Carnot cycle limitations as combustion and heat engines are, making them capable of higher energy conversion efficiencies. Nearly 80% of the chemical energy stored in the fuel can be converted into electrical energy, which is a considerable advantage when compared to the 40% efficiency that certain thermal power plants can

achieve.⁷⁷ The chemical energy stored in hydrogen and other hydrocarbon fuels, like methanol, is significantly higher than that of the materials used for batteries. Some of the advantages of using fuel cells include: efficient energy conversion; modular construction; fuel cells are non-polluting, low maintenance, and have a high energy density. However, they are complex to operate and commercial applications seem to be limited to primary energy sources for stationary central and dispersed power stations.⁵

Depending on the type of electrolyte used, fuel cells can be classified as alkaline fuel cells (AFCs), with potassium hydroxide-based electrolytes; polymer electrolyte fuel cells (PEMFCs); phosphoric acid fuel cells (PAFCs); molten carbonate fuel cells (MCFC); or solid oxide fuel cells (SOFCs).⁵

2.1. Hydrogen Proton Exchange Membrane Fuel Cells (PEMFCs)

First developed for the Gemini space vehicle, PEMFCs are one of the most promising types of fuel cells for commercial applications.⁷⁷ PEMFCs are unique among other fuel cell types, with the exception of the solid oxide fuel cells, because they possess a solid proton conducting electrolytes.

For PEMFC applications, the electrolyte material must be a good proton conductor while being a good barrier to hydrogen and oxygen gasses, since a cross-over of these materials would significantly lower the efficiency of the fuel cell by lowering the amount of work that it would be able to do.⁶

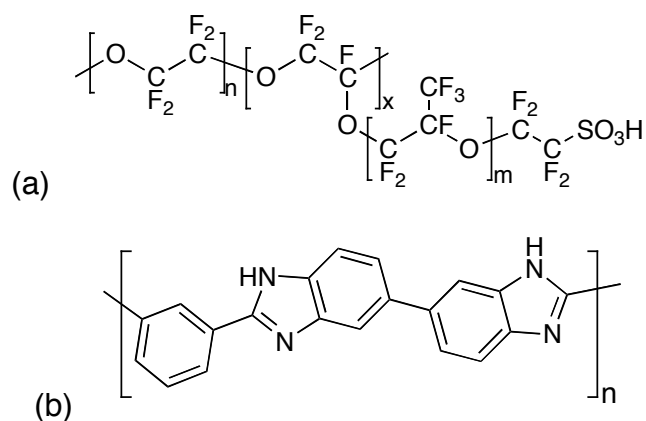


Figure 1.7. Structure of (a) Nafion® and (b) Poly(benzimidazole)

Nafion® is one of the polymer electrolytes used for these types of fuel cells and its structure involves a poly(tetrafluoroethylene) backbone with a perfluorinated side chain that is terminated with a sulfonic acid group (See Fig. 1.7(a)).^{5,78} Hydration of the membrane is necessary to allow proton mobility and solvation of the acid group.⁵ Conductivities in well-hydrated systems can be as high as 0.2 S.cm⁻¹. However, there are disadvantages to the use of this material: cost, safety concerns due to toxic gases liberated when operated at temperatures above 150°C, and the need for a hydration system limits the applicability of this technology on vehicles and adds complexity to the operation of the systems. Furthermore, the conductivity of the material at 80°C is diminished as much as ten times relative to the conductivity reported at 60°C due to dehydration of the polymer.^{5,78} Studies have shown that fuel cell performance improves at higher temperatures, mainly due to an increase in the rate of the reaction and reduction of catalyst poisoning by absorbed carbon monoxide. Operation at high

temperatures also helps to minimize problems regarding electrode flooding,⁷⁸ which makes it desirable to have an alternative material to Nafion[®] for PEMFC applications.

Mehta and Cooper have summarized some of the polymers that have been studied as an alternative to Nafion[®] for the manufacturing of membrane electrode assemblies (MEAs).⁷⁸

Fig. 1.7(b) shows the structure of poly(benzimidazole) (PBI). This polymer, when doped with acid is considered an alternative to Nafion[®] thanks to its high conductivity and thermal stability.⁷⁸ However, the drawback for these systems is the processing of the material. In order to prepare the film, PBI has to be dissolved in dimethylacetamide and spread on a glass plate. Then the solvent is evaporated by heating at 100°C for 5 hours and then any residual solvent is removed by further heating the sample up to 200°C for 2 hours. The doping process involves dipping the PBI film in anhydrous sulfuric acid or 11M phosphoric acid solutions for at least 16 hours. The amount of acid doping achieved depends on the ability of the acid to diffuse into the film and the time that the film is submerged in the acid. Phosphoric acid doped systems have shown better performance than other acids.⁷⁹⁻⁸¹

Acid-doped poly(ethylenimine) has also been considered an alternative to Nafion[®] as proton conductor materials.^{75,82} The interest in PEI as an electrolyte material for PEMFC applications was limited due to its water solubility and concerns about its thermal stability.⁷⁸ These concerns may be addressed by

developing a crosslinked PEI system.^{74,76}

Conductivity studies on crosslinked PEI-based electrolyte membranes will be presented in chapter 4 of this dissertation. Preliminary fuel cell testing of LPEI·HCl/H₃PO₄ based membrane electrode assemblies (MEAs) will be presented in chapter 5 of this dissertation.

References

- (1) UN Framework Convention on Climate Change (UNFCCC), *Kyoto protocol to the United Nations framework convention on climate change*, 1998, <http://unfccc.int/resource/docs/convkp/kpeng.pdf>
- (2) General Motors, "Fuel Economy & Alternative Fuels", General Motors, http://www.gm.com/experience/fuel_economy/ (accessed 08/18/2008)
- (3) Honda, "Environmental Technology Overview", Honda, <http://corporate.honda.com/environment/overview.aspx> (accessed 08/18/2008)
- (4) Toyota, "Hybrid synergy view", Toyota, <http://www.toyota.com/html/hybrid synergy view/2004/october/hybrids201.html> (accessed 08/18/2008)
- (5) Winter, M.; Brodd, R. J. *Chem. Rev.* **2004**, *104*, 4245-4269.
- (6) Linden, D. In *Handbook of batteries*; Linden, D., Reddy, T. B., Eds.; McGraw-Hill: New York, 2002, p 1.3-1.18.
- (7) Laidler, K. J.; Meiser, J. H.; Sanctuary, B. C. *Physical Chemistry*, 4th Edition ed.; Houghton Mifflin Company: Boston, 2003.
- (8) Linden, D.; Reddy, T. B. In *Handbook of batteries*; Linden, D., Reddy, T. B., Eds.; McGraw-Hill: New York, 2002, p 22.3-22.24.
- (9) Anglin, D. L.; Sadoway, D. R. In *AccessScience@McGraw-Hill* 2008; Vol. 2008.
- (10) Reddy, T. B.; Hossain, S. In *Handbook of batteries*; Linden, D., Reddy, T. B., Eds.; McGraw-Hill: New York, 2002, p 34.1-34.62.

- (11) Nishi, Y. In *Solid state ionics for batteries*; Minami, T., Tatsumisago, M., Wakihara, M., Iwakura, C., Kohjiya, S., Tanaka, I., Eds.; Springer - Verlag: Tokyo, 2005, p 5-11.
- (12) Ehrlich, G. M. In *Handbook of batteries*; Linden, D., Reddy, T. B., Eds.; McGraw-Hill: New York, 2002, p 35.1-35.94.
- (13) Fu, L. J.; Liu, H.; Li, C.; Wu, Y. P.; Rahm, E.; Holze, R.; Wu, H. Q. *Prog. Mater. Sci.* **2005**, *50*, 881-928.
- (14) Huggins, R. A. *Solid State Ionics* **2002**, *152-153*, 61-68.
- (15) Kohjiya, S. In *Solid state ionics for batteries*; Minami, T., Tatsumisago, M., Wakihara, M., Iwakura, C., Kohjiya, S., Tanaka, I., Eds.; Springer - Verlag: Tokyo, 2005, p 187-191.
- (16) Nanno, T.; Yoshizawa, H.; Ikoma, M. In *Solid State Ionics for Batteries*; Minami, T., Tatsumisago, M., Wakihara, M., Iwakura, C., Kohjiya, S., Tanaka, I., Eds.; Springer-Verlag: Tokyo, 2005, p 12-18.
- (17) Robertson, A. D.; West, A. R.; Ritchie, A. G. *Solid State Ionics* **1997**, *104*, 1-11.
- (18) Gray, F. M. *Polymer Electrolytes*; The Royal Society of Chemistry: Cambridge, 1997.
- (19) Bruce, P. G.; Gray, F. M. In *Solid state electrochemistry*; 1st ed.; Bruce, P. G., Ed.; Cambridge University Press: Cambridge, 1995, p 119-162.
- (20) Shriver, D. F.; Bruce, P. G. In *Solid state electrochemistry*; Bruce, P. G., Ed.; Cambridge University Press: Cambridge, 1995, p 95-118.
- (21) Hiemenz, P. C.; Lodge, T. P. *Polymer Chemistry*; 2nd. ed.; CRC Press: Boca Raton, 2007.
- (22) Young, R. J.; Lovell, P. A. *Introduction to Polymers*; 2nd. ed.; Chapman & Hall: London, 1991.
- (23) Kohjiya, S.; Ikeda, Y. In *Solid state ionics for batteries*; Minami, T., Tatsumisago, M., Wakihara, M., Iwakura, C., Kohjiya, S., Tanaka, I., Eds.; Springer-Verlag: Tokyo, 2005, p 191-196.
- (24) Ratner, M.; Nitzan, A. *Faraday Discuss. Chem. Soc.* **1989**, *88*, 19-42.
- (25) Bruce, P. G.; Vincent, C. A. *Faraday Discuss. Chem. Soc.* **1989**, *88*, 43-54.

- (26) Chintapalli, S.; Frech, R. *Electrochim. Acta* **1995**, *40*, 2093-2099.
- (27) Chintapalli, S.; Frech, R. *Electrochim. Acta* **1998**, *43*, 1395-1400.
- (28) Frech, R.; Chintapalli, S.; Bruce, P. G.; Vincent, C. A. *Chem. Commun.* **1997**, 157-158.
- (29) Frech, R.; Chintapalli, S.; Bruce, P. G.; Vincent, C. A. *Macromolecules* **1999**, *32*, 808-813.
- (30) Frech, R.; Giffin, G. A.; Yopez Castillo, F.; Glatzhofer, D. T.; Eisenblatter, J. *Electrochim. Acta* **2005**, *50*, 3963-3968.
- (31) Frech, R.; York, S.; Allcock, H.; Kellam, C. *Macromolecules* **2004**, *37*, 8699-8702.
- (32) Hu, L. Y.; Frech, R.; Glatzhofer, D. T.; Mason, R.; York, S. S. *Solid State Ionics* **2008**, *179*, 401-408.
- (33) Papke, B. L.; Ratner, M. A.; Shriver, D. F. *J. Electrochem. Soc.* **1982**, *129*, 1434-1438.
- (34) Petersen, G.; Jacobsson, P.; Torell, L. M. *Electrochim. Acta* **1992**, *37*, 1495-1497.
- (35) Rhodes, C. P.; Frech, R. *Solid State Ionics* **1999**, *121*, 91-99.
- (36) Rhodes, C. P.; Frech, R. *Solid State Ionics* **2000**, *136*, 1131-1137.
- (37) Sanders, R. A.; Snow, A. G.; Frech, R.; Glatzhofer, D. T. *Electrochim. Acta* **2003**, *48*, 2247-2253.
- (38) Snow, A. G.; Sanders, R. A.; Frech, R.; Glatzhofer, D. T. *Electrochim. Acta* **2003**, *48*, 2065-2069.
- (39) York, S.; Frech, R.; Snow, A.; Glatzhofer, D. *Electrochim. Acta* **2001**, *46*, 1533-1537.
- (40) Stephan, A. M. *Eur. Polym. J.* **2006**, *42*, 21-42.
- (41) Fenton, D. E.; Paker, J. M.; Wright, P. V. *Polymer* **1973**, *14*, 589.
- (42) Wright, P. V. *Br. Polym. J.* **1975**, *7*, 319-327.
- (43) Berthier, C.; Gorecki, W.; Minier, M.; Armand, M. B.; Chabagno, J. M.; Rigaud, P. *Solid State Ionics* **1983**, *11*, 91-95.

- (44) Armand, M. *Solid State Ionics* **1994**, *69*, 309-319.
- (45) MacCallum, J. R.; Tomlin, A. S.; Vincent, C. A. *Eur. Polym. J.* **1986**, *22*, 787-791.
- (46) Frech, R.; Huang, W. *Solid State Ionics* **1994**, *72*, 103-107.
- (47) Huang, W.; Frech, R. *Polymer* **1994**, *35*, 235-242.
- (48) Huang, W.; Frech, R.; Johansson, P.; Lindgren, J. *Electrochim. Acta* **1995**, *40*, 2147-2151.
- (49) Huang, W.; Frech, R.; Wheeler, R. A. *J. Phys. Chem.* **1994**, *98*, 100-110.
- (50) Lightfoot, P.; Mehta, M. A.; Bruce, P. G. *Science* **1993**, *262*, 883-885.
- (51) Blonsky, P. M.; Shriver, D. F.; Austin, P.; Allcock, H. R. *J. Am. Chem. Soc.* **1984**, *106*, 6854-6855.
- (52) Saegusa, T.; Ikeda, H.; Fujii, H. *Macromolecules* **1972**, *5*, 108.
- (53) Tanaka, R.; Koike, M.; Tsutsui, T.; Tanaka, T. *J. Polym. Sci. Polym. Lett.* **1978**, *16*, 13-16.
- (54) Tanaka, R.; Ueoka, I.; Takaki, Y.; Kataoka, K.; Saito, S. *Macromolecules* **1983**, *16*, 849-853.
- (55) Meyer, W. H. *Adv. Mater.* **1998**, *10*, 439-448.
- (56) Nagaoka, K.; Naruse, H.; Shinohara, I.; Watanabe, M. *J. Polym. Sci. Polym. Lett.* **1984**, *22*, 659-663.
- (57) Fish, D.; Khan, I. M.; Smid, J. *Makromol. Chem., Rapid Commun.* **1986**, *7*, 115-120.
- (58) Fish, D.; Khan, I. M.; Wu, E.; Smid, J. *Br. Polym. J.* **1988**, *20*, 281-288.
- (59) Jones, G. D.; Langsjoen, A.; Neumann, S. M. M. C.; Zomlefer, J. *J. Org. Chem.* **1944**, *9*, 125-147.
- (60) Jones, G. D.; MacWilliams, D. C.; Braxton, N., A. *J. Org. Chem.* **1965**, *30*, 1994-2003.
- (61) Chiang, C. K.; Davis, G. T.; Harding, C. A.; Takahashi, T. *Macromolecules* **1985**, *18*, 825-827.

- (62) Chiang, C. K.; Davis, G. T.; Harding, C. A.; Takahashi, T. *Solid State Ionics* **1986**, *18-19*, 300-305.
- (63) Harris, C. S.; Ratner, M. A.; Shriver, D. F. *Macromolecules* **1987**, *20*, 1778-1781.
- (64) Harris, C. S.; Shriver, D. F.; Ratner, M. A. *Macromolecules* **1986**, *19*, 987-989.
- (65) Paul, J.-L.; Jegat, C.; Lassègues, J. C. *Electrochim. Acta* **1992**, *37*, 1623-1625.
- (66) Takahashi, T.; Davis, G. T.; Chiang, C. K.; Harding, C. A. *Solid State Ionics* **1986**, *18-19*, 321-325.
- (67) Erickson, M.; Frech, R.; Glatzhofer, D. T. *Electrochim. Acta* **2003**, *48*, 2059-2063.
- (68) Erickson, M. J. Ph. D. Dissertation, The University of Oklahoma, 2004.
- (69) Erickson, M. J.; Frech, R.; Glatzhofer, D. T. *Polymer* **2004**, *45*, 3389-3397.
- (70) Hu, L. Y.; Frech, R.; Glatzhofer, D. T. *Polymer* **2006**, *47*, 2099-2105.
- (71) Tanaka, R.; Fujita, T.; Nishibayashi, H.; Saito, S. *Solid State Ionics* **1993**, *60*, 119-123.
- (72) Daniel, M. F.; Desbat, B.; Cruege, F.; Trinquet, O.; Lassègues, J. C. *Solid State Ionics* **1988**, *28-30*, 637-641.
- (73) Daniel, M. F.; Desbat, B.; Lassègues, J. C. *Solid State Ionics* **1988**, *28-30*, 632-636.
- (74) Tanaka, R.; Yamamoto, H.; Shono, A.; Kubo, K.; Sakurai, M. *Electrochim. Acta* **2000**, *45*, 1385-1389.
- (75) Tanaka, R.; Yamamoto, H.; Kawamura, S.; Iwase, T. *Electrochim. Acta* **1995**, *40*, 2421-2424.
- (76) Glatzhofer, D. T.; Erickson, M. J.; Frech, R.; Yopez, F.; Furneaux, J. E. *Solid State Ionics* **2005**, *176*, 2861-2865.
- (77) Viswanathan, B.; Aulice Scibioh, M. *Fuel cells: Principles and applications*; CRC Press: Boca Raton, 2007.
- (78) Mehta, V.; Cooper, J. S. *J. Power Sources* **2003**, *114*, 32-53.

- (79) Bouchet, R.; Siebert, E. *Solid State Ionics* **1999**, *118*, 287-299.
- (80) Bouchet, R.; Siebert, E.; Vitter, G. *J. Electrochem. Soc.* **1997**, *144*, L95-L97.
- (81) Wainright, J. S.; Wang, J.-T.; Weng, D.; Savinell, R. F.; Litt, M. *J. Electrochem. Soc.* **1995**, *142*, L121-L123.
- (82) Schoolmann, D.; Trinquet, O.; Lassegues, J. C. *Electrochim. Acta* **1992**, *37*, 1619-1621.

Chapter 2: PEI-based electrolytes for lithium battery applications

Portions of this chapter were taken from: Frech, R.; Giffin, G. A.; Yopez Castillo, F.; Glatzhofer, D. T.; Eisenblatter, J. *Electrochim. Acta* **2005**, *50*, 3963-3968.

The research presented in this chapter was performed in close collaboration with Dr. Nathalie M. Rocher and Ms. Guinevere A. Giffin in Dr. Roger Frech's research group at the University of Oklahoma. Part of the results presented in this chapter have already been published elsewhere.¹

Even though the research on polymer electrolytes for battery application has concentrated on poly(ethylene oxide)-based electrolytes, the conductivity of these systems is less than ideal at room temperature due to the formation of non-conductive crystalline PEO-lithium triflate phases.^{2,3} This fact has prompted researchers to look for alternative polymer host materials. Linear poly(ethylenimine), LPEI, is a polymer analog to PEO with secondary amine groups instead of oxygen groups.⁴ However, LPEI is highly crystalline and its complexes with alkali metals exhibit very low ionic conductivities at room temperature. This is due, in part, to the hydrogen bonding interactions that are present in the material.

Branched poly(ethylenimine), BPEI, has also been studied because it is a highly branched and amorphous type of poly(ethylenimine) and its complexes with alkali metals, much like those of LPEI, are conductive.^{5,6} BPEI also has the

advantage of being commercially available. BPEI has a lower T_g than that of LPEI and that it has a primary-to-secondary-to-tertiary amine ratio of 1:2:1.⁵ Lithium, and sodium triflate complexes of BPEI are amorphous at salt concentrations that range between repeat unit to salt ratios of 20:1 to 6:1.^{5,6} Table 2.1 shows the T_g values BPEI and LPEI complexes with lithium and sodium triflate.

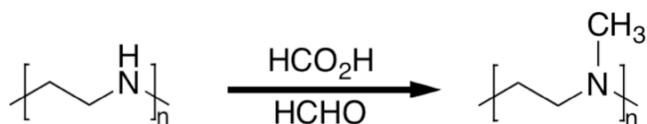
Table 2.1. Glass transition temperatures for BPEI, LPEI and their complexes with sodium and lithium triflate.

	T_g (°C)	Ref.
BPEI	-47	5
N:NaSO ₃ CF ₃		
20:1	-31	5
12:1	-12	5
6:1	12	5
N:LiSO ₃ CF ₃		
25:1	-36	6
20:1	-31	6
16:1	-27	6
8:1	-5	6
LPEI	-23	7
N:NaSO ₃ CF ₃		
6:1	-5	7
N:LiSO ₃ CF ₃		
15:1	ca. -19	9
10:1	ca. -12	9
6:1	ca. 12	9
4:1	ca. 25	9

As observed with LPEI complexes, the addition of salt to BPEI increases the T_g of the resulting complex.^{5,6} In the case of BPEI complexes, changes in T_g are more significant in magnitude than those observed in LPEI complexes. As seen in table 2.1, BPEI complexes with lithium and sodium triflate at low salt concentrations have lower T_g values than those for the LPEI. However, as the salt concentration increases, the T_g of BPEI complexes become higher than those of linear polyimine complexes.⁵⁻⁸

Harris *et al.* postulated that in BPEI the primary nitrogens at the chains ends are the ones that preferentially coordinate the metal ions, restricting the movements of the chain ends upon formation of polymer-salt complexes, increasing the T_g .⁵ Since BPEI has a much higher content of chain end groups than LPEI, it is expected that the amount of salt added to the polymer would cause a much bigger impact on the glass transition temperature of BPEI complexes than in LPEI complexes.

Hydrogen bonding interactions in PEI can be reduced or eliminated through the alkylation of secondary and primary amine groups. Tanaka *et al.* was the first to report the synthesis of linear poly(*N*-methylethylenimine), LPMEI, through a Clarke-Eschweiler reductive methylation of low molecular weight LPEI as shown in scheme 2.1.¹⁰



Scheme 2.1. Clarke-Eschweiler reductive methylation of LPEI.¹⁰

The synthesis, as described by Tanaka and co-workers, involves the reaction of LPEI or poly(*N*-formylethylenimine), POXZ, with a large excess of formalin (35% solution) – formic acid (85% assay) mixture, at 105°C for over two days. The solvent is removed under reduced pressure and hydrochloric acid is added to the residue in excess to form the hydrochloride salt of LPMEI.¹⁰

LPMEI hydrochloride is neutralized using an anion–exchange resin to quantitatively recover the neutral polymer.¹⁰ Conductivity and thermal data for LPMEI complexes with LiClO₄ and LiSO₃CF₃ have been reported by Tanaka *et al.*,⁹ and comparative studies of thermal and conductivity properties as well as vibrational spectroscopy data have also been reported elsewhere.¹¹

1. Branched PEI-based electrolytes: Synthesis of branched poly(*N*-methylethylenimine), BPMEI.

While the synthesis of branched poly(*N*-methylethylenimine), BPMEI, has been reported under similar Clarke-Eschweiler conditions to those used for LPMEI,¹⁰ a detailed spectroscopic study of BPMEI complexes with lithium triflate has not been published yet.

BPMEI - LiSO₃CF₃ complexes were studied using FT-IR spectroscopy, differential scanning calorimetry (DSC) and impedance spectroscopy. The study of these complexes was done in collaboration with Dr. Nathalie M. Rocher. Dr. Rocher was responsible for IR spectra collection and analysis, as well as the

DSC and conductivity data collection and analysis. I was responsible for the synthesis and initial characterization of BPMEI. Some of the results from this study are summarized in this chapter.

Branched PEI (Aldrich, \overline{M}_n ca. 10,000) was methylated under Clarke-Eschweiler conditions previously reported elsewhere.^{1,10,11} The branched poly(*N*-methylethylenimine) was a dark brown and extremely viscous material. The molecular weight of the resulting polymer, \overline{M}_n ca. 14,000, was derived from the molecular weight of the starting BPEI, assuming no polymer degradation during the methylation reaction. Fig. 2.1 shows the ¹H-NMR spectra of BPEI and BPMEI in *d*₄-methanol. The reaction yielded a BPMEI residue with a 100% of methyl substitution. This was determined by the integration of the peaks from the methylene (CH₂) and methyl (CH₃) units.

As shown in Fig. 2.1, after the methylation reaction, the ¹H-NMR spectra of the polymer presents several overlapping singlet peaks at $\delta \sim 2.3$ ppm that correspond to the protons of the newly added methyl groups. The appearance of more than one peak for the methyl group attached to the nitrogen atoms on the polymer backbone is consistent with the small differences that arise from the chemical environments of those methyl groups in the polymer backbone.

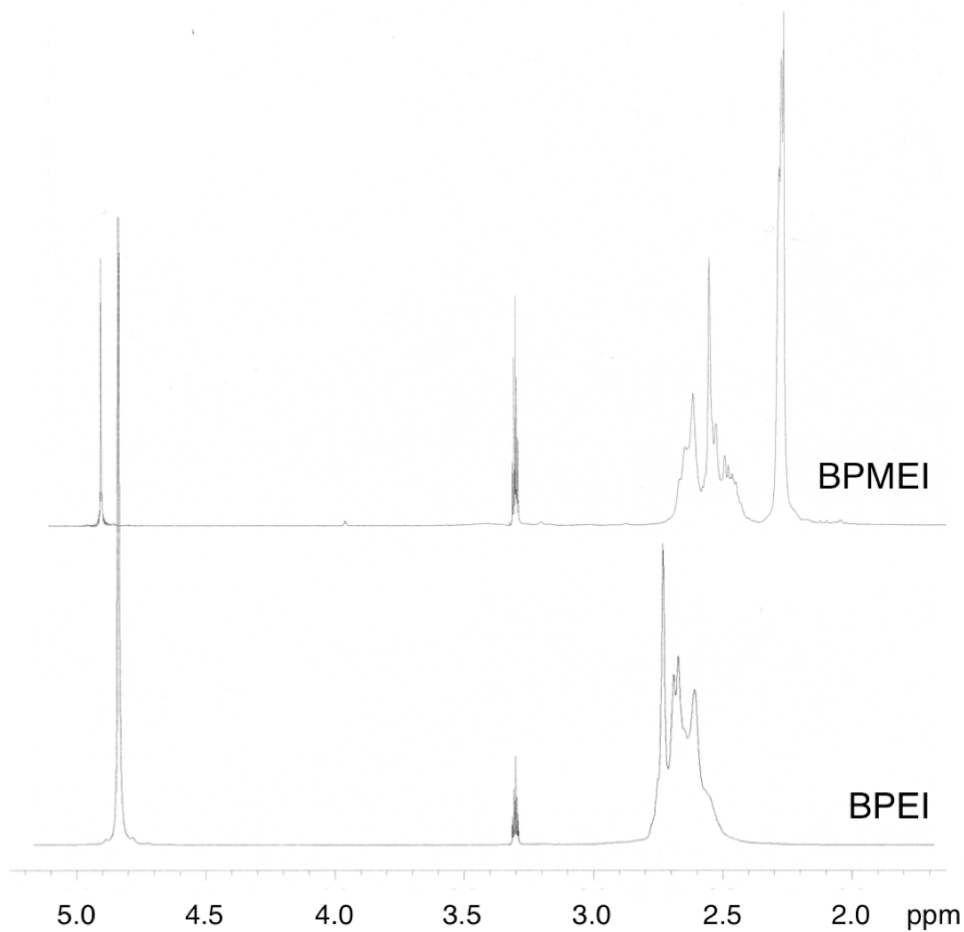


Figure 2.1. $^1\text{H-NMR}$ spectra of branched poly(ethylenimine) and branched poly(*N*-methylethylenimine) in methanol- d_4 .

Polymer salt complexes were made with BPMEI solutions in dry acetonitrile and various amounts of lithium triflate were added to the polymer solution. The N:Li molar ratio for the BPMEI- LiSO_3CF_3 complexes ranged from 30:1 to 5:1. Table 2.2 shows T_g values for BPMEI and LPMEI and the complexes with lithium triflate.

Table 2.2. Glass transition temperatures, T_g ($^{\circ}\text{C}$) of BPMEI and LPMEI and their lithium triflate complexes at various N:Li molar ratios.¹²

Composition N:Li	BPMEI-LiSO₃CF₃	LPMEI-LiSO₃CF₃[†]
Neat polymer	-91	-93
30:1	-88	
20:1	-81	-79
15:1	-43	
10:1	-18	-60
5:1	13	-14

[†] Values for LPMEI are taken from the literature.¹

When compared with previously collected LPMEI data,^{1,11} it was found that both polymers have similar T_g values even after adding small amounts of salt, N:Li molar ratios 20:1 or higher. Data in table 2.2 shows that at salt concentrations higher than 20:1 the glass transition temperature of the BPMEI-LiSO₃CF₃ complexes increases dramatically compared to the values obtained from LPMEI complexes. This trend is consistent with that observed previously for BPEI and LPEI complexes.^{5,6}

It has been reported that primary amine groups in BPEI preferentially form complexes with transition metal ions.⁵ Earlier in the chapter it was mentioned that Harris and co-workers have postulated that this was also the case for alkali metal ions.⁵ Coordination of primary amines to metal ions causes a restriction of movements of the chain ends upon formation of the polymer-salt complex.

The trend observed in table 2.2 could be explained in terms of the branched structure of the methylated polymer. BPMEI has only tertiary amine groups.

There is a difference in the mobility of amine groups located on the side chains and the ones located in the backbone of the polymer. The amine groups located on the side chains and chain ends, like the primary amines in BPEI, would coordinate more easily with metal cations due to their mobility and reduced steric hindrance compared to that of nitrogen atoms along the backbone of the BPMEI.

Formation of these complexes would constrain segmental motions of the side chains, effectively increasing the T_g of the branched system. It is found that, at high salt concentrations, the glass transition temperature of BPMEI complexes is consistently higher than that of LPMEI complexes of equivalent salt concentration. This observation suggests that a “stronger” lithium–nitrogen coordination takes place in the branched system.¹²

A careful study of the infrared spectra of BPMEI – LiSO₃CF₃ and LPMEI – LiSO₃CF₃ complexes shows that the changes seen in the spectra upon salt addition are similar for both linear and branched polymer hosts. Figures 2.2 and 2.3 show the spectra of BPMEI and LPMEI complexes with lithium triflate (N:Li molar ratios of 10:1 and 5:1) in the 735 – 1000 cm⁻¹ and in the 1000 – 1400 cm⁻¹ regions, respectively.

Modes in the 735 – 1000 cm⁻¹ region, illustrated in Fig. 2.2, are comprised mainly of CH₂ rocking and C–N stretching motions, while bands present in the 1000 – 1400 cm⁻¹ region (see Fig. 2.3) are assigned to mixed modes with contributions from CH₂ rocking and twisting, C–C and C–N stretching, and CH₃ wagging motions.¹²

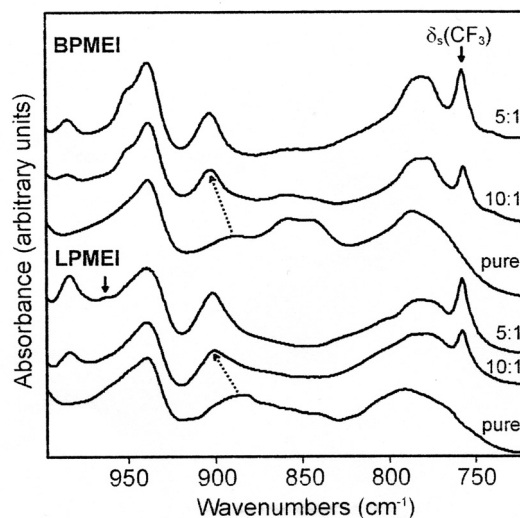


Figure 2.2. IR spectra of high M_w BPMEI and LPMEI and their complexes with lithium triflate (N:Li molar ratios 10:1 and 5:1) in the 735 – 1000 cm^{-1} region.¹²

Upon addition of lithium triflate to each of the polymer hosts, a few changes in the spectra of each of the systems become evident. For example, the addition of salt causes a large shift and increase of intensity of a polymer band at 887 cm^{-1} to higher frequencies; this change is common to both polymer systems.¹² Additionally, the symmetric deformation mode, $\delta_s(\text{CF}_3)$, of the triflate ion appears in the 750 – 770 cm^{-1} region of the spectra.^{13,14} Changes in the intensities of these bands, as well as frequency shifts, are evidence of changes in the ion-ion coordination.^{1,15} Tables 2.3 and 2.4 summarize the frequencies of the symmetric deformation band of the CF_3 group in the triflate anion for BPMEI- LiSO_3CF_3 and LPMEI- LiSO_3CF_3 , respectively.

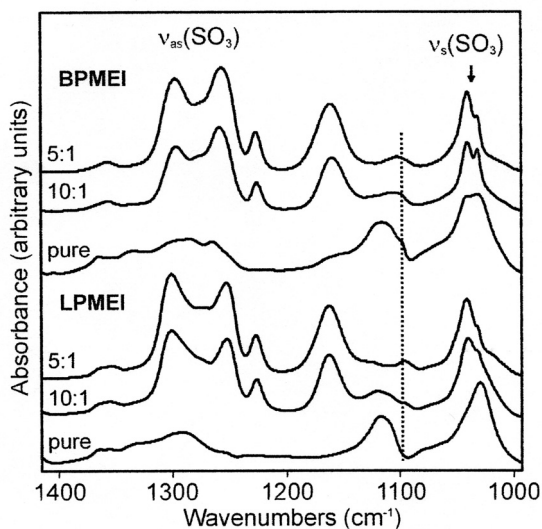


Figure 2.3. IR spectra of high M_w BPMEI and LPMEI and their complexes with lithium triflate (N:Li molar ratios 10:1 and 5:1) in the 1000 - 1400 cm^{-1} region.¹²

Table 2.3. Frequencies (cm^{-1}) in the $\delta_s(\text{CF}_3)$ region for BPMEI-LiSO₃CF₃ complexes. Relative intensities (%) are given next to frequency.¹²

Composition	$\delta_s(\text{CF}_3)$		
	Aggregate	Pair	“Free”
20:1		756 (78%)	752 (22%)
10:1		757 (78%)	752 (22%)
5:1	762 (6%)	758 (81%)	752 (13%)

An analysis of the $\delta_s(\text{CF}_3)$ region shows that contact ions pairs are the dominant species present in PMEI complexes with lithium triflate. However, there is an important difference between the linear and the branched polymer system. Aggregate formation seems to occur at lower salt concentrations and to a greater

extent for LPMEI complexes. Table 2.4 shows that a band at 762 cm^{-1} appears in 15:1 LPMEI-triflate complexes, and the relative intensity of this band increases with the salt content. A similar trend is observed in the branched system. For BPMEI-triflate complexes, the appearance of an aggregate band in the $\delta_s(\text{CF}_3)$ region of the IR spectra does not occur until the composition reaches 5:1.

Table 2.4. Frequencies (cm^{-1}) in the $\delta_s(\text{CF}_3)$ region for LPMEI- LiSO_3CF_3 complexes. Relative intensities (%) are given next to frequency.^{11,12}

Composition	$\delta_s(\text{CF}_3)$		
	Aggregate	Pair	“Free”
20:1		757 (64%)	752 (36%)
15:1	762 (12%)	758 (61%)	752 (27%)
10:1	762 (14%)	758 (60%)	752 (26%)
5:1	761 (20%)	758 (56%)	752 (24%)

It is possible to envision that the speciation differences between the linear and the branched systems are related to the structure of the polymer host. As was mentioned earlier in this chapter, evidence suggests that there is “stronger” lithium coordination in the branched system. The increased number of end amine groups in BPMEI provides more lithium coordination sites, which in turn inhibits the formation of aggregates. However, this effect seems to be coupled to a decrease in the relative concentration of free ions, which negatively impacts the conductivity of the resulting electrolyte.

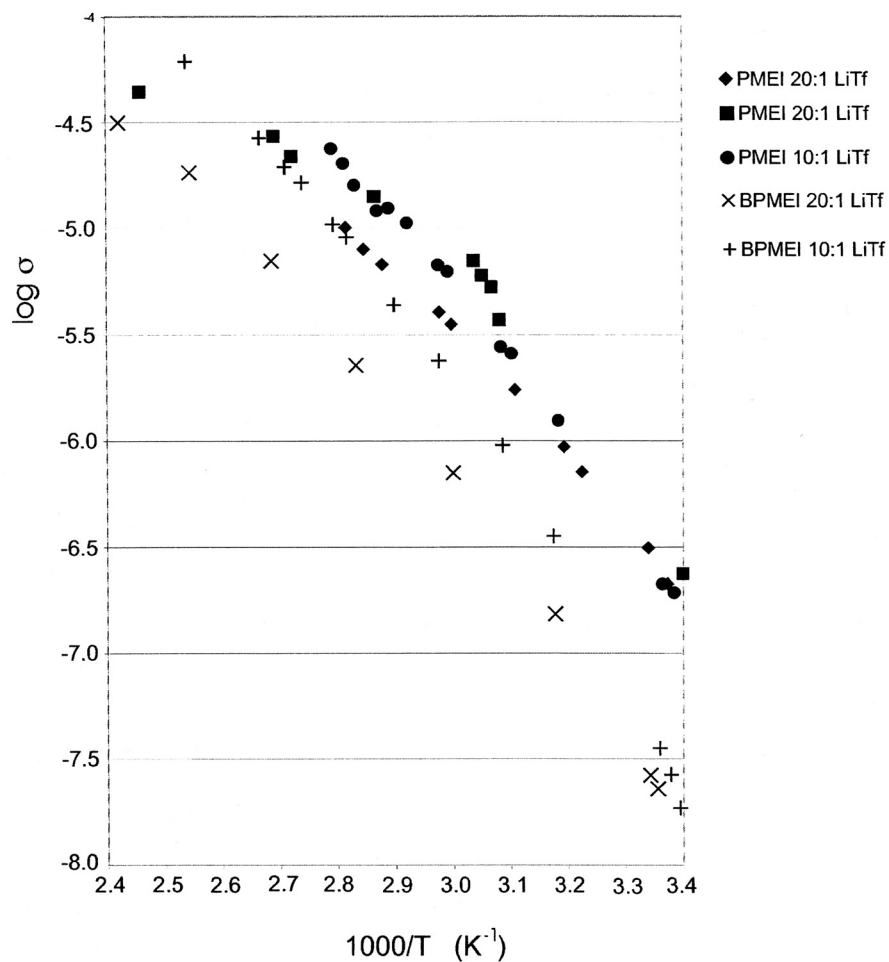
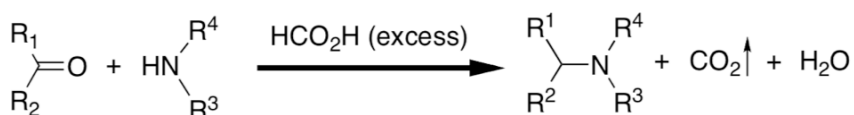


Figure 2.4. Temperature-dependent conductivity data of BPMEI-LiSO₃CF₃ and LPMEI-LiSO₃CF₃.^{12,16}

BPMEI-salt electrolytes exhibit an overall lower ionic conductivity than that of their linear analogs (see Fig. 2.4). BPMEI samples with a 10:1 N:Li molar ratio shows the highest conductivity values at all temperatures studied. The conductivity of the 20:1 sample was lower than that of the 10:1 composition, which is surprising given that both samples exhibit similar speciation (see table 3) and the 20:1 sample has a lower T_g .

2. Linear PEI-based electrolytes: Synthesis of linear poly(*N*-ethylethylenimine), LPEEI, and linear poly(*N*-butylethylenimine), LPBEI

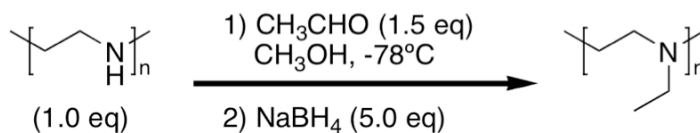
In addition to the methylation of LPEI and BPEI, Tanaka *et al.* also tried to attach longer alkyl chains onto the nitrogen atom on the backbone of poly(ethylenimine) with little success.¹⁰ Tanaka and co-workers attempted reductive alkylation of LPEI, via the Leuckart–Wallach reaction, using higher aldehydes such as propanal, butanal and pentanal.¹⁰ Illustrated in scheme 2.2 is the Leuckart-Wallach reaction. This reaction is a variation of the Clarke-Eschweiler reductive alkylation of amines in which other carbonyl species can be reacted with an amine to form an imine that is then reduced by formic acid.¹⁷



Scheme 2.2. Leuckart-Wallach reaction.¹⁷

Implementing a similar approach to that taken by Tanaka *et al.*, the reductive alkylation of LPEI was accomplished by using the two-step reaction shown in scheme 2.3. First, acetaldehyde was allowed to react with a methanol solution of the LPEI to form iminium ions that were then reduced using sodium borohydride, in excess, to obtain neutral linear poly(*N*-ethylethylenimine), LPEEI. The resulting

polymer can then be purified by filtration and extractions with non-polar solvents, such as methylene chloride or benzene.



Scheme 2.3. Synthesis of linear poly(*N*-ethylethylenimine), LPEEI.¹

LPEEI is a viscous, light yellow-brown material at room temperature. IR spectroscopy and ¹H-NMR were used to characterize the polymer. IR spectra showed complete disappearance of the N–H stretching bands of LPEI in the 3400-3100 cm⁻¹ region, indicating that complete substitution had occurred on the nitrogen atoms.¹

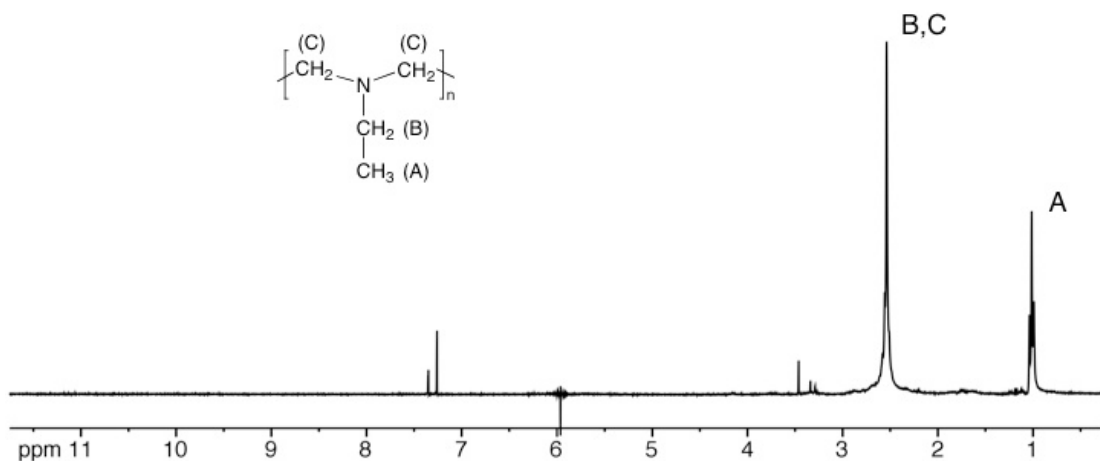
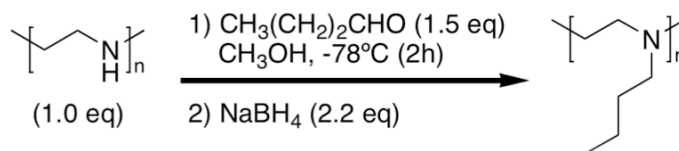


Figure 2.5. ¹H-NMR spectrum of linear poly(*N*-ethylethylenimine), LPEEI, in CDCl₃ (300.1 MHz ¹H).

Figure 2.5 illustrates the ¹H-NMR spectrum of LPEEI in chloroform-*d*. The

proton NMR shows overlapping peaks (*s* and *q*, 6H) at δ ca. 2.58, corresponding to the three methylene units around each nitrogen, and a triplet at δ 1.06 (3H) that has been assigned to the methyl group at the end of the ethyl substituent.

This synthetic method was also used successfully to synthesize linear poly(*N*-butylethylenimine), LPBEI, as shown in scheme 2.4. It was found that letting the reaction mixture reach room temperature after the initial two hours, and allowing it to stir for two additional hours increased the amount of alkyl substitution on nitrogen atoms. LPBEI was an amber-brown color, very viscous material.



Scheme 2.4. Synthesis of linear poly(*N*-butylethylenimine), LPBEI.

LPBEI was characterized by 1D and 2D NMR spectra in methanol- d_4 , and the ^1H -NMR spectrum of LPBEI is shown in Fig. 2.6. As can be observed, the singlet at δ 2.71 ppm, characteristic of the methylene protons in the backbone of LPEI, is affected by the reaction and several broad peaks appear at δ ca. 0.95 ppm (m, 3H), 1.35 -1.5 ppm (m, 2.5H) , 2.10 ppm (m, 1H), and 2.4 – 2.7 ppm (m, 6H).

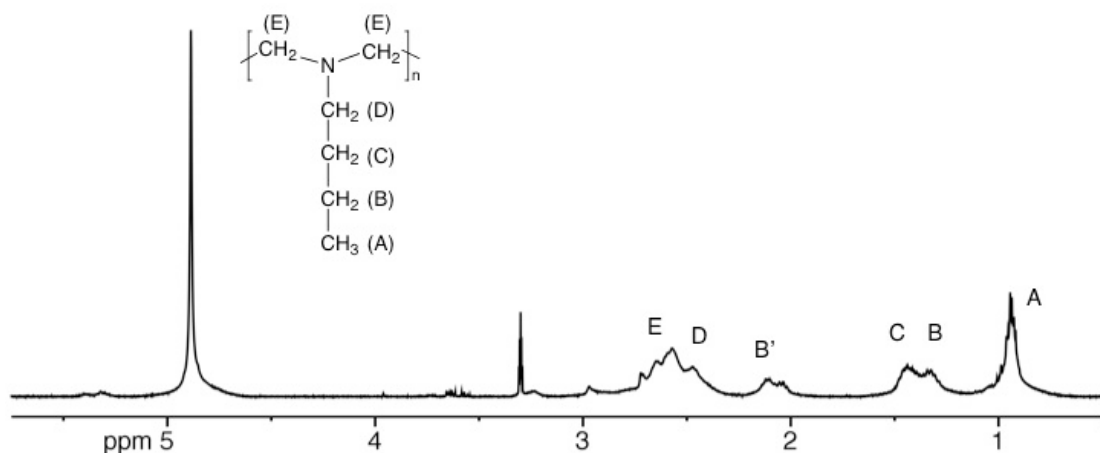


Figure 2.6. ^1H -NMR spectrum of linear poly(*N*-butylethylenimine), LPBEI, in CD_3OD (400.0 MHz ^1H).

^1H - ^1H correlation spectroscopy reveals that the peak at $\delta = 0.94$ ppm is coupled to a peak at $\delta = 1.35$ ppm; this is consistent with the coupling expected between the methyl group at the end of the side chain and the CH_2 group adjacent to it, labeled B in Fig. 2.6. The splitting pattern of the peak from the protons on the methyl group ($\delta = 0.94$ ppm) observed in Fig. 2.6 is not the expected triplet. It is possible that a slower relaxation time, often observed in polymer samples, might have caused the appearance of what seems to be multiple peaks around 0.94 ppm.

Coupling is also observed between the methyl signal and a peak at $\delta = 2.10$ ppm. This coupling is unexpected. Both protons on the B position could be considered diastereotopic and this could provide an explanation to the features shown in Fig. 2.7. The appearance of a couple of small cross peaks off the diagonal seems to support this hypothesis. Coupling between the peak with a

chemical shift of 1.35 ppm and the one at 1.46 ppm was also observed.

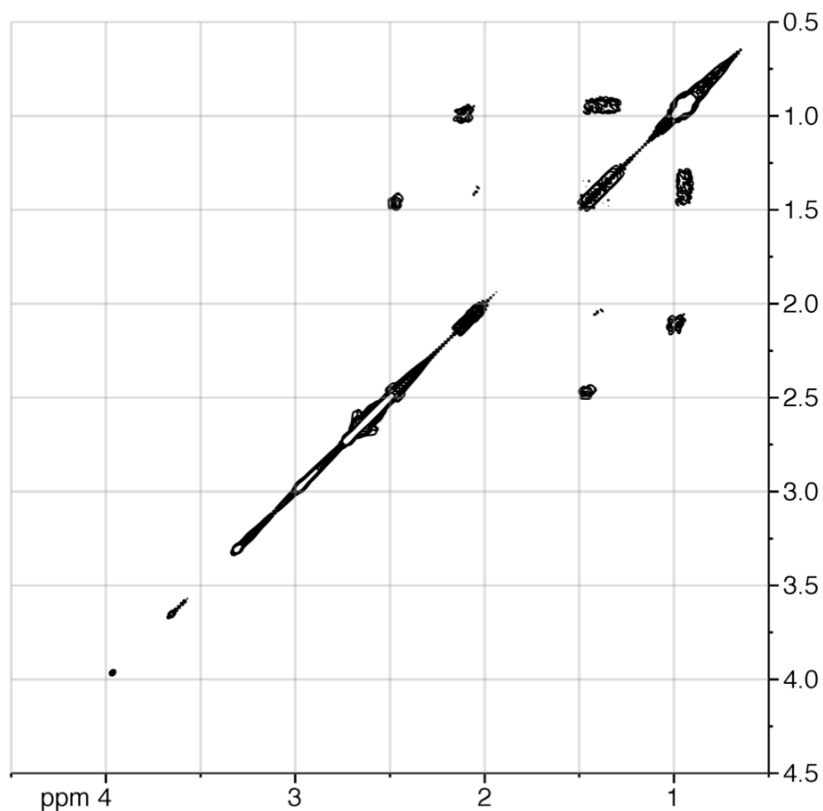


Figure 2.7. ^1H - ^1H COSY spectrum of LPBEI in CD_3OD (400.0 MHz ^1H).

Cross peaks also indicate the coupling of the peak at 1.46 ppm with that at 2.47 ppm. This is consistent with the coupling that would be observed between the proton signals of the methylene units α and β to the amine group (labeled D and C, respectively, in Fig. 2.6).

^1H NMR integration values reveal that almost a 100% substitution on the nitrogen was achieved. IR studies indicated that a small amount of unsubstituted amines was still present on the polymer, as was evident on the N-H stretch region of the infrared, around $3400 - 3100 \text{ cm}^{-1}$.

The synthesis of LPEEI provided an excellent opportunity to investigate the effect of the length of the substituent alkyl chain on important properties of several of their complexes with varying amounts of lithium triflate. This investigation was made in collaboration with Guinevere A. Giffin, a graduate student in Dr. Frech's research group. Ms. Giffin was responsible for sample preparation, as well as performing IR spectroscopy and differential scanning calorimetry (DSC) on samples for this study. Some of the results are summarized below.

A comparative spectroscopic study was made between linear poly(*N*-methylethylenimine), LPMEI, and LPEEI. Both polymers were synthesized from LPEI (avg. DP = ca. 2000);^{9,18} and LPMEI was prepared as previously reported in the literature.^{10,11} Differential scanning calorimetry was used to determine the glass transition temperature of polymer electrolytes of different LiSO₃CF₃ composition. Table 2.5 summarizes the values obtained for LPMEI and LPEEI – based electrolytes.

Table 2.5. Glass transition temperature (°C) of linear poly(*N*-methyl ethylenimine) (LPMEI), linear poly(*N*-ethylethylenimine) (LPEEI), and linear poly(*N*-butylethylenimine) (LPBEI), and LPMEI and LPEEI–based electrolytes.¹

Composition	LPMEI	LPEEI	LPBEI
Pure	-93	-80	-50
20:1	-79	-77	
10:1	-60	-41	
5:1	-14	-4	

As can be observed in table 2.5, increasing the length of the alkyl side chain attached to the nitrogen on the polymer backbone causes the glass transition to take place at higher temperatures. Addition of salt to the polymer hosts increases the T_g of the electrolyte, which is consistent with trends observed in previous studies.

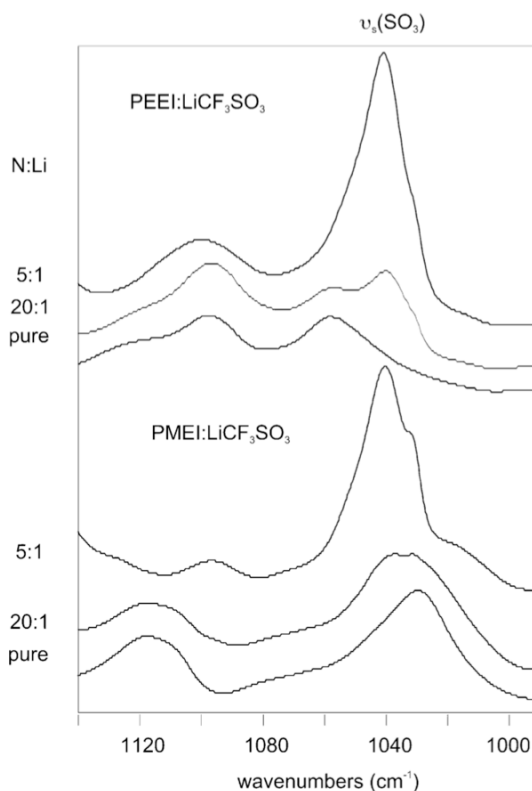


Figure 2.8. Infrared absorbance spectra from 1000 to 1140 cm⁻¹ of pure LPMEI and LPPEI and its complexes with different concentrations of LiSO₃CF₃.¹

Figures 2.8 and 2.9 show the infrared absorbance spectra of LPMEI and LPPEI – based electrolytes, with different salt compositions, from 1000 – 1140 cm⁻¹ and from 700 – 1000 cm⁻¹, respectively.

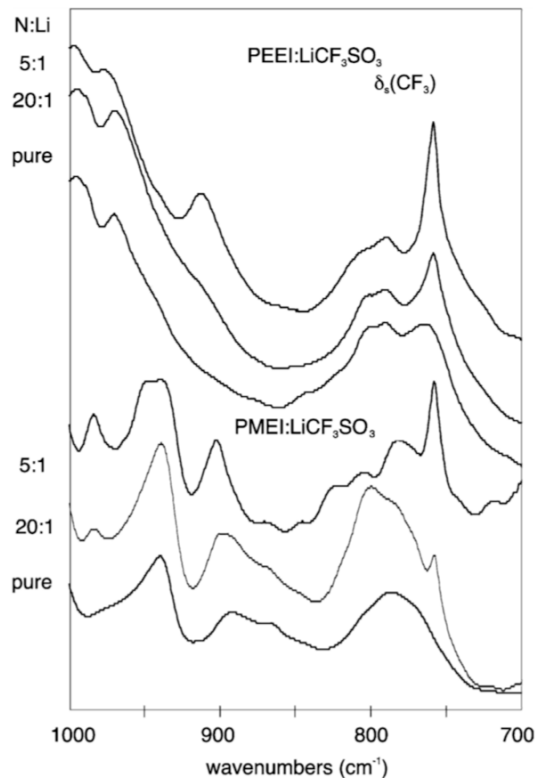


Figure 2.9. Infrared absorbance spectra from 700 to 1000 cm^{-1} of pure LPMEI and LPEEI and its complexes with different concentrations of LiSO_3CF_3 .¹

Vibrational spectroscopy studies performed on LPMEI has shown that IR spectra from the 1000 – 1140 cm^{-1} region (see Fig. 2.8) contains polymer modes that result from a complex mixture of CH_3 wagging, CH_2 twisting and rocking motions, as well as C–C and C–N stretching modes.^{11,19,20} As illustrated in figure 2.9, a band at 786 cm^{-1} splits into three components at 781, 804 and 822 cm^{-1} , while features in LPEEI at 764, 790 and 806 cm^{-1} remain relatively unshifted. This is consistent with previously reported work.¹¹ Compared to LPMEI, LPEEI presents fewer changes upon salt addition. Spectra in the $\nu_s(\text{SO}_3)$ and $\delta_s(\text{CF}_3)$ regions indicate that the speciation in these systems is mostly as contact ion

pairs.

LPMEI-LiSO₃CF₃ and LPEEI-LiSO₃CF₃ complexes showed an interesting hysteresis effect upon thermal cycling. Figure 2.10 shows the spectra of a 10:1 N:Li molar ratio complex of LPEEI and lithium triflate at room temperature after two heating and cooling cycles.

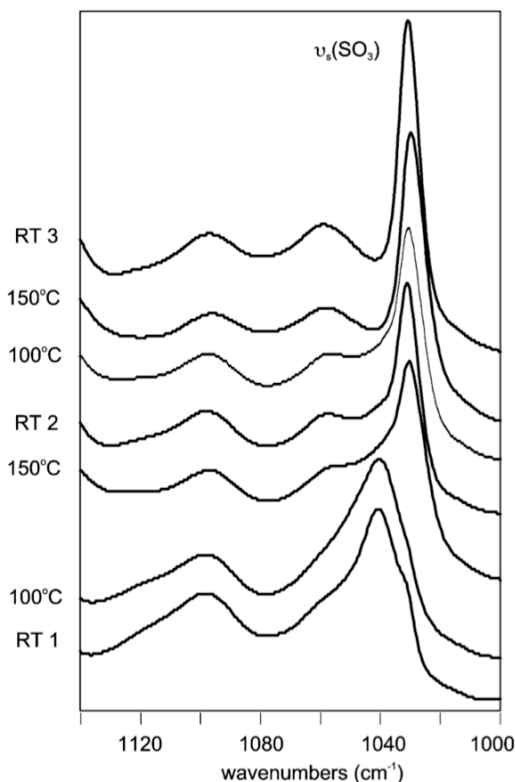


Figure 2.10. Temperature-dependent infrared absorbance spectra from 1000 to 1140 cm⁻¹ of a LPEEI-LiSO₃CF₃ complex (N:Li = 10:1). RT 1 is the initial spectrum at room temperature; RT 2 and RT 3 are the room temperature spectra after the first and second cycles of heating the sample up to 150°C and cooling, respectively.

Upon heating the samples up to 150°C, the contact ion pair band around 1040

cm^{-1} disappears while an intense free ion band appears at 1032 cm^{-1} . Surprisingly, the contact ion pair does not reappear upon cooling. Similar behavior was observed in a LPMEI- LiSO_3CF_3 complex of equal composition.¹ The observed shift in ionic association was unexpected. Previous studies on poly(propylene oxide)-based electrolyte systems indicate that salts dissolved into the polymer tend to aggregate and phase separate at higher temperatures. It is thought that metal cations lose their ability to coordinate to the oxygen atoms on the polyether chains as the thermal motion of these complexes increases.^{1,21,22} The opposite trend seems to take place in the *N*-alkylated polyamine systems studied in this chapter.

3. Conclusions

The glass transition temperature of branched poly(*N*-methylethylenimine) is more sensitive to salt concentration than that of LPMEI complexes of similar composition. This is consistent with the thermal property differences observed between BPEI and LPEI systems with both, sodium and lithium triflate. This observation, along with the differences in speciation determined through IR spectroscopy, suggests that the significant number of mobile short side-chains with terminal amine groups present in BPMEI have a great impact on the amount of lithium cations that the polymer can coordinate. The ability of the polymer host to coordinate Li^+ ions seems to have decreased the amount of aggregate formation, however, it also decreases the relative amount of “free” ions available

in the branched polymer complex.

LPMEI-LiSO₃CF₃ complexes exhibit higher conductivities than those of the branched system with comparable compositions. This may be caused by several factors. Samples with a 20:1 composition have very similar T_g values (-79°C and -81°C for LPMEI and BPMEI systems, respectively), which indicates that the difference in conductivity is most likely due in the difference in the relative concentrations of “free” ions. LPMEI samples presented a higher amount of “free” ions over the entire range of compositions studied than that of BPMEI samples. Samples with a 10:1 composition exhibit a comparable amount of “free” ions. However, there is a significant difference in the thermal properties of both polymers. The linear polymer complex has a T_g of -60°C while the branched PMEI complex has a much higher T_g (-18°C). Even though conductivity measurements were made at temperatures above the glass transition temperature for all complexes, it is still possible that the difference in T_g values would have an impact on the ion mobility and ultimately on the conductivity of the system.

A new method to successfully alkylate linear poly(ethylenimine) using aliphatic aldehydes has been proposed. It was possible to synthesize and isolate linear poly(*N*-ethylethylenimine) and poly(*N*-butylethylenimine). Differential scanning calorimetry reveals that when compared to LPMEI, increasing the length of the alkyl side chain on the backbone nitrogen increases the values of the glass transition temperatures. In general, increasing the length of the side chains in

polymers increases the free volume around the molecule, causing a decrease of the glass transition temperature. This was not the case in this study. Increasing the length of the alkyl group on the amine groups along the PEI backbone resulted in higher T_g s for the modified polymers. These observations were unexpected and could not be explained in the present study.

A spectroscopic study of LPEEI and LPMEI complexes with lithium triflate showed that the addition of a methylene unit to the alkyl group attached to the nitrogen on the polymer backbone rendered the polymer spectroscopic signatures largely insensitive to the addition of the lithium salt. Upon heating and cooling cycling, both systems showed a shift in the ion speciation from contact ion pairs to “free” triflate upon heating. This shift was found not to be reversible after cooling the sample back to room temperature.

References

- (1) Frech, R.; Giffin, G. A.; Yopez Castillo, F.; Glatzhofer, D. T.; Eisenblatter, J. *Electrochim. Acta* **2005**, *50*, 3963-3968.
- (2) Chintapalli, S.; Frech, R. *Electrochim. Acta* **1998**, *43*, 1395-1400.
- (3) Lightfoot, P.; Mehta, M. A.; Bruce, P. G. *Science* **1993**, *262*, 883-885.
- (4) Chiang, C. K.; Davis, G. T.; Harding, C. A.; Takahashi, T. *Macromolecules* **1985**, *18*, 825-827.
- (5) Harris, C. S.; Ratner, M. A.; Shriver, D. F. *Macromolecules* **1987**, *20*, 1778-1781.
- (6) Paul, J.-L.; Jegat, C.; Lassègues, J. C. *Electrochim. Acta* **1992**, *37*, 1623-1625.
- (7) Harris, C. S.; Shriver, D. F.; Ratner, M. A. *Macromolecules* **1986**, *19*, 987-989.

- (8) Tanaka, R.; Ueoka, I.; Takaki, Y.; Kataoka, K.; Saito, S. *Macromolecules* **1983**, *16*, 849-853.
- (9) Tanaka, R.; Fujita, T.; Nishibayashi, H.; Saito, S. *Solid State Ionics* **1993**, *60*, 119-123.
- (10) Tanaka, R.; Koike, M.; Tsutsui, T.; Tanaka, T. *J. Polym. Sci. Polym. Lett.* **1978**, *16*, 13-16.
- (11) Sanders, R. A.; Snow, A. G.; Frech, R.; Glatzhofer, D. T. *Electrochim. Acta* **2003**, *48*, 2247-2253.
- (12) Rocher, N. M. Ph.D. Dissertation, University of Oklahoma, 2006.
- (13) Huang, W.; Frech, R.; Wheeler, R. A. *J. Phys. Chem.* **1994**, *98*, 100-110.
- (14) Petersen, G.; Jacobsson, P.; Torell, L. M. *Electrochim. Acta* **1992**, *37*, 1495-1497.
- (15) Seneviratne, V.; Frech, R.; Furneaux, J. E. *Electrochim. Acta* **2003**, *48*, 2221-2226.
- (16) Rocher, N. M.; Yopez Castillo, F.; Frech, R.; Glatzhofer, D. T. *to be submitted for publication*.
- (17) Li, J. J. *Name Reactions: A collection of detailed reaction mechanisms*; 2nd ed.; Springer-Verlag: New York, 2003.
- (18) York, S.; Frech, R.; Snow, A.; Glatzhofer, D. *Electrochim. Acta* **2001**, *46*, 1533-1537.
- (19) Sanders, R. A.; Frech, R.; Khan, M. A. *J. Phys. Chem. B* **2003**, *107*, 8310-8315.
- (20) Sanders, R. A.; Frech, R.; Khan, M. A. *J. Phys. Chem. B* **2004**, *108*, 12729-12735.
- (21) Greenbaum, S. G.; Pak, Y. S.; Wintersgill, M. C.; Fontanella, J. J. *Solid State Ionics* **1988**, *31*, 241-245.
- (22) Teeters, D.; Frech, R. *Solid State Ionics* **1986**, *18-19*, 271-276.

Chapter 3: Crosslinked LPEI·HCl-based membranes for hydrogen fuel cell applications: Structural characterization.

Portions of this chapter have been taken from Giffin, G. A.; Yopez Castillo, F.; Frech, R.; Glatzhofer, D. T.; Burba, C. M. *Polymer* **2009**, *50*, 171-176.

Portions of the research presented in this chapter have been published previously.^{1,2} The research presented in this chapter was performed in close collaboration with Ms. Guinevere A. Giffin in Dr. Roger Frech's research group at the University of Oklahoma.

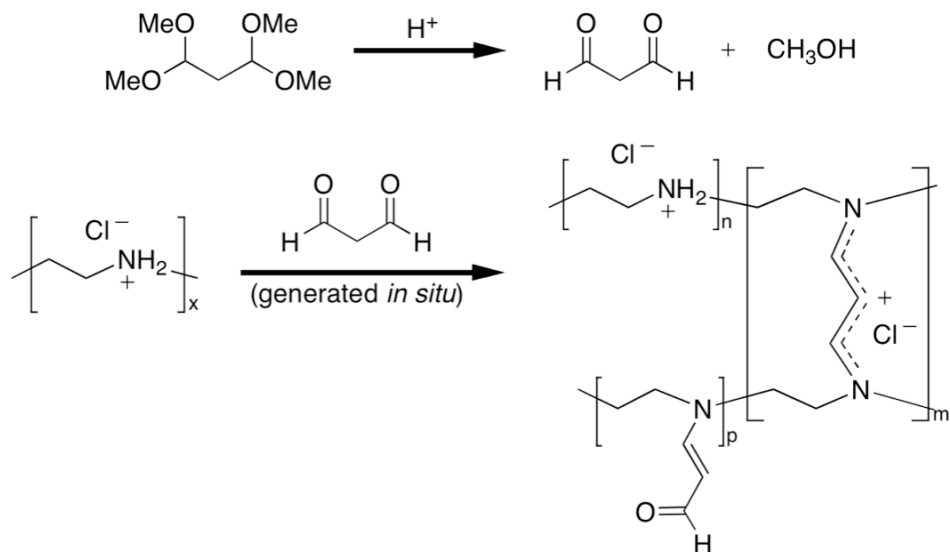
Ms. Guinevere A. Giffin was responsible for the collection of vibrational spectra as well as its analysis, while I was responsible for the collection of solution ¹H NMR and impedance spectroscopy presented in this chapter, as well as interpretation of the solution and solid-state ¹H NMR data. Interpretation of the conductivity data was done in a collaborative fashion by Ms. Giffin and myself. HR-MAS Solid State ¹H NMR data was collected by Dr. Christopher M. Burba, in Dr. Charles Rice's laboratory at the University of Oklahoma.

1. Introduction

Poly(ethylenimine) has great potential as proton conductor material due to its chemical structure. The abundance of amine groups along the polymer backbone provides sites for proton coordination that are necessary for conduction to occur. With this in mind, acid-doped poly(ethylenimine) has been studied by several groups around the world, including Dr. Glatzhofer's and Dr. Frech's at the

University of Oklahoma, as potential proton-conducting membrane alternative for hydrogen fuel cells.²⁻⁷ Currently, membrane development has focused on poly(perfluorosulfonic acids),^{8,9} sulfonated poly(arenes),¹⁰⁻¹⁵ and acid-doped polymer complexes.¹⁶⁻²¹

Glatzhofer *et al.* proposed a crosslinked linear poly(ethylenimine) hydrochloride/phosphoric acid doped system, using 1,1,3,3-tetramethoxypropane as the crosslinker (Scheme 3.1).² This system presents good conductivity, mechanical integrity and thermal stability up to 150°C,² and while crosslinking has a significant effect on the physical properties of the resulting material, a thorough study to determine the nature and degree of crosslinking was not reported in the literature. Thus, ¹H NMR, IR, Raman and impedance spectroscopic studies on these systems are presented in this chapter.



Scheme 3.1. Crosslinking reaction of LPEI, using malonaldehyde as crosslinker.

2. Structural characterization and determination of degree of crosslinking.

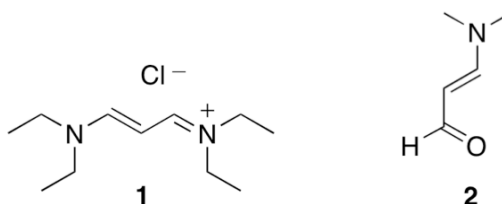
Due to the complexity of proton-exchange membrane systems based on crosslinked poly(ethylenimine) hydrochloride/phosphoric acid, it was necessary to simplify our approach to the analysis of this system. This was accomplished by taking two steps: (1) the crosslinked network was examined without phosphoric acid and (2) small molecules were used to model portions of the polymer network, which allowed the identification of various spectroscopic signatures of the polymer network.

Glatzhofer and coworkers previously described the general process by which crosslinking occurs in this system.² In the presence of a catalytic amount of acid, 1,1,3,3-tetramethoxypropane can be used to generate malonaldehyde *in situ*, which can then react with amine sites to form β -aminoacrolein moieties.²² The β -aminoacrolein moieties can further react with amine sites to form β -aminoethenyliminium salts.²³ Thus there are three possible species that may be found in the crosslinked membranes as illustrated in Scheme 3.1. There may be some remaining protonated amine sites, designated by n , in addition to the new β -aminoethenyliminium crosslinked moieties, designated by m . At high crosslinker concentrations non-reacted β -aminoacrolein branching units may remain, designated by p , due to the inaccessibility of the remaining amine sites.

2.1. ^1H NMR spectroscopy and degree of crosslinking

^1H NMR spectra of β -aminoethenyliminium salts have been reported in the

literature previously, making it possible to assign the chemical shifts observed for this polymer system. The ^1H -NMR spectrum of *N,N,N',N'*-tetraethyl-1,5-diazapentadienium chloride (**1**, TEDCI) in CD_3OD shows resonances at δ 1.27 (6H, t), 1.32 (6H, t), 3.56 (8H, q), 5.51 (1H, t), and 7.72 (2H, d).²⁴



A ^1H NMR spectrum of non-crosslinked LPEI·HCl in D_2O and HR-MAS ^1H NMR spectra of several crosslinked films are presented in Fig. 3.1. Similar spectra were obtained using solution-state NMR techniques for gelled samples.

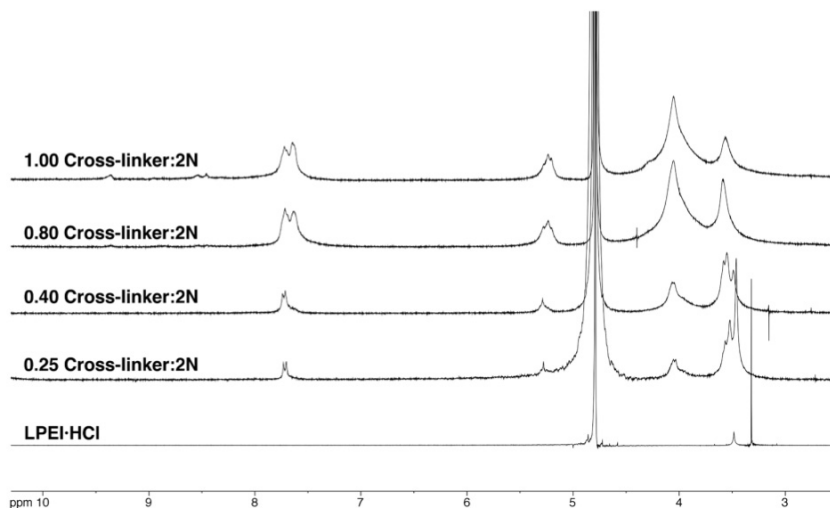


Figure 3.1. HR-MAS Solid State ^1H NMR spectra of crosslinked poly(ethylenimine) hydrochloride ($x\text{LPEI}\cdot\text{HCl}$) in water and solution ^1H NMR of linear poly(ethylenimine) hydrochloride in water- d_2 . The notation $x\text{linker}:2\text{N}$ designates the number of crosslinker molecules added to the solution for every two PEI·HCl nitrogen atoms.¹

As shown in Fig. 3.1, the sharp singlet at 3.32 ppm that is characteristic of the methylene protons in the backbone of LPEI·HCl is affected by the crosslinking reaction. The resonance shifts downfield as the number of neighboring iminium crosslink moieties increases and appears as a collection of overlapping peaks of decreasing relative intensity.

Other changes in the spectra include the appearance of a new, broad backbone hydrogen peak at 4.02 ppm, which corresponds to the ethyl methylenes in TEDCl at 3.56 ppm, shifted further downfield by neighboring ammonium or iminium moieties. As expected, the intensity of this peak increases when the amount of crosslinker added in the reaction is increased. A resonance at 5.23 ppm, corresponding to the β -methine hydrogen of TEDCl, appears when the polymer has been crosslinked. This peak appears to be a broad singlet at lower crosslinker concentrations but at higher concentrations a broad triplet becomes apparent. A doublet also appears around 7.65 ppm, corresponding to the α -methine hydrogens of TEDCl, which increases in intensity as crosslinking increases. At high crosslinker concentrations other features are visible, a broad peak above 9 ppm is consistent with the presence of β -acrolein branching moieties.

It has been reported that the aldehyde proton in 3-(*N,N*-dimethylamino)acrolein (**2**) has a resonance at 9.06 ppm, while the hydrogens at the 2 and 3 positions appear at 5.04 ppm and 7.41 ppm.²⁵ The presence of these branches increases the integrated area of the peaks in the region

corresponding to the hydrogen atoms from the crosslinking substituents (δ , 7.05-7.8). Fortunately, this can be corrected by subtracting branching unit hydrogen atoms from the integrated values as indicated by the number of aldehyde end groups.

Other peaks around 8.37-8.62 ppm are also consistent with the formation of the *O*-protonated 3-(*N,N*-dialkylamino)acrolein branch, but this moiety does not have hydrogens with resonances in the region of interest in the spectra analyzed.²⁵

Due to changes in chemical shift and broadening of signals as crosslinking took place, care was taken to integrate peaks for the PEI backbone protons at ca. 3.2 – 4.5 ppm (Fig. 3.1), for the crosslink protons at ca. 7.7 ppm, and the branch aldehyde protons at ca. 9.4 ppm over 1.100, 0.750, and 0.065 ppm ranges, respectively. A baseline correction was applied to each integration.

The integrated ¹H NMR spectra described above allow estimation of the degree of crosslinking for different samples from the ratio of backbone hydrogen atoms to hydrogen atoms from the crosslinking moieties. The degree of crosslinking is defined here as the percentage of nitrogen sites that effectively participate in the crosslinking of the polymer. A ratio of eight backbone hydrogens to three crosslink hydrogens would indicate a 100% degree of crosslinking. Thus, the degree of crosslinking within a particular sample may be estimated by comparing the measured ratio to this theoretical maximum. However, it was noted that the peak for the β -methine proton at 5.23 ppm in D₂O decreased in

intensity relative to the other peaks over time, indicating exchange. The integration for this peak was consequently considered unreliable. Therefore a ratio of eight backbone hydrogens to the two α -methine crosslink hydrogens was taken to indicate 100% degree of crosslinking and the degree of crosslinking was estimated by comparing the measured ratio to the theoretical maximum.

A plot of the estimated degree of crosslinking as determined from these NMR values versus the nominal values for the number of moles of crosslinker per two moles of PEI·HCl nitrogen atoms is shown in Fig. 3.2.

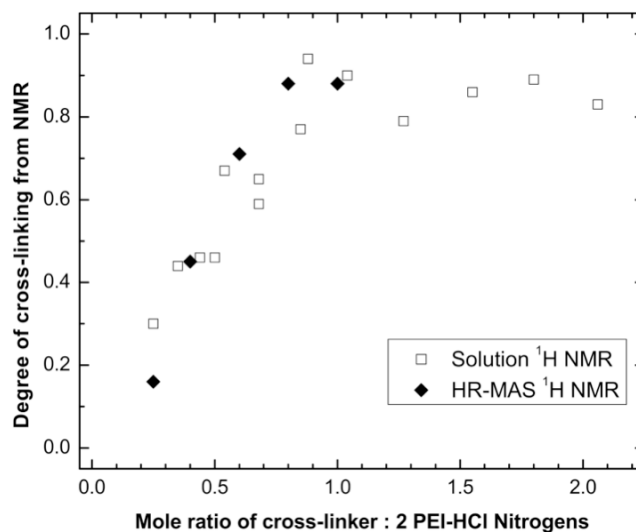


Figure 3.2. Calibration curve for degree of crosslinking determined from NMR data: (□) Solution ¹H NMR, (◆) HR-MAS ¹H NMR.¹

At most crosslinker concentrations, the degree of crosslinking increases roughly linearly as the number of moles of crosslinker is increased. However, at high crosslinker molar ratios, the degree of crosslinking plateaus at ca. 0.85 – 0.90 and even decreases slightly as fresh malonaldehyde molecules compete

with acrolein units to react with the remaining nitrogen atoms on the backbone.

Higher crosslinker concentrations promote substantial branching. Data points from the solution NMR experiments are also shown in Fig. 3.2 and agree well with the HR-MAS NMR results. Therefore, the plot shown in Fig. 3.2 can be used as a calibration curve to estimate the degree of crosslinking for samples simply from the nominal amount of crosslinker used in sample preparation.

2.2. Ionic Conductivity

The conductivity of crosslinked PEI·HCl was investigated as a function of the degree of crosslinking within the polymer films as determined by NMR spectroscopy. The logarithm of the conductivity as a function of the degree of crosslinking is shown in Fig. 3.3.

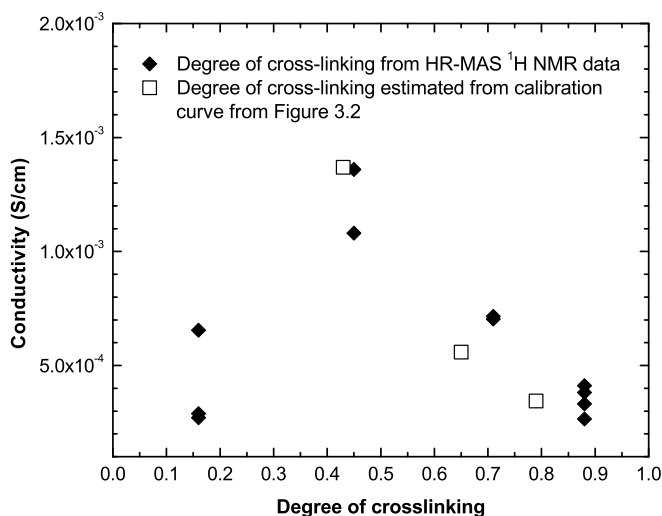


Figure 3.3. Log of conductivity as a function of degree of crosslinking. Degree of crosslinking as determined by: (◆) HR-MAS ¹H NMR, (□) estimation from the average calibration curve in Fig. 3.2.¹

The conductivity is highest, approximately 1×10^{-3} S/cm, at intermediate degrees of crosslinking (ca. 0.45) and decreases at both smaller and larger degrees of crosslinking. Similar conductivity behavior has been seen in both non-crosslinked linear and branched PEI·H₃PO₄ systems at low acid concentrations (< 0.4 mole ratio).⁴⁻⁷

Lassègues and co-workers studied branched poly(ethylenimine) complexes with sulfuric and phosphoric acids of the form BPEI·xH₂SO₄ and BPEI·xH₃PO₄, where x is the number of acid moles per BPEI repeat unit.^{4,5} Conductivity was measured for these systems at different concentrations and temperatures. Figs. 3.4a-b illustrate the conductivity ($\log \sigma$) dependence on the acid concentration at 300 K and at 373 K.⁴

It was found that the conductivity of the mixtures increases with increasing acid concentration. However, as can be observed in Figs. 3.4a and 3.4b, the conductivity reaches maxima at $x = 0.2$ after which the conductivity, at both temperatures, decreases until the acid concentration is increased to $x = 0.35$. Higher concentrations of acid increase the conductivity of the system.⁴ Similar behavior was reported by Tanaka and co-workers for both linear and branched PEI·xH₃PO₄ systems.⁷

It is thought that this behavior is associated with a change in the type of proton conduction above and below the maximum amount of protonation of PEI.^{4,5,7} Tanaka *et al.* postulated that in the $0 < x < 0.4$ region, proton hopping between neighboring ammonium and amino groups is the most important process

contributing to the conductivity.

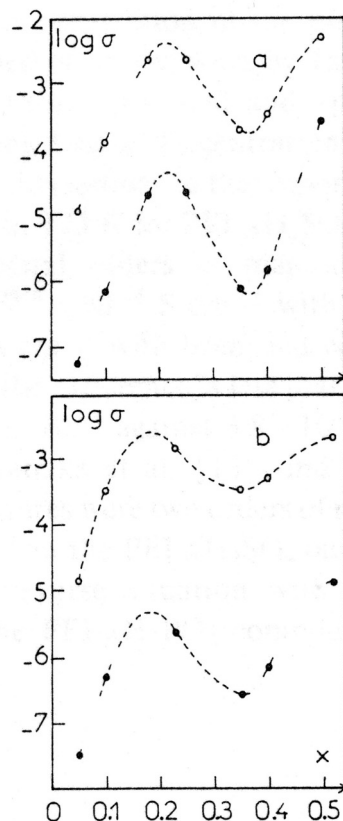


Figure 3.4. Concentration dependence of $\log \sigma$ (S/cm) for (a) BPEI· x H₂SO₄ and (b) BPEI· x H₃PO₄ at 300 K (●) and 373 K (○).⁴

However, once $x \approx 0.4$ is reached, nearly all the amino groups accessible in the polymer network are depleted, forcing the conductivity to reach a minimum. When the amount of acid is further increased, the phosphoric acid becomes the proton source, making the protonated PEI a mere framework in which the protons travel *via* HO(PO₂⁻)-O-H···O(PO₂⁻)-OH hydrogen-bond arrays.⁷

In the case of crosslinked PEI·HCl there are several factors that may influence the conductivity behavior as well. The initial increase in conductivity may be the

result of reduced crystallinity upon crosslinking and changes in the pK_a of the ammonium groups (n , in Scheme 3.1) neighboring the positively charged crosslinking moieties (m , in Scheme 3.1). Eventually, stiffening of the lattice and a decreasing number of labile ion sites lead to a decrease in the conductivity at high degrees of crosslinking. At high degrees of crosslinking, the presence of the branching units (m , in Scheme 3.1) may also have an undetermined effect.

It should also be noted that the conductivity measurements were made at 75% relative humidity. The absorbed water at equilibrium, which undoubtedly changes as a function of crosslinking, certainly plays a significant role in the conduction mechanism.

2.3. Vibrational Spectroscopy

IR and Raman spectroscopy were used to investigate the crosslinked network. The presence of the crosslinker unit can be identified through a series of bands between 1570 and 1640 cm^{-1} .

In the Raman spectra shown in Fig. 3.5, two bands at 1572 and 1638 cm^{-1} can be seen at lower crosslinker concentrations, with a third band appearing at 1602 cm^{-1} at higher concentrations. The 1602 cm^{-1} band is attributed to the presence of acrolein branching units that are only found at the higher crosslinker concentrations. This conclusion is supported by comparing the Raman spectrum of a highly crosslinked membrane with DMAA – a small molecule model compound for the branching units.

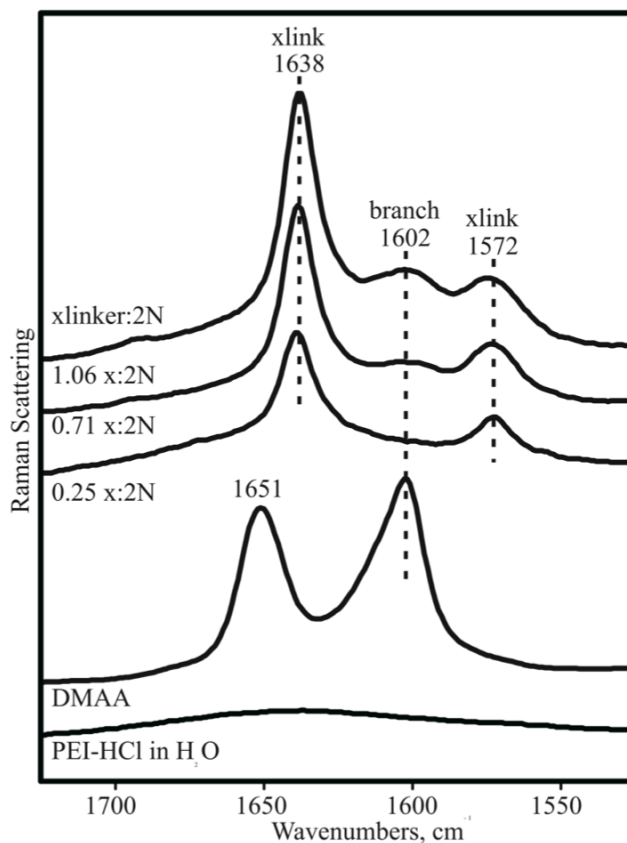


Figure 3.5. Raman spectra of crosslinker stretching region. Crosslinked poly(ethylenimine)-hydrochloride, 3-(diethylamino)-acrolein (DMAA) and linear poly(ethylenimine)-hydrochloride (LPEI·HCl) in water. The notation xlinker: 2N designates the number of crosslinker molecules added to the solution for every two PEI·HCl nitrogen atoms.¹

The model compound has two bands at 1651 and 1602 cm⁻¹. The bands at 1602 cm⁻¹ in both the DMAA model compound and the crosslinked membrane are assigned to the CO stretch from the aldehyde group. The 1638 and 1572 cm⁻¹ bands in the crosslinked membrane are primarily the result of the CC stretching motions from the crosslinker.²⁶

Fig. 3.6 shows the IR spectra of this region; the bands in the IR spectra are more complex than in the Raman spectra. Three bands at 1638, 1608, and 1572 cm^{-1} are seen at all crosslinker concentrations. The 1608 cm^{-1} band is significantly broadened as the crosslinker concentration increases; this broadening is accompanied by a slight frequency shift from 1608 to 1610 cm^{-1} .

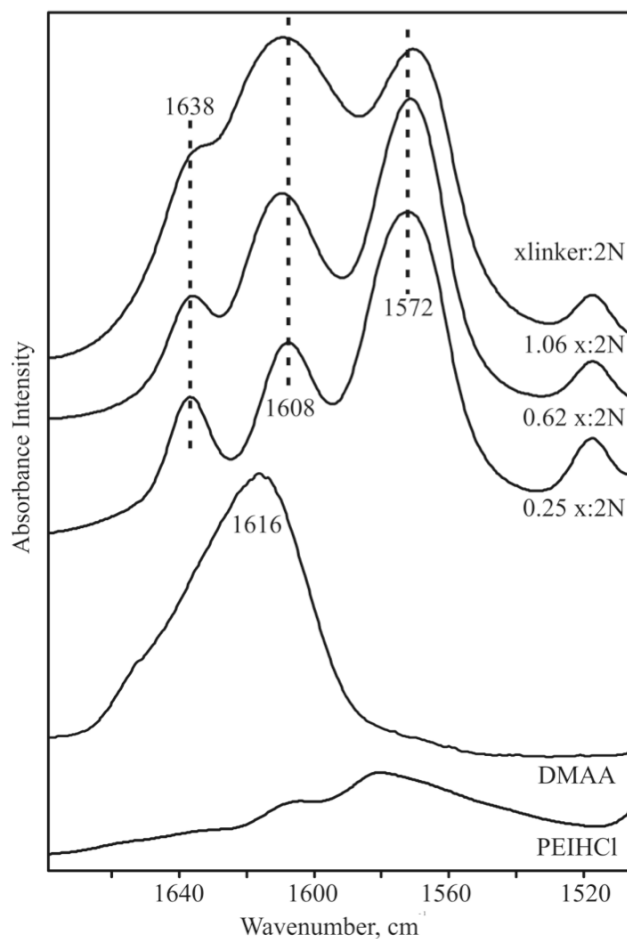


Figure 3.6. Infrared spectra of crosslinker stretching region. Crosslinked poly(ethylenimine)-hydrochloride, 3-(diethylamino)-acrolein (DMAA) and linear poly(ethylenimine)-hydrochloride (LPEI·HCl). The notation xlinker: 2N designates the number of crosslinker molecules added to the solution for every two PEI·HCl nitrogen atoms.¹

The IR spectrum of the model compound consists of one broad asymmetric band located at 1616 cm^{-1} that contains coupled CO stretching modes.²⁷ The mixing of these modes would lead to the broadening and slight frequency shift seen in the membrane at high crosslinker concentrations.

The stretching bands directly associated with the crosslink unit can be clearly identified in the region between 1570 and 1640 cm^{-1} . However, the lower frequency regions are more complicated because they contain bands that are associated with both the polymer backbone and the crosslink unit.

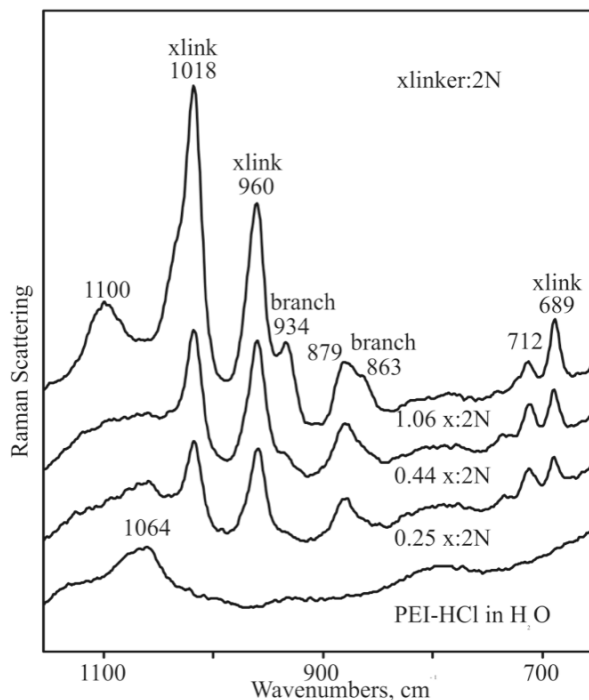


Figure 3.7. Raman spectra of lower frequency region. Crosslinked poly(ethylenimine)-hydrochloride and linear poly(ethylenimine)-hydrochloride (LPEI·HCl) in water. The notation xlinker: 2N designates the number of crosslinker molecules added to the solution for every two PEI·HCl nitrogen atoms.¹

Fig. 3.7 shows the Raman spectra between approximately 1100 and 600 cm^{-1} . Bands in this region contain mixed modes that are sensitive to the conformation of the polymer backbone.^{28,29}

There are three bands at 1018, 960 and 689 cm^{-1} that appear even at low crosslinker concentrations. These bands are probably associated with the crosslink unit itself. Most likely, the vibrational modes resulting in these bands are a mixture of CCC bending and CH in-plane bending motions.³⁰ In contrast, the band at 1064 cm^{-1} in the PEI-HCl spectrum shifts to 1100 cm^{-1} as the crosslinker concentration increases. The bands at 863 and 934 cm^{-1} appear only at high crosslinker concentrations and therefore may be attributed to the acrolein branching units.

Similar trends can be seen in the IR spectra of Fig. 3.8, which covers essentially the same range. Bands at 1010, 620 and 564 cm^{-1} are most likely associated directly with the crosslink unit, whereas the bands at 1064 and 1010 cm^{-1} are attributed to the polymer backbone. Bands in this range of the spectrum contain CN and CC stretching motions.

As the crosslinking reaction occurs, the nitrogen atoms of the polymer backbone become covalently bonded to the crosslinker molecule. This will necessarily result in a redistribution of electron density around the nitrogen and adjacent carbon atoms on the polymer backbone, changing both the effective force constants of the backbone CN and CC bonds as well as dipole moment and polarizability derivatives for these modes. Those changes will appear as

frequency shifts and intensity changes in the corresponding IR and Raman bands. Therefore, as the amount of crosslinker increases, the intensity of the 1062 cm^{-1} band decreases and the related band at 1010 cm^{-1} increases.

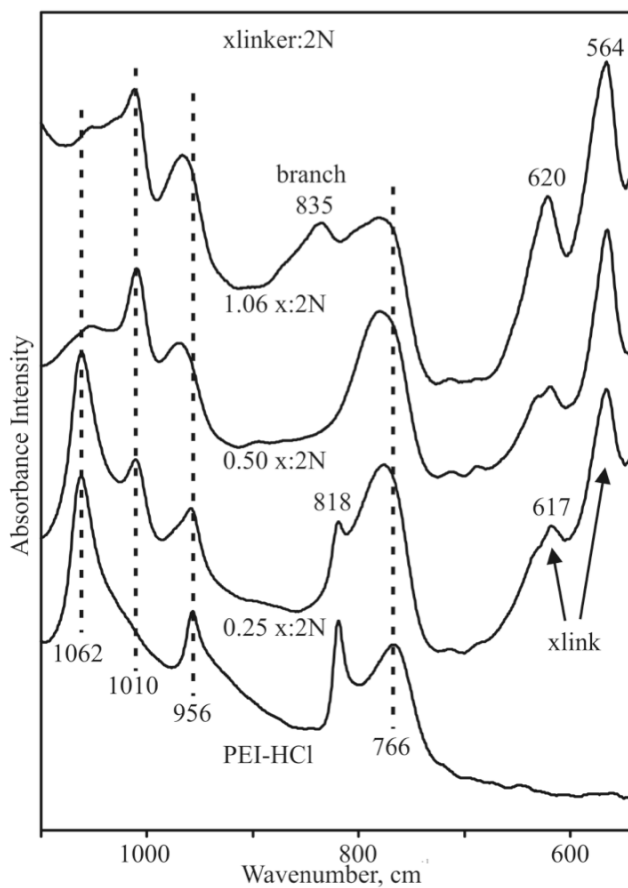


Figure 3.8. Infrared spectra of lower frequency region. Crosslinked poly(ethylenimine)-hydrochloride, and linear poly(ethylenimine)-hydrochloride (LPEI·HCl). The notation xlinker: 2N designates the number of crosslinker molecules added to the solution for every two PEI·HCl nitrogen atoms.¹

The band at 835 cm^{-1} may be attributed to the acrolein branching units, consistent with the assignment of the 863 cm^{-1} band in the Raman spectrum.

Finally, it is interesting to note that spectrum labeled 0.25:2N (crosslinker:2N) resembles a superposition of pure PEI·HCl and the 0.50:2N spectra. This would indicate that membranes with mole ratios less than 0.25:2N contain domains of pure PEI·HCl in addition to the crosslinked moieties.

3. Conclusions

Membranes made of crosslinked LPEI·HCl have been investigated as a function of the degree of crosslinking with a number of different spectroscopic techniques and measurements of the conductivity. The degree of crosslinking was determined using NMR spectroscopy. The maximum degree of crosslinking attained is approximately 85%. Above this crosslinking level, some of the remaining sites react with one end of a malonaldehyde molecule. However, there are no available amine sites sufficiently close to allow the malonaldehyde to react with a second nitrogen atom. This results in an acrolein branching unit whose presence is inferred from spectroscopic data.

Vibrational modes associated with the crosslink unit can be identified in both the IR and Raman spectra from bands that are present even at low crosslinker concentrations, but are not present in the pure polymer. In comparison, bands that are present in pure PEI·HCl but exhibit shifts in frequency and intensity as the amount of crosslinker increases are attributed to the polymer backbone. These shifts are associated with a redistribution of electron density along the backbone due to the reaction of the crosslinker molecule with the polymer. The

bands associated with the acrolein branching units can be distinguished from those associated with both the crosslinker and the polymer backbone as they are present only at high crosslinker concentrations.

The conductivity of crosslinked PEI-HCl was highest, $\sim 1 \times 10^{-3}$ S/cm, at intermediate degrees of crosslinking and may be attributed to the movement of protons and/or chloride ions. The shape of the ionic conductivity curve observed in this study resembles curves characteristic of almost all polymer-salt electrolyte systems. In those systems, the ionic conductivity decreases at high salt concentrations because of a reduction in the segmental motion and the number of available coordination sites of the polymer. This decrease in segmental motion is usually considered to result from an increase in the coordination of ions between sites on the polymer chains, where the ions act as transitory crosslinks.³¹

In this case, the peak in the conductivity data may reflect a balance between the stiffening of the polymer network and the number of labile ion sites available but having water present during the measurements at 75% relative humidity complicates these interpretations.

References

- (1) Giffin, G. A.; Yepez Castillo, F.; Frech, R.; Glatzhofer, D. T.; Burba, C. M. *Polymer* **2009**, *50*, 171-176.
- (2) Glatzhofer, D. T.; Erickson, M. J.; Frech, R.; Yepez, F.; Furneaux, J. E. *Solid State Ionics* **2005**, *176*, 2861-2865.
- (3) Dabrowski, J.; Kamieńska-Trela, K. *Org. Magn. Reson.* **1972**, *4*, 421-425.

- (4) Daniel, M. F.; Desbat, B.; Cruege, F.; Trinquet, O.; Lassègues, J. C. *Solid State Ionics* **1988**, 28-30, 637-641.
- (5) Schoolmann, D.; Trinquet, O.; Lassegues, J. C. *Electrochim. Acta* **1992**, 37, 1619-1621.
- (6) Tanaka, R.; Yamamoto, H.; Shono, A.; Kubo, K.; Sakurai, M. *Electrochim. Acta* **2000**, 45, 1385-1389.
- (7) Tanaka, R.; Yamamoto, H.; Kawamura, S.; Iwase, T. *Electrochim. Acta* **1995**, 40, 2421-2424.
- (8) Basnayake, R.; Peterson, G. R.; Casadonte, D. J.; Korzeniewski, C. J. *Phys. Chem. B* **2006**, 110, 23938-23943.
- (9) Mehta, V.; Cooper, J. S. *J. Power Sources* **2003**, 114, 32-53.
- (10) Carretta, N.; Tricoli, V.; Picchioni, F. *J. Membr. Sci.* **2000**, 166, 189-197.
- (11) Cho, C. G.; Kim, Y. S.; Yu, X.; Hill, M.; McGrath, J. E. *J. Polym. Sci., Part A: Polym. Chem.* **2006**, 44, 6007-6014.
- (12) Hofmann, M. A.; Ambler, C. M.; Maher, A. E.; Chalkova, E.; Zhou, X. Y.; Lvov, S. N.; Allcock, H. R. *Macromolecules* **2002**, 35, 6490-6493.
- (13) Lee, H.-S.; Badami, A. S.; Roy, A.; McGrath, J. E. *J. Polym. Sci., Part A: Polym. Chem.* **2007**, 45, 4879-4890.
- (14) Sankir, M.; Kim, Y. S.; Pivovarov, B. S.; McGrath, J. E. *J. Membr. Sci.* **2007**, 299, 8-18.
- (15) Yang, Y.; Holdcroft, S. *Fuel Cells* **2005**, 5, 171-186.
- (16) Asensio, J. A.; Borrós, S.; Gómez-Romero, P. *J. Electrochem. Soc.* **2004**, 151, A304-A310.
- (17) Bouchet, R.; Siebert, E. *Solid State Ionics* **1999**, 118, 287-299.
- (18) Kim, H.-J.; Lim, T.-H. *J. Ind. Eng. Chem. (Seoul, Korea)* **2004**, 10, 1081-1085.
- (19) Lobato, J.; Canizares, P.; Rodrigo, M. A.; Linares, J. J.; Aguilar, J. A. *J. Membr. Sci.* **2007**, 306, 47-55.
- (20) Lobato, J.; Canizares, P.; Rodrigo, M. A.; Linares, J. J.; Manjavacas, G. J. *J. Membr. Sci.* **2006**, 280, 351-362.

- (21) Xiao, L.; Zhang, H.; Jana, T.; Scanlon, E.; Chen, R.; Choe, E. W.; Ramanathan, L. S.; Yu, S.; Benicewicz, B. C. *Fuel Cells* **2005**, *5*, 287-295.
- (22) Noguchi, M.; Yamada, H.; Takamura, S.; Uchida, T.; Hironaka, M.; Kekehi, A.; Yamamoto, H. *Eur. J. Org. Chem.* **2000**, 1489-1496.
- (23) Nair, V.; Cooper, C. S. *J. Org. Chem.* **1981**, *46*, 4759-4765.
- (24) Wypych, J.-C.; Nguyen, T. M.; Bénéchie, M.; Marazano, C. *J. Org. Chem.* **2008**, *73*, 1169-1172.
- (25) Bürgi, D.; Sterchi, A.; Neuenschwander, M. *Helv. Chim. Acta* **1977**, *60*, 2195-2207.
- (26) Socrates, G. *Infrared characteristic groups frequencies*; John Wiley & Sons: New York, 1980.
- (27) Dabrowski, J.; Kamienzka-Trela, K. *Roczniki Chemii N. Soc. Chim. Polonorum* **1966**, *40*, 831-834.
- (28) Boesch, S. E.; York, S. S.; Frech, R.; Wheeler, R. A. *PhysChemComm* **2001**, *4*, 10.
- (29) Matsuura, H.; Fukuhara, K. *J. Polym. Sci., Part B: Polym. Phys.* **1986**, *24*, 1383-1400.
- (30) Aly, M. M. A.; Baron, M. H.; Favrit, J.; Romain, F.; Revault, M. *Spectrochim. Acta, Part A* **1984**, *40A*, 1037-1056.
- (31) Gray, F. M. *Solid polymer electrolytes: Fundamentals and technological applications*; VCH: New York, 1991.

Chapter 4: Crosslinked LPEI·HCl-based membranes for hydrogen fuel cell applications: Ionic conductivity studies

An important amount of research has been dedicated to the development of proton conducting materials for hydrogen fuel cell applications. Most of the research in this area has focused on perfluoro-sulfonic acid materials (e.g. Nafion®), sulfonated poly(aromatics) and poly(benzimidazole)-type polymers.¹⁻⁴ Developing new alternative materials can offer solutions to some of the shortcomings that these membranes possess.

Linear poly(ethylenimine), LPEI, has been recognized as a potential proton-conducting polymer.⁵⁻⁹ However, without functionalization, the use of LPEI in proton exchange membranes for hydrogen fuel cells is limited due to its water solubility.³

Research done in Dr. Glatzhofer's laboratory at the University of Oklahoma has shown that linear poly(ethylenimine) hydrochloride, LPEI·HCl, can be successfully crosslinked with malonaldehyde generated *in situ* in aqueous phosphoric acid to form freestanding, thermally stable, homogeneous gel membranes that exhibit ionic conductivities up to 0.01 S/cm at 150°C and 0% relative humidity.¹⁰ The ionic conductivity of these materials depends on the temperature, the amount of crosslinker added during the formation of the membrane and the amount of phosphoric acid used in the formulation.¹⁰

Preliminary studies indicate that the degree of crosslinking, determined

through ^1H NMR spectroscopy, has an influence on the ionic conductivity performance of crosslinked LPEI·HCl systems.¹¹ A detailed study on the effects of relative humidity, temperature, degree of crosslinking and amount of phosphoric acid added to the system on the conductivity has not been reported yet. Such studies are presented in this chapter.

1. Background

Complexes of poly(ethylenimine) with acids such as hydrochloric, sulfuric and phosphoric acids, have been studied in the past and the proton conductivity of branched PEI: $x\text{H}_3\text{PO}_4$ complexes, where x is the number of moles of acid per mole of PEI repeat unit have been reported.^{5,12}

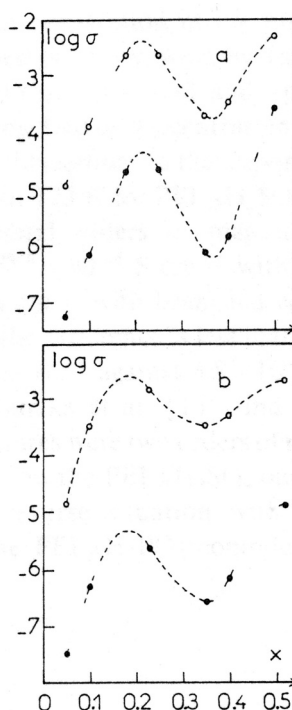


Figure 4.1. Concentration dependence of $\log \sigma$ (S/cm) for anhydrous BPEI· $x\text{H}_2\text{SO}_4$ (a) and BPEI· $x\text{H}_3\text{PO}_4$ (b) at 25°C (●) and 100°C (○).¹²

It is known that the conductivity of the complexes increases with increasing acid concentration, to reach maxima at x ca. 0.2, after which the conductivity decreases until the acid concentration is increased to x ca. 0.35.¹² Figs. 4.1a-b illustrates the conductivity behavior of these systems.

Similar behavior was noted in samples of linear and branched PEI with different amounts of phosphoric and sulfuric acids by Tanaka and co-workers.^{7,8} Fig. 4.2 shows the conductivity dependence on the amount of acid in the complex at 30, 60 and 100°C.

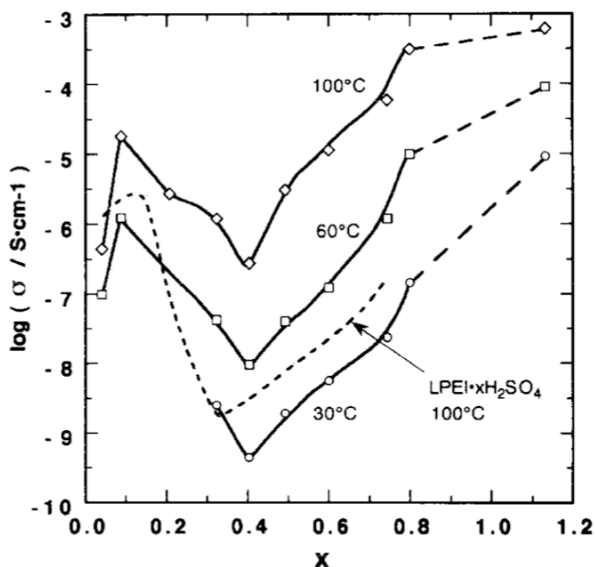
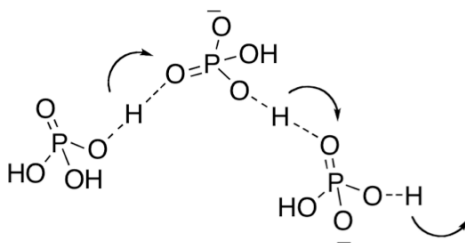


Figure 4.2. Composition, x , dependence of proton conductivities of PEI: x H₃PO₄ at 30, 60 and 100°C. Values for LPEI: x H₂SO₄ are shown for comparison.⁸

Even though the actual conductivity values reported by Tanaka in his studies varied significantly from the ones reported by Lassègues *at al.* the behavior of the

samples is very similar. It is believed that the trend observed results from changes in the proton conducting mechanism within the samples.^{5,7,8,13}

At low acid concentration, ca. $x < 0.4$, proton conductivity takes place through a proton hopping mechanism in which the most important contributions come from processes that involve ammonium groups ($^-\text{NH}_2^+$) along the polymer backbone acting primarily as proton donors, while neutral amino groups act as proton acceptors. Upon increasing the amount of acid past this point ($x > 0.4$), phosphoric acid competes with ammonium groups as the proton source. However, higher H_3PO_4 concentrations change the proton conduction in such a way that the protonated polymer provides a medium in which proton conduction occurs mainly through proton hopping *via* hydrogen bond arrays involving phosphoric acid in different stages of deprotonation as shown in Scheme 4.1 below.⁸



Scheme 4.1. Proposed proton hopping mechanism in $\text{PEI}:\text{xH}_3\text{PO}_4$, where $x > 0.4$ moles of acid per mole of repeat unit of the polymer. Arrows denote general direction of the proton movement.

While these results are promising, $\text{PEI}:\text{xH}_3\text{PO}_4$ complexes are water soluble at

concentrations higher than $x = 0.5$, which limits its application in hydrogen fuel cells, where water management can be challenging.

In an attempt to overcome this problem Tanaka and coworkers proposed crosslinking PEI with ethylene glycol diglycidyl ether (EGDGE). The crosslinked material was pulverized and soaked in a methanol solution containing the required amount of phosphoric acid. Methanol would be then removed and the resulting material pulverized once more and compacted.⁷

Conductivity studies on these materials revealed that, while the conductivity of the crosslinked system was lower than that of non-crosslinked samples with comparable amounts of acid, the dependence of conductivity on the sample composition for crosslinked PEI: $x\text{H}_3\text{PO}_4$ exhibits a similar pattern to non-crosslinked systems previously reported in the literature.^{5,8,12} However, it was noted that the minimum in conductivity occurred at lower acid concentrations, indicating that crosslinking the polymer lowers the number of available nitrogens, decreasing the upper limit of neutralization.⁷

These initial attempts at a viable crosslinked poly(ethylenimine) based system rendered mechanically incoherent materials due to the way they were processed. Research done by Dr. Michael J. Erickson, in Dr. Glatzhofer's group at the University of Oklahoma, resulted in the development of new crosslinked LPEI·HCl based materials doped with phosphoric acid.¹⁰

Linear poly(ethylenimine) hydrochloride was crosslinked with malonaldehyde, generated *in situ* from 1,1,3,3-tetramethoxypropane, in water and the appropriate

amount of phosphoric acid.¹⁰ Freestanding films were cast onto Teflon® coated Petri dishes and sealed tightly to prevent evaporation of the crosslinker for two days. Later, water was allowed to slowly evaporate over a period of three days.¹⁰

The possible mechanism through which the crosslinking of these systems take place have been described elsewhere,¹⁰ and the degree of crosslinking achieved have been determined by IR, Raman and ¹H NMR spectroscopy as reported in chapter 3 of this dissertation.¹¹

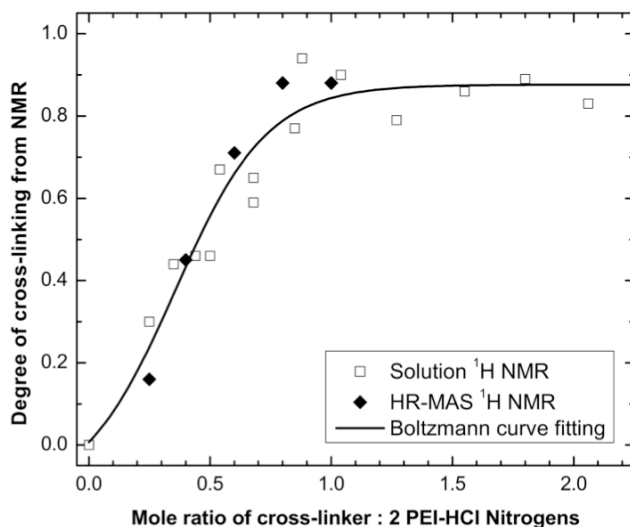


Figure 4.3. Calibration curve for degree of crosslinking determined from NMR data: (□) Solution ¹H NMR, (◆) HR-MAS ¹H NMR.¹¹

For the purposes of this study, the degree of crosslinking of each of the samples studied was determined by using the calibration curve shown in Fig. 4.3. Solution ¹H NMR was performed on samples with phosphoric acid and it was found that even though the presence of acid in the polymer solution affects the

kinetics of the crosslinking reaction, it does not change the final degree of crosslinking (data not shown).

It is possible to fit data collected through solid-state HR-MAS ^1H NMR and solution ^1H NMR to a Boltzmann-type sigmoidal model of the form

$$y = A_2 + \frac{A_1 - A_2}{1 + e^{(x-x_0)/dx}} \quad (4.1)$$

where A_1 is the initial y value ($x = -\infty$), A_2 is the final y value ($x = +\infty$), x_0 is the center (point of inflection), and dx is approximately the width of range of x over which y changes the most. These fitting constants have the following values for our system: $A_1 = 0.0 \pm 0.1$, $A_2 = 0.88 \pm 0.03$, $x_0 = 0.36 \pm 0.08$, and $dx = 0.19 \pm 0.05$. For our system, y will be defined as the degree of crosslinking and x is the mole ratio of crosslinker to 2 nitrogens in the polymer backbone. Using this equation allows us to obtain a calibration curve that can be used to determine the degree of crosslinking of any given sample by knowing the amount of crosslinker used in the formulation of the membrane.

Initial studies showed that the conductivity of this system varies as a function of acid content, degree of crosslinking and temperature.^{10,11} While keeping the concentration of phosphoric acid constant and increasing the degree of crosslinking, it was noted that the conductivity of the samples increased. However, as can be seen in Fig. 4.4, no significant changes in the conductivity were observed from increasing the degree of crosslinking from 0.76 to 0.84.¹⁰ This is consistent with observations made by Tanaka *et al.* in which it was noted that in crosslinked systems the minimum in conductivity was reached at lower

acid concentrations.⁷ It could be expected that higher degrees of crosslinking will lead lower upper limits of neutralization, as described by Tanaka,⁷ effectively increasing the amount of “free” phosphoric acid contained in the sample. Higher “free” phosphoric acid content is responsible for higher conductivity values. This effect seems to reach a saturation point, upon which, no more “free” phosphoric acid is produced.

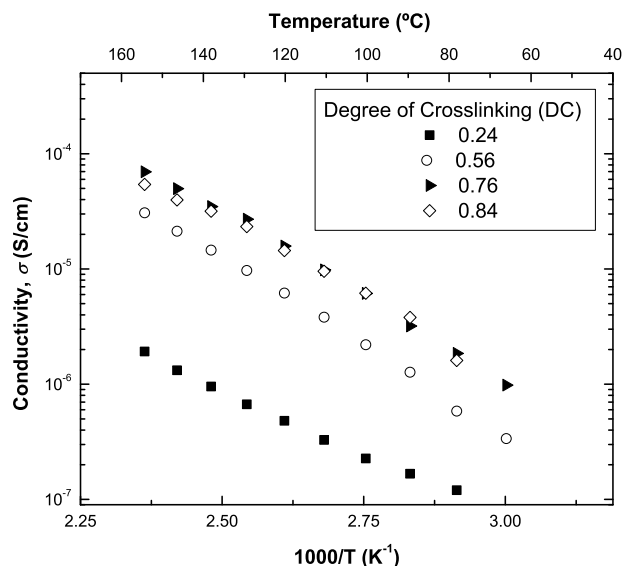


Figure 4.4. Conductivity dependence on temperature for anhydrous samples with P:N molar ratio of 0.69 and different degrees of crosslinking. Data taken from ref. 10.

Research showed that the conductivity of crosslinked LPEI·HCl, at a constant degree of crosslinking and with different amounts of H₃PO₄, would rise by increasing the concentrations of acid.¹⁰ Fig. 4.5 illustrates the change in conductivity as a function of the phosphorus to nitrogen molar ratio in

LPEI·HCl:xH₃PO₄ complexes over a range of temperatures.

From the data in Fig. 4.5 it is possible to determine an apparent energy of activation, E_{app} for the conductivity processes by using an Arrhenius-type expression. E_{app} values reveal that there's a change in the amount of energy needed for the conduction process cause by changes in the phosphoric acid content.

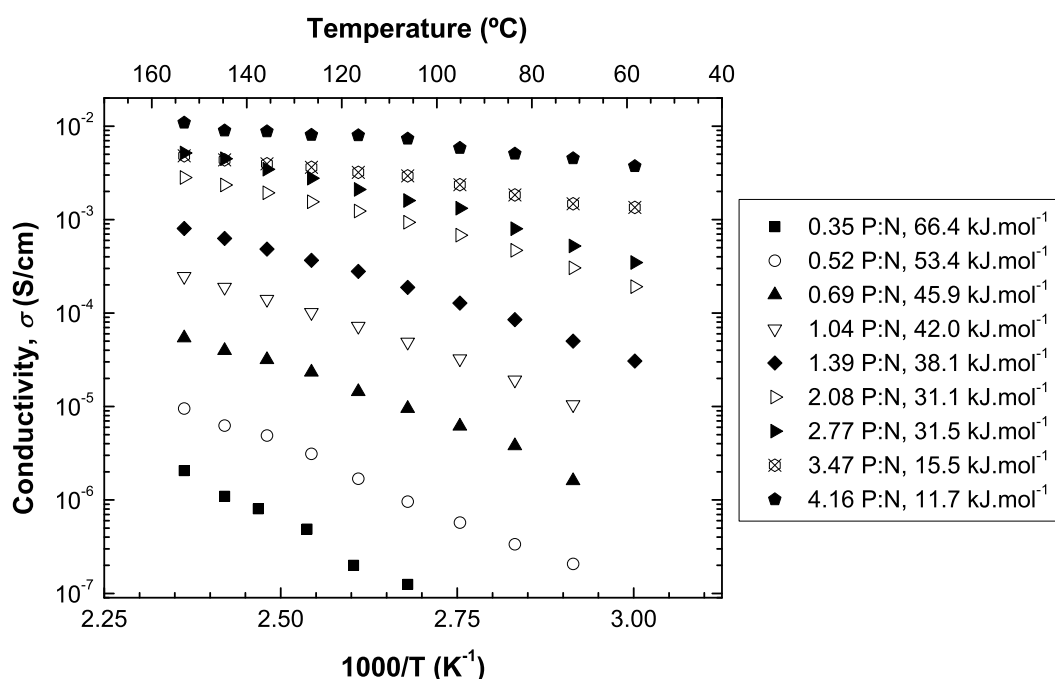


Figure 4.5. Ionic conductivity of crosslinked linear poly(ethylenimine) hydrochloride with different phosphoric acid concentration, as a function of temperature; legend indicates the phosphorus to nitrogen (P:N) molar ratio and apparent energy of activation derived from the plot.¹⁰

At low acid content, E_{app} is 66.4 kJ·mol⁻¹ and this value gradually decreases as

the H_3PO_4 concentration in the system is increased, reaching $11.7 \text{ kJ}\cdot\text{mol}^{-1}$ at 4.16 P:N molar ratio. This trend is consistent with the proposed conduction mechanism. As mentioned before, the conduction mechanism for membranes with low acid content would rely strongly on ammonium-amine proton transfer, while transport mechanisms in high phosphoric acid content membranes would involve phosphate mediated proton hopping.⁸ Enthalpies of dissociation of ammonium ions in aqueous systems are in agreement with the apparent energies of activation reported by Glatzhofer *et al.*,^{8,10} supporting the mechanism described above.

2. Ionic conductivity studies

While previous studies in our group provide important insight into the composition-property relationships for these systems, more work is needed to fully understand the important role that water has in the proton transport mechanism. The presence of water in these systems takes on more importance as we consider that water is produced during fuel cell operation. Water absorption is an important issue for existing polymer electrolyte membranes, such as Nafion[®], because water is essential for this material to achieve useful conductivity values.

The effect of the degree of crosslinking on the conductivity of xLPEI-HCl / H_3PO_4 membranes is not clear yet, and additional studies have been carried out to improve our understanding of this system in order to be able to better tailor it to

different applications. Additionally, films with different amounts of phosphoric acid were evaluated at different temperatures and relative humidities to provide a more detailed view of the system.

A.C. conductivity of xLPEI-HCl with a degree of crosslinking of 0.84 and different amounts of phosphoric acid, 0.5 and 0.7 P:N, was measured at 25°C using a four-probe technique as described in the literature.^{10,11} Two different setups were used to control the relative humidity. At room temperature, the relative humidity in the measurement chamber was controlled using a saturated salt solution as a constant activity source.^{14,15} Samples were allowed to equilibrate over 24 hours prior to measuring the conductivity. For samples evaluated at higher temperatures, from 30°C to 130°C, an in-plane conductivity test system, model BT512, from BakkTech, LLC. was used. The system consists of a Teflon® insert that supported a sample with longitudinal geometry. The insert included four platinum wires evenly spaced along the sample. The testing system allows control of the temperature of the sample. The equipment is coupled to a dew point saturator to control the relative humidity inside the conductivity cell. Typical sample dimensions were 2.5 cm x 0.06 cm x 0.5 cm. Fig. 4.6 shows the conductivity as a function of relative humidity for xLPEI-HCl samples with 0.5 and 0.7 P:N molar ratios.

As can be observed in Fig. 4.6, the ionic conductivity of the samples appears to increase exponentially when the relative humidity increases. The same behavior is observed for both samples. However, as expected, the ionic

conductivity for the 0.7 P:N sample is higher than that of the 0.5 P:N at comparable relative humidities over the range evaluated.

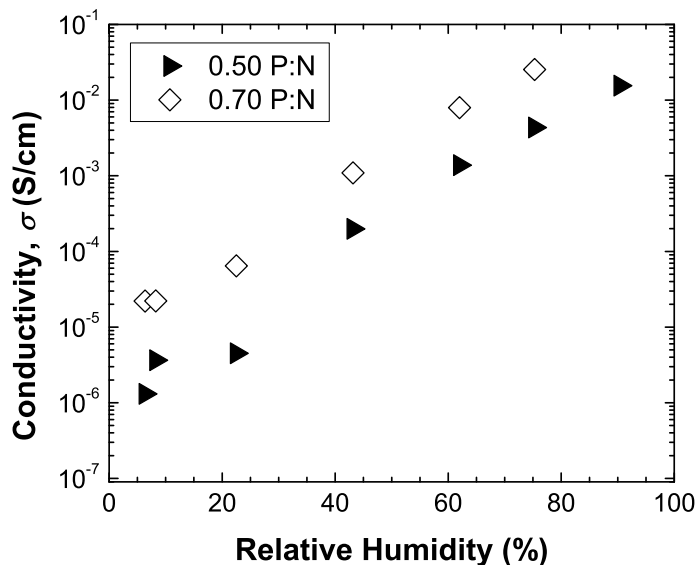


Figure 4.6. Conductivity as a function of relative humidity for x LPEI·HCl/ H_3PO_4 membranes at 25°C with different phosphorus to nitrogen molar ratios, P:N. Both membranes have a degree of crosslinking of 0.84.

Relative humidity can be considered an indirect indication of how much water has been absorbed by the membrane. LPEI-based films are highly hygroscopic and judging by the data shown in Fig. 4.6, no water saturation effect is observed under these conditions.

Water molecules absorbed into the polymer matrix can participate in the proton conduction mechanism by providing coordination sites for protons. It can be inferred that water molecules are distributed throughout the cross-section of

the polymer membrane, providing additional pathways through which protons can be transferred.

Fig. 4.7 presents conductivity vs. temperature curves for a 0.5 P:N xLPEI·HCl / H₃PO₄, and DC = 0.84, at different relative humidities. Similar curves were obtained for samples with a 0.7 P:N molar ratio and a degree of crosslinking of 0.84 (not shown).

The conductivity of this membrane while held at constant relative humidity changes significantly when temperature is increased. The ionic conductivity of the samples decreases to a minimum when the temperature is ca. 50-60°C. However, the conductivity increases again as the temperature is increased further.

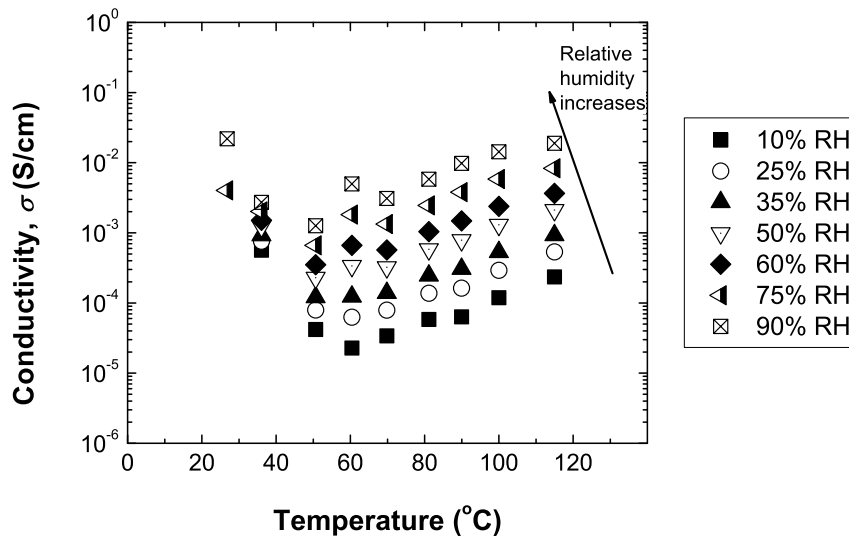


Figure 4.7. Conductivity as a function of temperature for a crosslinked LPEI·HCl/ H₃PO₄ membrane with a 0.5 P:N molar ratio, and degree of crosslinking of 0.84, at different relative humidities.

This curious behavior might be indicative of two different conduction mechanisms taking place in the sample. It is postulated here that water is mainly responsible for the transport of protons through the polymer matrix at low temperatures. This process is hindered by evaporation when temperature is increased, causing a decrease in the conductivity values reached by the membranes. However, phosphoric acid is known to participate in the conduction mechanism in LPEI-based materials.

As was noted earlier by Lassègues,^{5,13} Tanaka,^{7,8} and Glatzhofer,¹⁰ conduction mechanisms involving phosphoric acid are thermally activated processes. When the temperature is high enough, the contribution of these processes can be significant enough to produce an increase in the conductivity, thereby overcoming the effects of water loss.

Conductivity measurements on samples with a wider range of phosphoric acid content at 100°C revealed that the behavior observed in Fig. 4.6 was more complex than originally thought.

Fig. 4.8 shows that samples with different amounts of phosphoric acid present different sensitivities to the relative humidity in their environment. Samples with lower acid content (0.5, 0.8 and 1.0 P:N) seem relatively less sensitive to the relative humidity, only registering a change of an order of magnitude or two at the most, while samples with higher acid content present a more significant change in their conductivity, similar to that seen in Fig. 4.6. However, there is a significant

difference: the 1.5 P:N presents a significant jump in conductivity followed by a plateau in which the conductivity increased slightly with relative humidity. Coincidentally, the 2.0 P:N presented a plateau at lower conductivity values followed by a marked increase in the conductivity.

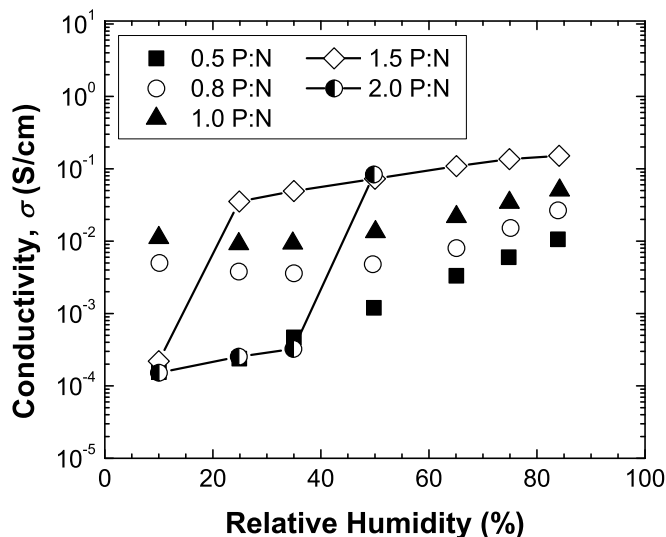


Figure 4.8. Conductivity as a function of relative humidity for xLPEI·HCl films with a degree of crosslinking of 0.84 and different phosphorus to nitrogen molar ratios. Measurements carried out at 100°C.

Fig. 4.9 shows the conductivity as a function of relative humidity for crosslinked LPEI·HCl / H₃PO₄ films with a 2.0 P:N molar ratio. Three samples with different degrees of crosslinking were studied. As can be observed, changes in the degree of crosslinking caused a transition from low to high conductivity values similar to the ones seen in samples with different amounts of acid. It is remarkable that samples with lower degrees of crosslinking, i.e. 0.46 and 0.66,

exhibit very little sensitivity to changes in relative humidity, maintaining conductivity values below and around 0.1 S/cm, the DOE target conductivity for PEM fuel cell applications at 100°C. Similar transitions are observed when the degree of crosslinking and H₃PO₄ content are kept constant while measuring the conductivity at different temperatures, as evidenced in Fig. 4.10.

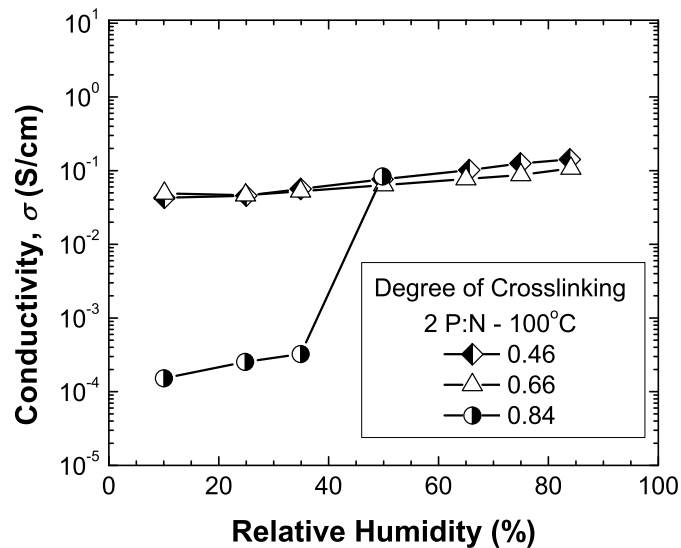


Figure 4.9. Conductivity at 100°C as a function of relative humidity for crosslinked LPEI·HCl membranes containing 2.0 P:N molar ratio. Samples had degrees of crosslinking varying from 0.46 to 0.84.

These transitions from lower to higher conductivity values take place at different “onset” relative humidities, depending on the degree of crosslinking, amount of phosphoric acid in the membrane and temperature of the measurement, which leads us to believe that the transition depends on the formulation of the film rather than testing conditions.

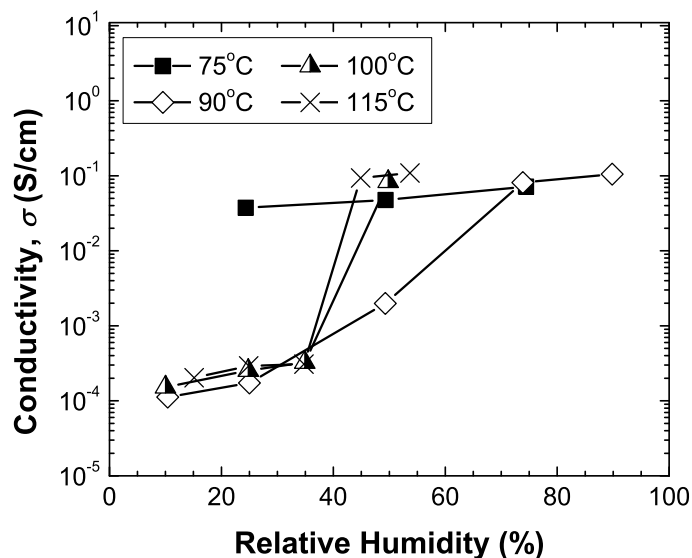


Figure 4.10. Conductivity as a function of relative humidity for a crosslinked LPEI·HCl / H₃PO₄ membrane with a degree of crosslinking of 0.84 and a 2.0 P:N molar ratio.

The ability of crosslinked poly(ethylenimine) hydrochloride-based membranes to absorb and retain water depends strongly on its formulation. Even though the exact relationship between the physical properties exhibited and the structure and characteristics of the crosslinked polymer network is not known, it is possible to recognize that the conductivity of the system shows a behavior similar to that of other physical properties of polymers that follow a Williams-Landel-Ferry relationship, WLF, not unlike the time-temperature superposition.¹⁶

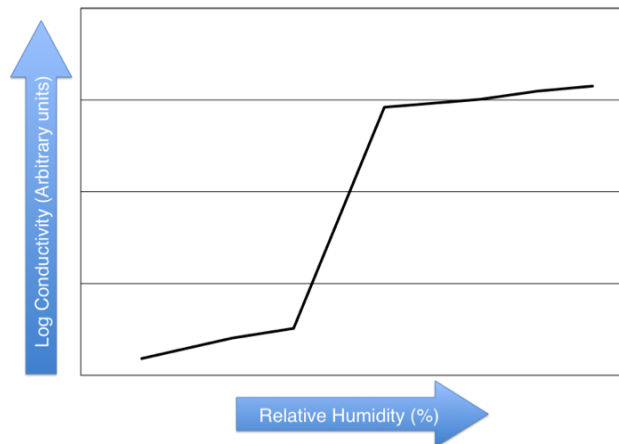


Figure 4.11. WLF master curve for conductivity of crosslinked LPEI·HCl / H₃PO₄ systems.

Thus, it is possible to envision that the conductivity behavior shown in Fig. 4.6 represents only a section of the entire curve for that system, and that under the right conditions or membrane formulation it would be possible to obtain membranes that only exhibit high conductivities with little or no variation with relative humidity. Evidence of such systems is easily found in Figs. 4.8, 4.9 and 4.10.

3. System optimization

In order to optimize crosslinked poly(ethylenimine) hydrochloride based membranes, it was necessary to evaluate several formulations at temperatures ranging from 75°C to 115°C. Formulations were changed by adjusting the degree of crosslinking and phosphoric acid content of these membranes.

Membranes with different amounts of phosphoric acid were submerged under

distilled water over 24 hour periods at 25°C, the water would then be removed. Samples would then be allowed to dry over 72 hours in an oven at 45°C. The treatment was repeated twice more and the water collected from each extraction was evaluated separately. Silver nitrate was used in portions of the water to test for chlorine content. ³¹P NMR was used to determine if there was any phosphoric acid in the water.

Results showed that hydrochloric acid would slowly migrate out of the membranes while no trace of phosphoric acid was observed in the water from samples with a P:N < 2.0. Even though these results are only qualitative and highly empirical, they are important in setting parameters to further tailor the formulation of membranes for fuel cell applications.

Samples with phosphorus to nitrogen molar ratios going from 0.5 to 2.0 P:N were evaluated in membranes with a degree of crosslinking, DC, of 0.46. Membranes with a DC = 0.84 were tested with three different phosphoric acid contents (0.2, 0.4 and 1.0 P:N). Both systems were tested at four different temperatures.

Figs. 4.12 and 4.13 present conductivity values for the DC=0.84 and DC=0.46, respectively. Samples from the DC = 0.84 system showed the expected behavior: higher conductivities were obtained by increasing the amount of phosphoric acid. Slight increases in the conductivity were observed as the relative humidity was increased.

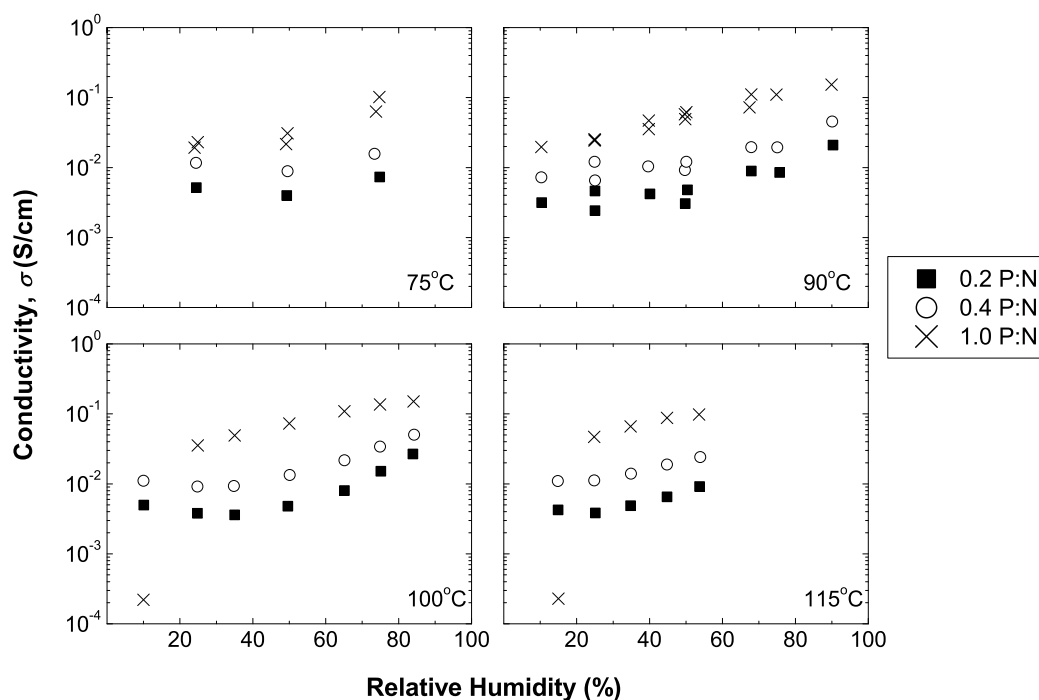


Figure 4.12. Conductivity as a function of relative humidity for xLPEI·HCl membranes with a degree of crosslinking, DC, of 0.84, and different amounts of phosphoric acid. Samples were evaluated at 75, 90, 100 and 115°C.

Surprisingly, samples with a lower degree of crosslinking revealed a more complex picture. The membrane containing phosphoric acid in a 0.8 P:N molar ratio had the lowest conductivity, on average, over all the temperatures evaluated. Additionally, this system seems particularly less sensitive to the changes in relative humidity.

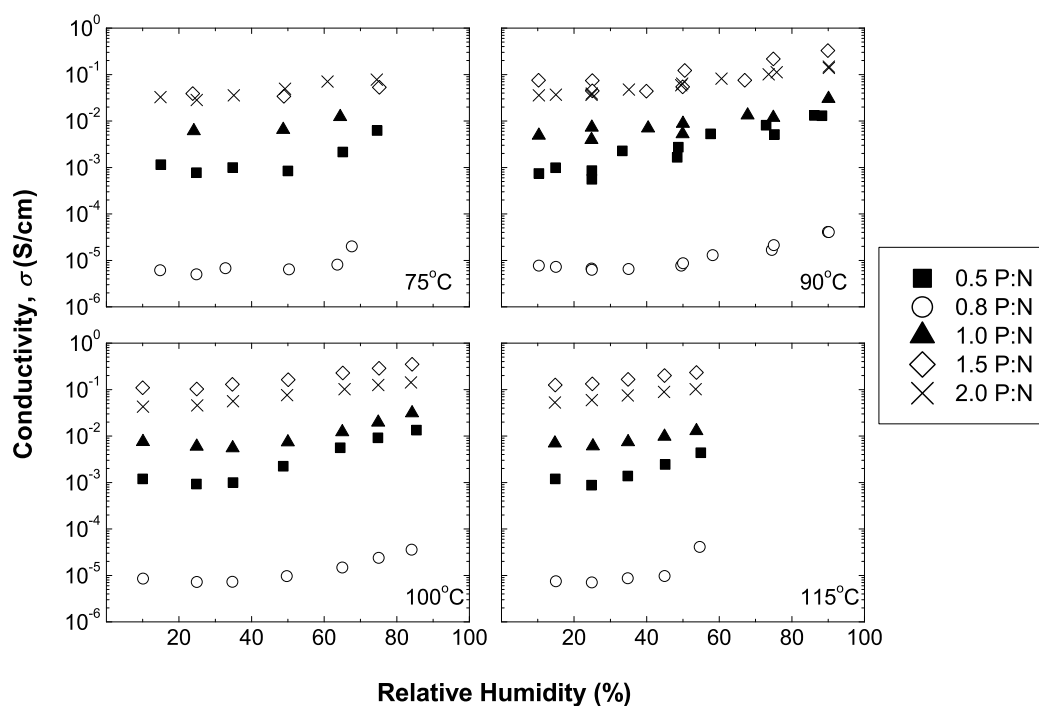


Figure 4.13. Conductivity as a function of relative humidity for xLPEI·HCl membranes with a degree of crosslinking, DC, of 0.46, and different amounts of phosphoric acid. Samples were evaluated at 75, 90, 100 and 115°C.

In order to better illustrate these observations, conductivity was plotted against the P:N molar ratio for both systems in Figs. 4.14 and 4.15. Data for 50% relative humidity was chosen as a representative set of data for both systems. It can be observed in Fig. 4.14 that conductivity values increase slightly with temperature as was expected from previous reports.

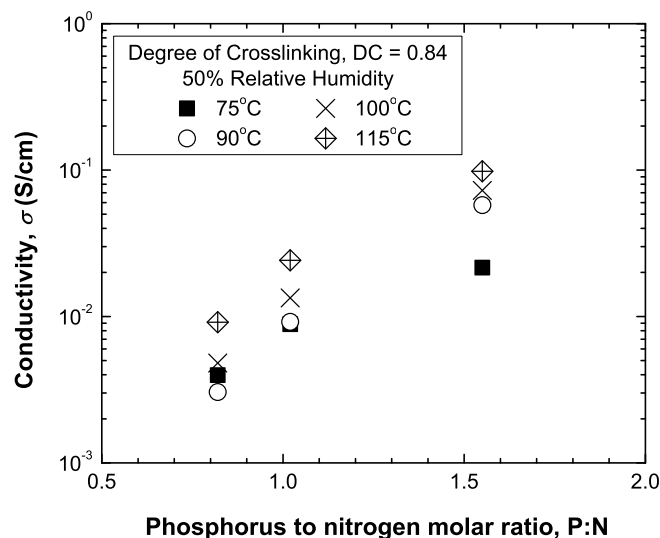


Figure 4.14. Conductivity as a function of acid content for xLPEI·HCl membranes with a degree of crosslinking, DC, of 0.84, at 50% relative humidity. Samples were evaluated at 75, 90, 100 and 115°C.

Fig. 4.15 reveals a similar behavior to that reported by Tanaka and Lessègues,^{5,7,8,12} and later by our group.¹¹ A minimum in the conductivity is observed for samples with phosphoric acid in a 0.8 P:N molar ratio. It is possible to explain these results in the same terms used by Tanaka.^{7,8} However, this interpretation should be made carefully as the introduction of positively charged crosslink units certainly complicates the intricate coordination between phosphoric acid and the host polymer network.

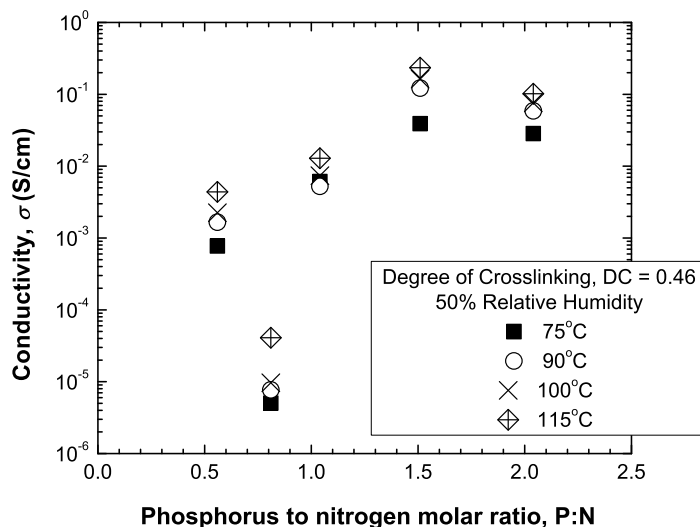


Figure 4.15. Conductivity as a function of acid content for xLPEI·HCl membranes with DC = 0.46 at 50% relative humidity. Samples were evaluated at 75, 90, 100 and 115°C.

Since the polymer host is crosslinked, the mobility of the amine groups along the polymer chain is hindered, diminishing the contribution of these groups in the proton transport process responsible for the conductivity. Each crosslink unit reduces the nitrogen atoms available for protonation by one, effectively reducing the number of moles of phosphoric acid necessary to generate “free” phosphoric acid within the host network. This could explain why a minimum in conductivity is not observed in samples with a degree of crosslinking of 0.84. This type of interaction results in membranes exhibiting higher conductivity values than comparable samples with lesser amounts of “free” H₃PO₄ available.

Taking all these factors into consideration, a sample was prepared with

phosphoric acid in a 1.5 P:N molar ratio and a degree of crosslinking of 0.45. Results are summarized in Fig. 4.16. As expected, this system exhibits a slight sensitivity to relative humidity and shows conductivity values above 0.1 S/cm, at temperatures 90°C or higher, over relative humidities ranging from 10% to 90%.

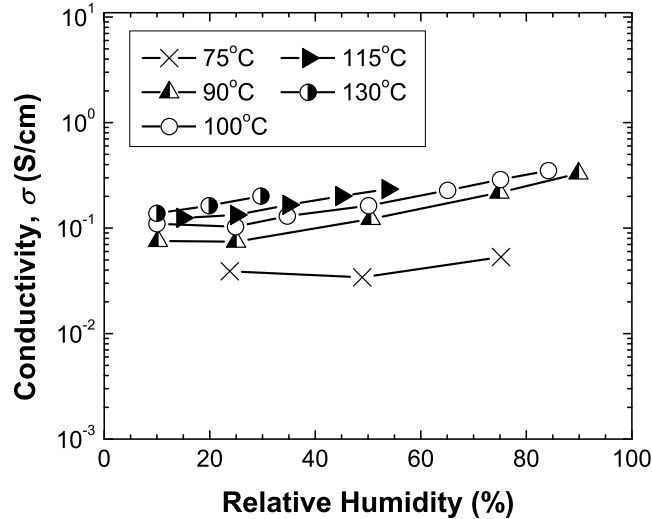


Figure 4.16. Conductivity as a function of relative humidity for a crosslinked LPEI·HCl / H₃PO₄ membrane with a degree of crosslinking of 0.45 and a 1.5 P:N molar ratio.

4. Conclusions

The ionic conductivity of membranes made of LPEI·HCl crosslinked with malonaldehyde generated *in situ*, and doped with phosphoric acid, has been determined as a function of the degree of crosslinking, amount of phosphoric acid, temperature and relative humidity.

Results showed that the dependence of the conductivity on these factors is

complex and that it involves a drastic transition in which the conductivity increases by several orders of magnitude. The onset of this transition appears to be related to the composition of the polymer membranes.

^{31}P NMR and silver nitrate titrations were used to qualitatively determine if phosphoric or hydrochloric acids can be leached from crosslinked membranes. It was found that, even though HCl can be removed from crosslinked membranes by evaporation or extraction with water, this was not the case for H_3PO_4 . No traces of phosphoric acid were found in the water used in the extractions performed on the crosslinked polymer membranes with acid contents below 2.0 P:N. It is necessary to test the materials at fuel cell operating temperatures to know if this is still the case at higher temperatures. Results presented in this chapter, along with strong interactions reported before in the literature,^{5,7,8,12} indicate that there might be more than an acid-base interaction between poly(ethylenimine) and phosphoric acid.

It was demonstrated that it is possible to tailor the amount of phosphoric acid and the degree of crosslinking necessary to obtain a crosslinked LPEI·HCl based membrane with conductivities around 0.1 S/cm over 90°C and relative humidity as low as 10%.

References

- (1) Hickner, M. A.; Ghassemi, H.; Kim, Y. S.; Einsla, B. R.; McGrath, J. E. *Chem. Rev.* **2004**, *104*, 4587-4612.
- (2) Lee, J. S.; Quan, N. D.; Hwang, J. M.; Lee, S. D.; Kim, H.; Lee, H.; Kim, H. *S. J. Ind. Eng. Chem.* **2006**, *12*, 175-183.

- (3) Mehta, V.; Cooper, J. S. *J. Power Sources* **2003**, *114*, 32-53.
- (4) Miyatake, K.; Watanabe, M. *Electrochemistry* **2005**, *73*, 12-19.
- (5) Schoolmann, D.; Trinquet, O.; Lassegues, J. C. *Electrochim. Acta* **1992**, *37*, 1619-1621.
- (6) Senadeera, G. K. R.; Careem, M. A.; Skaarup, S.; West, K. *Solid State Ionics* **1996**, *85*, 37-42.
- (7) Tanaka, R.; Yamamoto, H.; Shono, A.; Kubo, K.; Sakurai, M. *Electrochim. Acta* **2000**, *45*, 1385-1389.
- (8) Tanaka, R.; Yamamoto, H.; Kawamura, S.; Iwase, T. *Electrochim. Acta* **1995**, *40*, 2421-2424.
- (9) Watanabe, M.; Ikezawa, R.; Sanui, K.; Ogata, N. *Macromolecules* **1987**, *20*, 968-973.
- (10) Glatzhofer, D. T.; Erickson, M. J.; Frech, R.; Yepez, F.; Furneaux, J. E. *Solid State Ionics* **2005**, *176*, 2861-2865.
- (11) Giffin, G. A.; Yepez Castillo, F.; Frech, R.; Glatzhofer, D. T.; Burba, C. M. *Polymer* **2009**, *50*, 171-176.
- (12) Daniel, M. F.; Desbat, B.; Cruège, F.; Trinquet, O.; Lassègues, J. C. *Solid State Ionics* **1988**, *28-30*, 637-641.
- (13) Daniel, M. F.; Desbat, B.; Lassègues, J. C. *Solid State Ionics* **1988**, *28-30*, 632-636.
- (14) Greenspan, L. *J. Res. NBS A: Phys. Chem.* **1977**, *81A*, 89-96.
- (15) Wexler, A. In *CRC Handbook of Chemistry and Physics*; CRC Press: Boca Raton, 2004.
- (16) Young, R. J.; Lovell, P. A. *Introduction to Polymers*; 2nd. ed.; Chapman & Hall: London, 1991.

Chapter 5: Crosslinked LPEI·HCl-based membranes: Hydrogen fuel cell application.

Interest in the application linear poly(ethylenimine)-based systems for use in operating fuel cells has driven Dr. Glatzhofer's group at the University of Oklahoma to study the ionic conductivity of crosslinked LPEI·HCl membranes and the results, some of which are included in Chapter 4 of this dissertation, have been promising. Research on composite membrane electrode assemblies (MEAs) containing crosslinked LPEI·HCl/H₃PO₄ based films was initially presented by Dr. Michael J. Erickson with interesting results based on studies on a 0.7 P:N LPEI·HCl/H₃PO₄ membrane with a degree of crosslinking, DC, of 0.84.¹ This chapter is a continuation of his work. Two new LPEI-based systems were used in MEAs: a 1.0 P:N LPEI·HCl / H₃PO₄ with DC = 0.24, and a 2.0 P:N LPEI·HCl / H₃PO₄ with DC = 0.66. Their performance in fuel cells was measured as a function of temperature at low relative humidity and compared to that of Nafion®-containing MEAs under the same conditions.

1. Background

As mentioned in the introduction, fuel cells are electrochemical devices that consist of an electrolyte in contact with two electrodes that is capable of converting directly any consumable fuels to electrical energy through chemical reactions.²

PEMFCs operate at low temperatures ($< 200^{\circ}\text{C}$) when compared to other types of fuel cells, such as solid oxide or molten carbonate fuel cells, that operate at temperatures well above 500°C .³ In order to operate under those conditions, catalysts are needed to facilitate the redox reactions that take place on each electrode.^{2,4,5} A large amount of research is being conducted to reduce the catalyst loading, its CO tolerance, and to find lower cost alternatives to platinum.⁶ Additionally, as O_2 and H_2 dissociation kinetics are better at higher temperatures ($> 400^{\circ}\text{C}$), and CO sensitivity is reduced as well, there has been a lot of interest in finding polymer electrolytes that perform well under those conditions.⁶

Hydrogen is fed into the cell, where a catalyst oxidizes it to generate two H^+ and 2e^- . Electrons are conducted through the electrical circuit to produce work, while protons must flow from the anode, through the electrolyte, to the cathode, where they would participate in the reduction of oxygen by a catalytic reaction producing water. Fuel cells perform consistently, generating electricity, as long as a continuous stream of fuel is fed into the electrochemical cell.^{2,7}

Fuel cell performance is often judged in terms of voltage-current density and power-current density curves. Figure 5.1 shows a typical voltage-current curve for an operating fuel cell.⁶

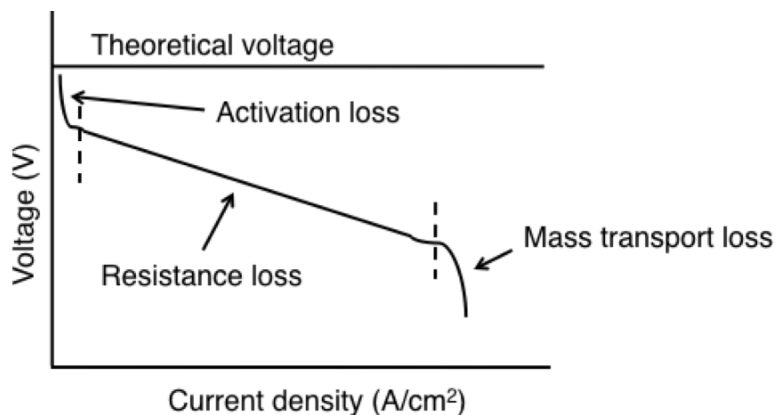


Figure 5.1. Typical cell potential vs. current density plot for a H₂/O₂ PEMFC.

Potential losses are indicated in the figure.

In general, operating voltages in fuel cells are significantly lower than the theoretical open circuit voltage value (OCV), $E^{\circ} = 1.23$ V for H₂/O₂ fuel cells, determined by the formula

$$E^{\circ} = -\frac{\Delta G^{\circ}}{zF} \quad (5.1)$$

where ΔG° is the standard Gibbs energy change of the reaction occurring in the electrochemical cell (the standard Gibbs energy of formation of H₂O (l) is -237.18 kJ/mol), z is the number of electrons that pass through the electrical circuit ($2e^{-}$), and F is the Faraday constant (96,485 C).^{4,6}

The activation, ohmic, and diffusion overpotential losses are responsible for the shape of the voltage-current density curve of a fuel cell.^{3,6} The activation overpotential occurs when reactions at the electrodes have slow kinetics. Part of the potential produced during the reaction is used to drive the reaction forward.⁴

Ohmic or resistive losses are related to the voltage loss due to the inherent

resistivity of the electrolyte. Electronic conduction through the electrolyte also makes a small contribution to ohmic losses.⁴ Finally, mass transport or concentration losses occur at high current densities due to lower concentrations of H₂/O₂ at the electrodes.³

The requirements for polymer electrolyte materials for fuel cell applications include properties such as low electronic conductivity, good barrier to hydrogen and oxygen gasses and good proton conductivity.⁷ These requirements reduce processes involved in potential losses that reduce the efficiency of an operating cell.

Several recent reviews have summarized some of the polymers that have been studied for the manufacturing of membrane electrode assemblies (MEAs).^{6,8} Poly(perfluorosulfonic acids),^{9,10} sulfonated poly(arylenes),¹¹⁻¹⁶ and acid-doped polymer complexes,¹⁷ are some of the membrane materials currently being studied.

Nafion® membranes require proper hydration in order to assure adequate solvation of sulfonic acid groups, thus allowing proton mobility.⁶ Reported conductivity values for well hydrated Nafion® membranes can be as high as 0.144 S/cm.¹⁸ However, the conductivity of the material at 80°C decreases up to 10 times relative to values measured at 60°C, due to dehydration of the membranes.^{6,8}

Dr. Erickson, in Dr. Glatzhofer's group at OU, conducted experiments that revealed that MEAs, prepared in the same way, using Nafion® and a crosslinked

LPEI·HCl/H₃PO₄ with a degree of crosslinking of 0.84 and 0.7 P:N molar ratio showed similar performances at room temperatures.¹

Crosslinked LPEI·HCl/H₃PO₄ films have shown remarkable ionic conductivities over a wide range of temperatures and relative humidities as evidenced in Fig. 5.2. However, little is known about the performance of MEAs containing these materials in operating fuel cells.

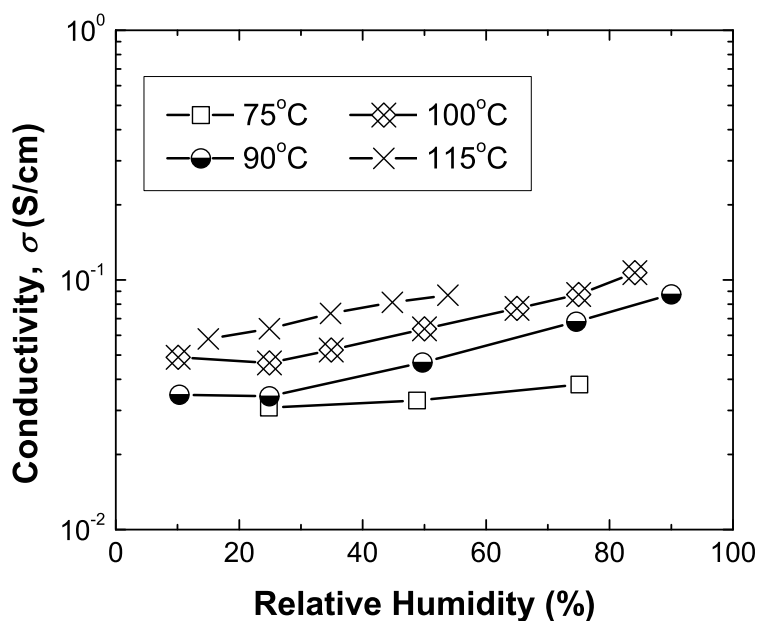


Figure 5.2. Conductivity as a function of relative humidity for a crosslinked LPEI·HCl/H₃PO₄ membrane with 2.0 P:N molar ratio and 0.66 degree of crosslinking.

2. Fuel cell testing.

MEAs were made using two high temperature ELAT® gas diffusion electrode (GDE) microporous layers, with 0.5 mg/cm² Pt loading on a carbon woven web

and a standard ionomer application (*E-TEK*, HT140EWSI), sandwiching a piece of electrolyte. The MEA was held in place by two square self-adhesive Mylar® gaskets, with 5 cm² holes cut in the center of them to expose the MEA, as illustrated in Fig. 5.3. MEAs were tested in a fuel cell hardware assembly purchased from *Fuel Cell Technologies*, which consisted of a pair of Poco graphite blocks with a precision, machined serpentine flow-pattern (5 cm²), and a pair of gold plated connectors fastened with aluminum end plates with gas inputs and outputs, a thermocouple well and two cartridge heaters to allow temperature control.

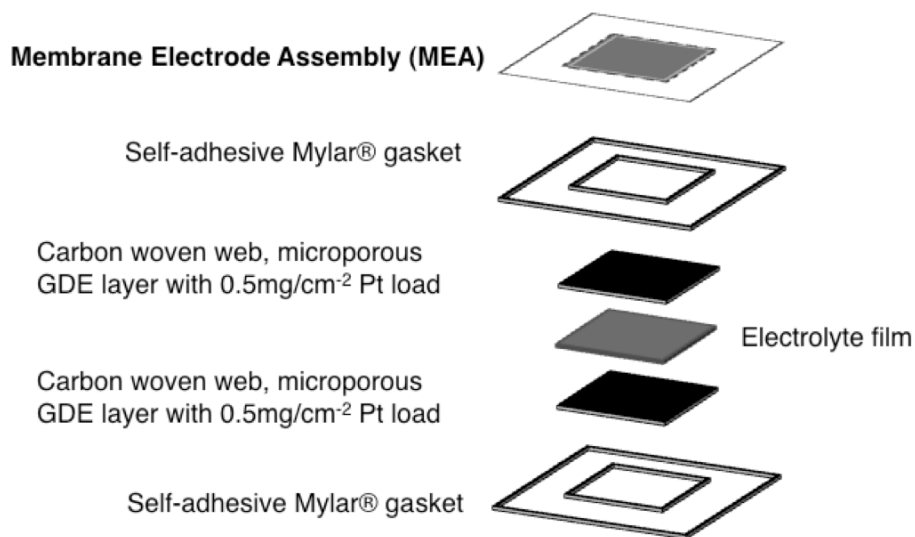


Figure 5.3. Schematic view of a typical MEA (as prepared). Diagram shows the different components of the MEA in their relative order.

Additional Teflon® coated fiberglass and Teflon® gaskets were used to avoid leaks or fuel crossover during the operation of the fuel cell. Experimental parameters for fuel cell testing were controlled by connecting the fuel cell to an

in-plane conductivity test system by *BekkTech, LLC*, model BT512. This system allowed thermal control of the fuel cell heating blocks, as well as the temperature of the H₂ inlet and outlet. Additionally, hydrogen (99.9%) was connected to a flow meter coupled to a needle valve that was used to regulate the flow rate of hydrogen into the cell and a dew point saturator, that was used to humidify and set the relative humidity of the hydrogen supplied into the fuel cell. The gas outlet on the anode of the fuel cell was connected to a regulator valve that was used to manually adjust the back pressure on the cell (avg. 10 psi). The hydrogen flow rate was kept at ca. 250 standard cubic centimeters. Compressed air was dried, filtered and injected into the cathode at constant pressure (10 psi). Our setup did not allow for a good control of the air flow rate into the cathode, nor did it provide an adequate way to maintain constant back pressure. Air was supplied in excess compared with the amount of hydrogen supplied to the anode.

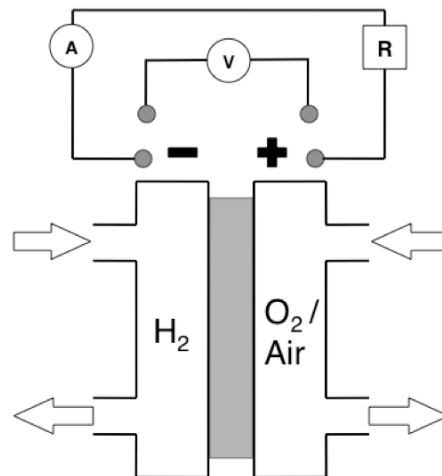


Figure 5.4. Diagram of a fuel cell setup including electrical and gas connections.

Resistors, with resistance values varying from 1Ω to $10M\Omega$, were used as resistive loads. Two *Kiethley* digital multimeters were used to measure the potential (V) and current output (A) of operating fuel cells. A diagram of the fuel cell is shown in Fig. 5.4.

Even though optimization of the fuel cell set up was not within the scope of this study, significant efforts were made to improve the performance of the fuel cell by changing the hydrogen flow rate, as well as setting up different values for the back pressure. These efforts were mildly successful but, as a general feature, all the MEAs studied exhibit very low current densities relative to the values reported in the literature. In order to make fair comparisons, an MEA using a Nafion® 117 film as the electrolyte was constructed and evaluated in our testing system as identically as possible. The performance for this MEA was measured at 60, 90, 100, 115 and 130°C at 30% relative humidity. Figures 5.5 and 5.6 show voltage-current density and power-current density curves for Nafion® 117 at different temperatures and at 30% relative humidity.

The potential between the terminals of the fuel cell increases as the load applied to the cell is increased while the current decreases. The curves shown in Fig. 5.5 resemble the one illustrated in Fig. 5.1 above. However, it should be noted that potential-current density curves in Fig. 5.5 do not seem to reach the mass transport losses region characteristic of high current densities.^{3,4}

According to Fig. 5.5, activation losses appear to be the most important ones exhibited by this system. These losses are associated with slow kinetics of the

reactions that take place at the electrodes. In theory, this problem could be addressed by improving the contact between the GDE layer containing the catalyst and the electrolyte membrane. Several reviews show that these losses can be minimized by changing the way the MEA is put together.^{3,6,8}

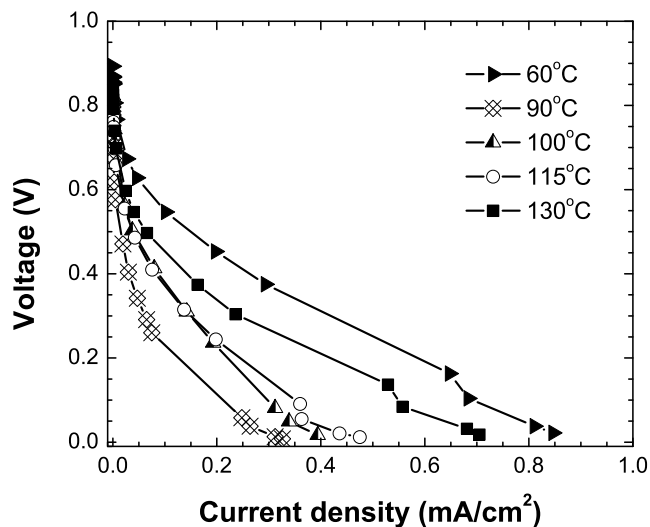


Figure 5.5. Potential (V) vs. current density (mA/cm²) curves for fuel cell operating at 30% relative humidity with an MEA containing a Nafion® 117 film.

Fig. 5.6 shows power-current density curves for the Nafion® 117 MEA. As expected, parabolic curves were obtained. Surprisingly, the performance of the cell at 60°C is superior to the performance at all the other temperatures measured. However, as would be expected, fuel cell performance is improved as temperature is increased up to 130°C relative to the performance of the cell at 90°C.

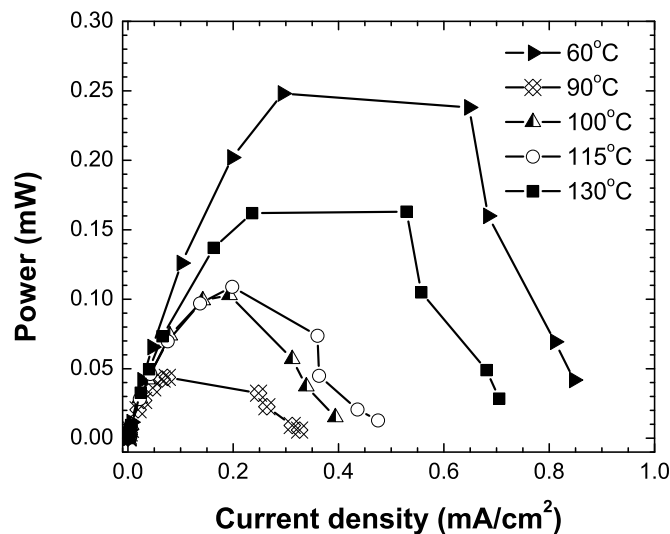


Figure 5.6. Power (mW) vs. current density (mA/cm²) curves for fuel cell operating at 30% relative humidity with an MEA containing a Nafion® 117 film.

Two crosslinked LPEI·HCl/H₃PO₄ systems were evaluated under similar conditions: a crosslinked poly(ethylenimine) hydrochloride film containing phosphoric acid in a 1.0 P:N molar ratio and a degree of crosslinking of 0.25; and a similar film containing 2.0 P:N molar ratio and a degree of crosslinking of 0.66.

The rationale behind the selection of these two formulations takes into consideration that previous studies revealed that lower degrees of crosslinking produced films with lesser sensitivity to relative humidity at elevated temperatures, resulting in films that would exhibit little change in ionic conductivity over a wide range of relative humidity. More importantly, this observation would extend to relative humidities lower than 30%. Additionally, Erickson reported that fully crosslinked membranes (degree of crosslinking ca.

0.84) with phosphoric acid in a 0.7 P:N molar ratio showed fuel cell performance comparable to that of Nafion® at room temperature;¹ films with a higher phosphoric acid content could potentially show better performance, especially since higher phosphoric acid content is associated with higher conductivity values in poly(ethylenimine)-based membranes.¹⁹⁻²¹

Figs. 5.7 and 5.8 show the potential-current density and power-current density curves for fuel cells with MEAs containing crosslinked poly(ethylenimine) hydrochloride electrolyte films with H₃PO₄ in 1.0 P:N molar ratio.

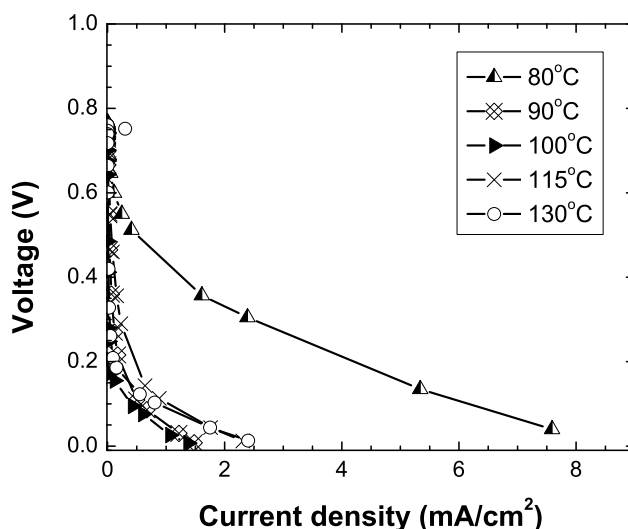


Figure 5.7. Potential (V) vs. current density (mA/cm²) curves for fuel cell operating at 30% relative humidity with an MEA containing a crosslinked LPEI·HCl / H₃PO₄ film with 1.0 P:N molar ratio and a degree of crosslinking of 0.24.

As can be observed on Fig. 5.7, at 60°C, current densities close to 8 mA/cm²

were achieved before any transport losses were measured.

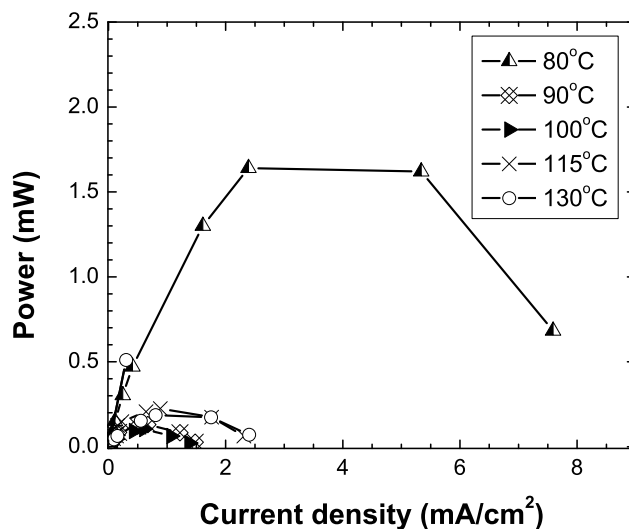


Figure 5.8. Power (mW) vs. current density (mA/cm²) curves for fuel cell operating at 30% relative humidity. Crosslinked LPEI·HCl / H₃PO₄ MEA with 1.0 P:N molar ratio and DC = 0.24.

The performance of this membrane showed similar features to those of the Nafion® 117 MEA. Even though performance seems to improve with increasing temperatures, there is a significant decrease in current density when the temperature reaches 90°C. This is consistent not only with these two membranes, but also with results observed in LPEI·HCl / H₃PO₄ membranes with 2.0 P:N molar ratio and a degree of crosslinking of 0.66 shown in Figs. 5.9 and 5.10.

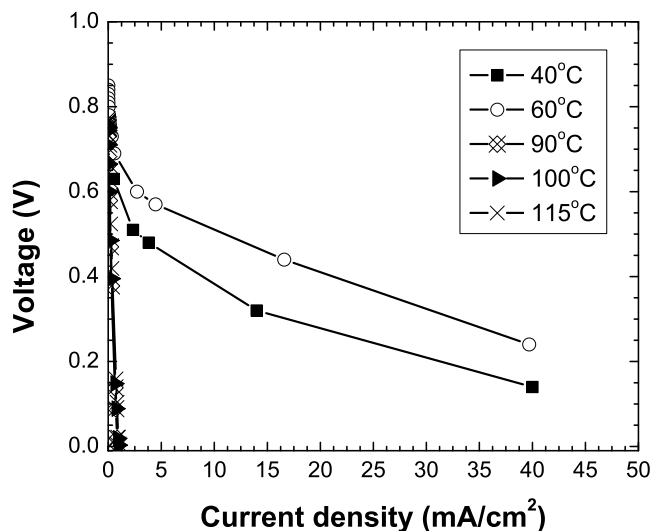


Figure 5.9. Potential (V) vs. current density (mA/cm²) curves for fuel cell operating at 30% relative humidity with an MEA containing a crosslinked LPEI·HCl / H₃PO₄ film with 2.0 P:N molar ratio and a degree of crosslinking of 0.66.

An increase in the amount of phosphoric acid present in the polymer electrolyte membrane is most likely responsible for the significant improvement in the current density output of the fuel cell. Current densities of 40 mA/cm² were obtained at 40 and 60°C with this system. However, a full characterization at temperatures below 90°C was not possible. Fig. 5.10 shows that the power-current density curves are incomplete. The fuel cell generates up to 20 mW at 60°C and 30% relative humidity, but it is not clear if this is the maximum point in the curve.

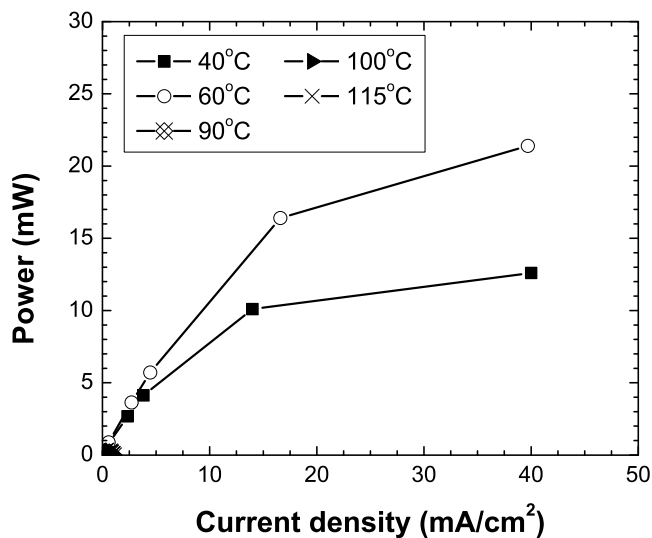


Figure 5.10. Power (mW) vs. current density (mA/cm²) curves for fuel cell operating at 30% relative humidity with an MEA containing a crosslinked LPEI·HCl / H₃PO₄ film with 2.0 P:N molar ratio and a degree of crosslinking of 0.66.

Since the details for the potential and power curves against current density for 90, 100 and 115°C cannot be seen clearly in the previous figures, Figs. 5.11 and 5.12 provide this data adequately. Performance was improved by increasing the temperature and current densities in the order of 1.0 mA/cm² were obtained for this system. More clearly defined potential-current density curves were obtained, with OCV potentials closer to 0.8 V.

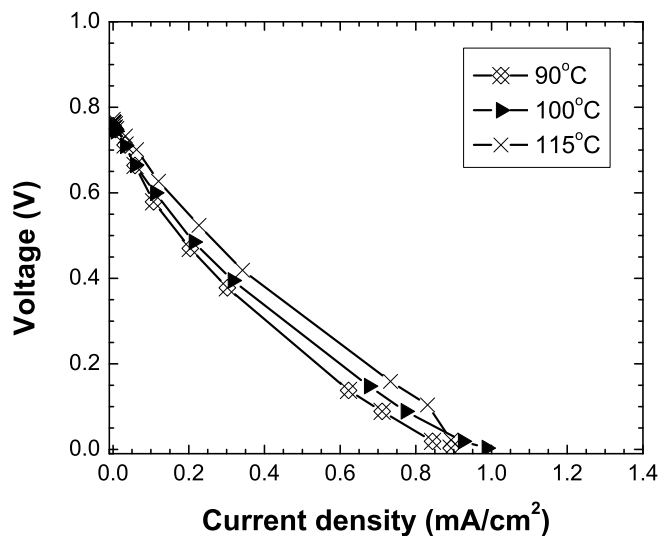


Figure 5.11. Potential (V) vs. current density (mA/cm²) curves for fuel cell operating at 30% relative humidity with an MEA containing a crosslinked LPEI·HCl / H₃PO₄ film with 2.0 P:N molar ratio and a degree of crosslinking of 0.66.

Power generated by this fuel cell peaked at 130°C with 0.32 mW and a current density of 0.34 mA/cm². All of the power curves obtained in this study, including those of fuel cells with Nafion® 117 MEAs were parabolic in shape, with no rapid decrease in power after the maxima were reached. This is consistent with the lack of mass transport loss regions in the potential-current density curves obtained in this study.³

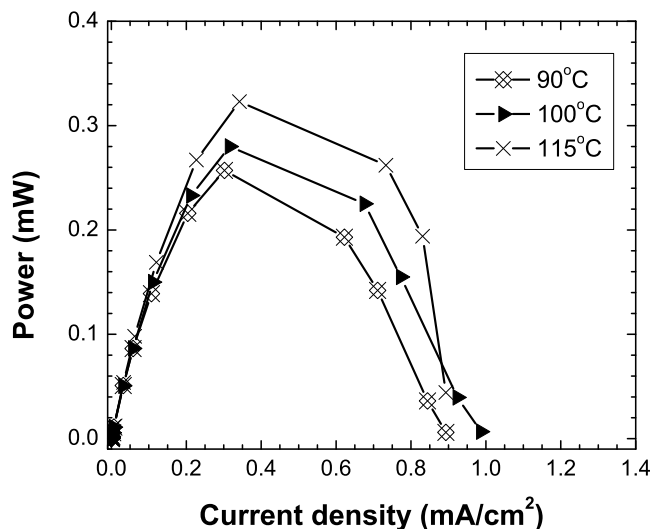


Figure 5.12. Power (mW) vs. current density (mA/cm²) curves for fuel cell operating at 30% relative humidity with an MEA containing a crosslinked LPEI·HCl / H₃PO₄ film with 2.0 P:N molar ratio and a degree of crosslinking of 0.66.

Figs. 5.13 and 5.14 show the potential-current density and power-current density curves for both xLPEI·HCl / H₃PO₄ studied at 90°C. Curves for Nafion® containing MEAs are also shown to provide a good comparison between the different systems.

Remarkably, both LPEI·HCl / H₃PO₄ systems provided current densities two or three times higher than that of Nafion®. As noted above, activation overpotentials seem to be somewhat diminished for the 2.0 P:N xLPEI·HCl / H₃PO₄ system relative to the ones observed for the other two films. However, this apparent advantage is quickly reversed when the fuel cell with a LPEI·HCl / H₃PO₄ MEA

and 1.0 P:N slows down the potential loss and is able to deliver current densities over 1.4 mA/cm^2 .

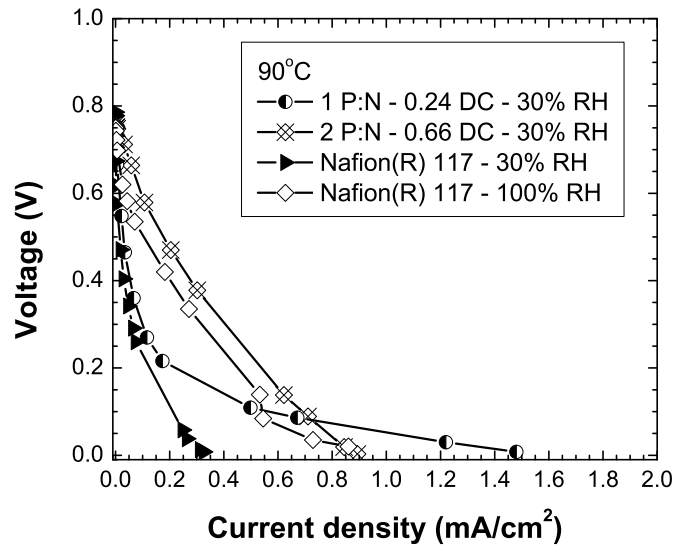


Figure 5.13. Potential (V) vs. current density (mA/cm^2) curves for fuel cells operating at 90°C and 30% relative humidity with different MEAs.

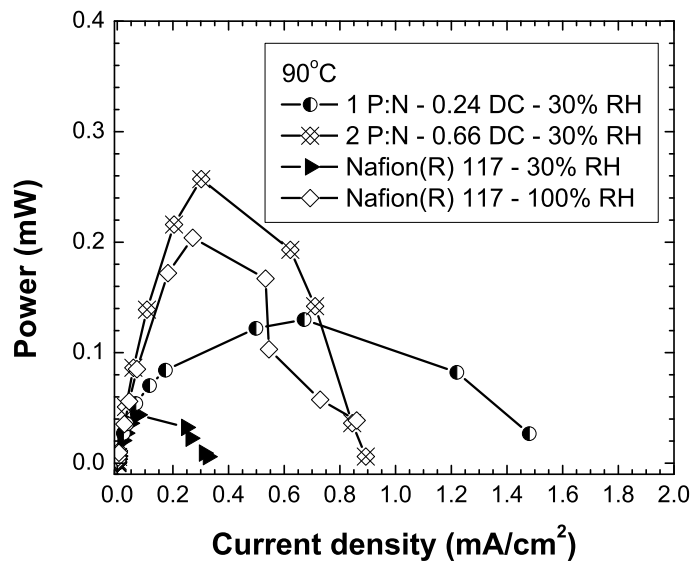


Figure 5.14. Power (mW) vs. current density (mA/cm^2) curves for fuel cells operating at 90°C and 30% relative humidity with different MEAs.

When we observe the power-current density curves on Fig. 5.14, it is easy to notice that the poly(ethylenimine)-based MEA with higher phosphoric acid content achieves higher power than its low acid counterpart, nearly doubling the power generated by the 1.0 P:N LPEI-based MEA. LPEI-based membranes used in MEAs for hydrogen fuel cells showed better performance than Nafion® at low relative humidity (30%). Furthermore, samples with a 2.0 P:N molar ratio, evaluated at 90°C and 30% relative humidity, produced higher power than Nafion® tested at the same temperature and 100% relative humidity (0.20 mW for Nafion® compared to 0.25 mW for the LPEI-based membrane. Data not shown).

3. Conclusions

Crosslinked linear poly(ethylenimine) hydrochloride membranes doped with phosphoric acid that have shown remarkable ionic conductivity values have been incorporated in membrane electrode assemblies (MEAs) and their performance in fuel cells have been tested. Even though overall potentials and current output measured were very low compared to results found in the literature for tested fuel cells, the performance of poly(ethylenimine)-based MEAs was superior than that of Nafion® 117 MEAs tested in our system. These results are very promising considering that no significant effort was made to improve contact between the catalyst in the gas diffusion electrode and the electrolyte film in the MEA. Further testing is necessary to determine if similar performance can be achieved with

LPEI-based MEAs with lower P:N molar ratios (P:N < 2.0).

References

- (1) Erickson, M. J. Ph. D. Dissertation, The University of Oklahoma, 2004.
- (2) Viswanathan, B.; Aulice Scibioh, M. *Fuel cells: Principles and applications*; CRC Press: Boca Raton, 2007.
- (3) Srinivasan, S.; Krishnan, L.; Marozzi, C. In *Fuel cells: From fundamentals to applications*; Springer: New York, 2006, p 189-233.
- (4) Larminie, J.; Dicks, A. *Fuel cell systems explained*; John Wiley & Sons: Chichester, 2003.
- (5) Srinivasan, S.; Krishnan, L. In *Fuel cells: From fundamentals to applications*; Srinivasam, A., Ed.; Springer: New York, 2006, p 189-233.
- (6) Winter, M.; Brodd, R. J. *Chem. Rev.* **2004**, *104*, 4245-4269.
- (7) Linden, D. In *Handbook of batteries*; Linden, D., Reddy, T. B., Eds.; McGraw-Hill: New York, 2002, p 1.3-1.18.
- (8) Mehta, V.; Cooper, J. S. *J. Power Sources* **2003**, *114*, 32-53.
- (9) Basnayake, R.; Peterson, G. R.; Casadonte, D. J.; Korzeniewski, C. *J. Phys. Chem. B* **2006**, *110*, 23938-23943.
- (10) Mauritz, K. A.; Moore, R. B. *Chem. Rev.* **2004**, *104*, 4535-4585.
- (11) Carretta, N.; Tricoli, V.; Picchioni, F. *J. Membr. Sci.* **2000**, *166*, 189-197.
- (12) Cho, C. G.; Kim, Y. S.; Yu, X.; Hill, M.; McGrath, J. E. *J. Polym. Sci., Part A: Polym. Chem.* **2006**, *44*, 6007-6014.
- (13) Hofmann, M. A.; Ambler, C. M.; Maher, A. E.; Chalkova, E.; Zhou, X. Y.; Lvov, S. N.; Allcock, H. R. *Macromolecules* **2002**, *35*, 6490-6493.
- (14) Lee, H.-S.; Badami, A. S.; Roy, A.; McGrath, J. E. *J. Polym. Sci., Part A: Polym. Chem.* **2007**, *45*, 4879-4890.
- (15) Sankir, M.; Kim, Y. S.; Pivovar, B. S.; McGrath, J. E. *J. Membr. Sci.* **2007**, *299*, 8-18.
- (16) Yang, Y.; Holdcroft, S. *Fuel Cells* **2005**, *5*, 171-186.

- (17) Asensio, J. A.; Borrós, S.; Gómez-Romero, P. *J. Electrochem. Soc.* **2004**, *151*, A304-A310.
- (18) Slade, S.; Campbell, S. A.; Ralph, T. R.; Walsh, F. C. *J. Electrochem. Soc.* **2002**, *149*, A1556-A1564.
- (19) Glatzhofer, D. T.; Erickson, M. J.; Frech, R.; Yopez, F.; Furneaux, J. E. *Solid State Ionics* **2005**, *176*, 2861-2865.
- (20) Tanaka, R.; Yamamoto, H.; Shono, A.; Kubo, K.; Sakurai, M. *Electrochim. Acta* **2000**, *45*, 1385-1389.
- (21) Tanaka, R.; Yamamoto, H.; Kawamura, S.; Iwase, T. *Electrochim. Acta* **1995**, *40*, 2421-2424.

Chapter 6: Future directions in poly(ethylenimine) research

It has been shown that poly(ethylenimine)-based materials can be used as electrolytes for batteries and fuel cell applications. *N*-Alkylated PEI derivatives have been used to study the interactions between nitrogen atoms along the polymer backbone and lithium ions and valuable insight has been gained.

BPMEI appears to coordinate lithium ions to a greater extent than LPMEI. This is evidenced by the absence of aggregate formation with addition of salt, as well as a decrease in the relative concentration of “free” ions present in the polymer-salt complexes. This is coupled to lower conductivities in BPMEI complexes.

New methods to *N*-alkylate PEI have been proposed and successfully used. Novel LPEEI and LPBEI have been synthesized. Interestingly, increasing the length of the alkyl chain on the nitrogen atom raises the glass transition temperature of the resulting polymer.

Spectroscopic studies of LPMEI and LPEEI showed that upon addition of salt, LPEEI does not seem to undergo significant conformational changes. However, a shift from ion pairs to “free” ions seems to take place upon heating and cooling cycling of PEI-LiSO₃CF₃ complexes.

LPEI can be crosslinked and doped with phosphoric acid to make proton-conducting membranes. A series of PEI-based membranes, crosslinked with malonaldehyde generated *in situ*, has been characterized. The chemical nature

of the crosslinking unit has been probed and ^1H NMR has been used to determine the degree of crosslinking of the resulting films.

Ionic conductivity experiments have been carried out on membranes with different degrees of crosslinking and with various acid concentrations and the effect of temperature and relative humidity on the conductivity of these membranes has also been studied.

Crosslinked PEI/ H_3PO_4 -based membranes with ionic conductivities, ca. $3.0 \times 10^{-2} - 3.0 \times 10^{-1}$ S/cm at high temperatures ($> 90^\circ\text{C}$) and over a wide range of relative humidity, were obtained.

Membrane electrolyte assemblies were made with these materials and tested in hydrogen fuel cells. When compared to Nafion® MEAs made in the same way, PEI-based MEAs exhibited better performance at lower relative humidity.

These results are promising. However, further research on linear poly(ethylenimine)-based membranes for fuel cell applications is needed to understand the way such an intricate polymer electrolyte network functions. Even though this work sheds light on some of the relationships between the composition of the membranes and their physical properties, we are still far from achieving a complete understanding of the exact role of phosphoric acid in the proton conductivity.

^{31}P NMR spectroscopy can be used to determine the nature of the different phosphorus species present in crosslinked LPEI gels as well as provide some

insight as to why no phosphoric acid is leached out of membranes with phosphoric acid content lesser than 2.0 P:N molar ratio at room temperature.

Additional tests are also needed to determine if phosphoric acid is lost when the membranes are submerged in water at elevated temperatures (ca. 100°C). These tests are relevant in the context of possible use of these membranes in fuel cell applications.

Pulse field gradient spin-echo ^1H NMR measurements could be used to determine proton diffusion coefficients in poly(ethylenimine) membranes in order to better understand the conduction mechanisms of these membranes. Such studies have been carried successfully on Nafion® - based systems by Zawodzinski *et al.*¹

LPEI-based membranes still exhibit behavior that could be considered problematic during their use in fuel cell applications. One of the most important ones is their hydrophilicity. Experiments should be carried to determine how much water could be absorbed by poly(ethylenimine) membranes. Differential Scanning Calorimetry could be used to determine how much water poly(ethylenimine) retains after being subjected to a drying process. Similar tests are being used by other research groups to determine how much water poly(arylsulfonic acids) can retain and use during high temperature – low relative humidity fuel cell operation.

Additionally, several approaches can be taken to address LPEI's hydrophilicity. Since fully crosslinked materials are not necessary to obtain good

proton conductivity values, researchers could take advantage of the synthetically versatile LPEI by partially functionalizing the backbone chains to increase the overall hydrophobicity of the material. Such chemical modifications could involve adding perfluorinated alkyl chains onto the polymer backbone. Care should be taken to estimate the extent to which these modifications could potentially change the stability and reactivity of the polymer, as well as the changes in morphology that would take place upon functionalization.

Fiberglass could be used as a reinforcing material by casting polymer solutions onto them and allowing the crosslinking reaction to take place, thus binding to the fiberglass. Similar approaches include the use of silica to improve the dimensional stability of the membranes. Such additions could also enhance the conductivity of the material and lower its final cost since less of the polymer would be used to make the membranes. This work could also help develop better methods to control the thickness of the finished films. Thick films increase the ohmic losses in fuel cell applications and reduce the current density and power that the cell is able to generate.

Finally, additional research is necessary to improve contact between the polymer electrolyte and the catalyst layer on the electrodes. Better contact between these elements of the MEA would facilitate the transfer of protons resulting from the oxidation of hydrogen deposited on the catalyst surface. This could be accomplished by casting LPEI solutions containing a crosslinking agent directly onto the GDE. If done correctly, the solution should wet the GDE material

and significantly improve contact with the polymer electrolyte. Other approaches include spraying or spreading catalyst paint onto LPEI-based membranes. Improvements on MEA manufacturing protocols will ultimately result in better fuel cell performance.

References

- (1) Zawodzinski, T. A.; Neeman, M.; Sillerud, L. O.; Gottesfeld, S. *J. Phys. Chem.* **1991**, *95*, 6040-6044.

Experimental Section

1. Polymer Synthesis

Synthesis of LPEI·HCl: In a 3 L round bottom flask, 20 g of poly(2-ethyl-2-oxazoline) (Aldrich, MW ca. 200,000 or 500,000) was dissolved in 1200 mL of 2.5 M HCl with stirring (magnetic). The solution was heated to reflux solvent for 5 days. Solvent was removed under reduced pressure using a rotary evaporator. The remaining material was an off-white flaky powder and was verified to be LPEI·HCl using ¹H NMR. ¹H-NMR (D₂O): δ (ppm)- 3.57 (s, variable peak area).^{1,2}

Neutralization of LPEI·HCl: Previously synthesized LPEI·HCl was dissolved in 1.5 L of distilled water and neutralized by adding NaOH (EM Science) until the pH of the solution was greater than 10, as determined using pH paper, causing the neutral polymer to precipitate out of solution. The resulting mixture was heated to ca. 75 °C to re-dissolve the neutral polymer and ensure complete neutralization. The solution was allowed to cool down to room temperature using an ice bath resulting in reprecipitation of neutral LPEI. The polymer was collected by vacuum filtration using a fritted glass funnel. The polymer was washed with fresh water until the filtrate was neutral. LPEI was dried under vacuum at ca. 50 °C for 24 hours and then at ca. 70 °C for 24 hours to ensure removal of any traces of water. ¹H-NMR (CD₃OD): δ (ppm)- 2.71 (4 H); ¹³C-NMR (CD₃OD) δ (ppm)- 49.8. Data is consistent with previously reported values.¹⁻³

Synthesis of branched poly(*N*-methylethylenimine), BPMEI: In a 1 L round bottom flask, BPEI (14.84 g, Aldrich, \overline{M}_n ca. 10,000) was added to 175 mL of distilled water, then heated. After the BPEI dissolved, formic acid (88 %, 275 ml) and formalin (37 %, 175 mL) were added to the solution. The solution was heated to reflux the solvent for 24 hours and, after cooling, 300 mL of concentrated HCl were added. The solvent was removed under reduced pressure to provide the quaternary ammonium hydrochloride salt. The salt was dissolved in distilled water (500 mL), and run through an ion exchange column (Amberlite® IRA-400 – OH form). The neutralized polymer water solution was dissolved in benzene, and any excess water was removed by azeotropic distillation. The resulting solution was centrifuged to remove any remaining solid impurities. The solvent was removed under reduced pressure using a rotary evaporator. The branched poly(*N*-methylethylenimine) was a dark brown and extremely viscous material. Yield: 70%. Calculated MW ca. 14,000. ¹H-NMR (CD₃OD): δ (ppm) 2.7 – 2.4 (m, -CH₂CH₂-, br), 2.3 (s, -CH₃, br).⁴⁻⁶

Synthesis of linear poly(*N*-ethylethylenimine), LPEEI: In a 150 mL round bottom flask, 3.03 g (0.0703 eq.) of LPEI (MW ca. 86,000) was dissolved in 120 mL of absolute methanol. The solution was stirred (magnetic) and cooled using a dry ice/acetone bath and 4.64 g (0.105 eq.) of acetaldehyde was added. The flask was sealed and the solution stirred for 1 hour. Sodium borohydride (3.32 g,

0.351 eq.) was added slowly to the solution. The solution was allowed to warm up to room temperature over a period of several hours. The solvent was removed under reduced pressure using a rotary evaporator. Methylene chloride was added to the flask, and the solution was stirred for 1-2 additional hours. Inorganic salts were removed by filtration and CH_2Cl_2 was removed under reduced pressure using a rotary evaporator. Benzene was used to extract the polymer, and remaining inorganic salts were removed by filtration. On standing, salt formation in the solution was not observed, so the benzene was removed under reduced pressure using a rotary evaporator to give near quantitative yield of LPEEI. LPEEI was dried under reduced pressure at 60°C overnight and transferred to a glove box under an argon atmosphere to prevent water uptake before characterization. LPEEI is a viscous, light yellow-brown material. Calculated avg. MW ca. 142,000. ^1H NMR (CDCl_3): δ (ppm) ca. 2.58 (overlapping s and q, 6H), 1.06 (t, 3H).⁴

Synthesis of linear poly(*N*-butylethylenimine), LPBEI: In a 150 mL round bottom flask, 3.0 g (1 eq.) of LPEI (MW ca. 86,000) was dissolved in 120 mL of absolute methanol. The solution was stirred (magnetic) and cooled using a dry ice/acetone bath and 7.5 g (1.5 eq.) of butyraldehyde was added. The flask was sealed and the solution stirred for 2 hour. Sodium borohydride (1.32 g, 2 eq.) was added slowly to the solution. The solution was allowed to warm up to room temperature over a period of several hours. The solvent was removed under

reduced pressure using a rotary evaporator. The polymer was extracted with methylene chloride as described in the LPEEI synthesis. LPBEI was dried under reduced pressure at 60°C overnight and transferred to a glove box under an argon atmosphere to prevent water uptake before characterization. LPBEI was an amber-brown color, very viscous material. Calculated avg. MW ca. 200,000. ^1H NMR (CDCl_3): δ (ppm) ca. 0.95 ppm (m, 3H), 1.35 -1.5 ppm (m, 2.5H) , 2.10 ppm (m, 1H), and 2.4 – 2.7 ppm (m, 6H).

2. Crosslinked LPEI·HCl based polymer electrolyte membranes

Crosslinked membranes were made as previously described;⁷ the procedure is briefly summarized as follows. LPEI·HCl, synthesized from poly(2-ethyl-2-oxazoline) (Aldrich, avg. MW ca. 500,000),^{2,8} was dissolved in water (~ 1.2 M in repeat units) and varying amounts of 1,1,3,3-tetramethoxypropane (Aldrich) were added while stirring, generating malonaldehyde *in situ*. The solutions were capped and allowed to stir for approximately 15 minutes. The solutions were cast onto a silicone rubber substrate and covered. After two days the samples were uncovered and placed in an oven at ~ 40°C for 72 hours to facilitate evaporation of residual water and form a freestanding membrane. The resulting membranes ranged in thickness from 0.3 to 0.9 mm.

Slight modifications were made to the procedure described above to prepare crosslinked membranes with phosphoric acid. Samples were prepared by dissolving LPEI·HCl, synthesized from poly(2-ethyl-2-oxazoline) (Aldrich, avg.

MW ca. 500,000),^{2,8} in water (10% solution by weight), followed by addition of varying amounts of phosphoric acid (Mallinckrodt, 98%). 1,1,3,3-tetramethoxypropane (Aldrich), in varying amounts, was added while stirring, generating malonaldehyde *in situ*. The rest of the experimental procedure to prepare crosslinked membranes remained unchanged. Compositions of the membranes were expressed as a nitrogen:phosphorus molar ratio.

3. Techniques

3.1. Polymer electrolyte preparation

BPMEI-salt electrolytes: Anhydrous acetonitrile (99.8%) and LiCF₃SO₃ (LiTf) were obtained from Aldrich. Dry acetonitrile was used as received. The LiTf was dried under vacuum at 120 °C for 48 hours before use. All the chemicals were stored and used in a dry argon atmosphere glove box (VAC, ≤ 1ppm H₂O) at room temperature. All polymer – salt solutions were prepared by dissolving weighed amounts of BMPEI and salt in dry acetonitrile and stirring for approximately 24 h to insure a homogeneous solution before casting as films. The compositions of the samples are reported as a nitrogen:cation molar ratio (N:M⁺).^{9,10}

LPPEI and LPBEI-salt electrolytes: Polymer electrolytes were prepared by dissolving weighed amounts of lithium triflate and the host polymer in dry methanol. The solutions were stirred for approximately 12 hours before casting

as films. All sample preparation and manipulation steps were carried out in a dry argon glove box (VAC, ≤ 1 ppm H₂O) at room temperature. Sample compositions are reported as a nitrogen:cation molar ratio.⁴

3.2. Vibrational spectroscopy

BPMEI-salt electrolytes: Samples were characterized using FT-IR. The FT-IR samples were made by casting the solutions directly onto zinc selenide (ZnSe) windows and drying under argon for 24 hours. The samples were then placed under vacuum at room temperature for an additional 24 hours to insure solvent removal. Infrared data were collected using a Bruker IFS66V FT-IR spectrometer (KBr beam splitter) under vacuum (11 mbar). The data were recorded over a range of 500-4000 cm⁻¹ with a spectral resolution of 1 cm⁻¹.^{9,10}

LP EEI and LP BEI-salt complexes: Samples were characterized using infrared and Raman spectroscopies. Samples for IR spectroscopic measurements were cast from solution (PEI·HCl, ~ 0.6 M) on ZnSe windows ~ 1.5 hours after mixing to form thin films. Approximately 12-24 hours after preparation, the cast films were dried under vacuum. Infrared spectra were collected using a Bruker IFS 66v spectrometer with a KBr beam splitter; 64 scans at a spectral resolution of 1 cm⁻¹ were averaged for each spectrum. Spectra of cast membranes were measured under vacuum (pressure = 11 mbar), while those of the liquid model compound, 3-(dimethylamino)acrolein (DMAA) (Aldrich, 90%), were measured under a dry

air purge. Samples for Raman were made from the same solutions (PEI-HCl, ~ 0.6 M) used for the IR experiments. These solutions were placed in glass tubes 15 minutes after mixing to form a gel. Raman spectra were collected on a Bruker Equinox 55 FRA 106/S with a Nd:YAG laser (1064 nm) and a CCD detector. Commercially available software (Thermo Galactic, Grams/AI 7.00) was used for spectral analysis.

3.3. NMR spectroscopy

Solution-state NMR experiments on non-crosslinked samples were carried out using a Varian Mercury-300 spectrometer (300.1 MHz ^1H). VnmrJ 1.1D software (Varian, Inc) was used for data collection, while iNMR 2.6.1 software (Mestrelab Research, 2008) was used for data processing. A deuterium lock was maintained throughout data acquisition to control the field frequency ratio over the sample. The sample temperature was controlled at 25°C.

Solution-state NMR experiments on the gels were carried out using a Varian Mercury-300 spectrometer (300.1 MHz ^1H). Crosslinked samples for NMR were made from the same solutions (PEI-HCl, ~ 0.6 M) used for the IR and Raman experiments. Water was suppressed from the spectra by pre-saturation using PRESAT pulse sequence as supplied by Varian, Inc. The spectra were collected after 48 scans and were referenced to d_4 -Methanol (δ 3.32 ppm). High-resolution magic-angle-spinning (HRMAS) NMR spectra were collected with a Varian

$^{13}\text{C}\{^1\text{H}\}$ HRMAS NanoProbe[®] and a Mercury VX 300 MHz NMR Spectrometer. VnmrJ 1.1D software (Varian, Inc) was used for data collection, while iNMR 2.6.1 software (Mestrelab Research, 2008) was used for data processing. The ^1H chemical shift values were referenced to the residual water signal (HOD) at 4.79 ppm. A deuterium lock was maintained throughout data acquisition to control the field frequency ratio over the sample. Crosslinked PEI·HCl membranes were soaked in D_2O for at least 1 hour prior to data collection and then loaded into a ceramic rotor. Subsequently, the rotor was filled with D_2O and spun at a rate of 2000 Hz. Sample spinning was achieved with a Torlon drive ring and dry air. The sample temperature was controlled at 25°C.¹¹

Degree of crosslinking: Due to changes in chemical shift and broadening of signals as crosslinking occurs, care was taken to integrate peaks for the PEI backbone protons at ca. 3.2 – 4.5 ppm, for the crosslink protons at ca. 7.7 ppm, and the branch aldehyde protons at ca. 9.4 ppm over 1.100, 0.750, and 0.065 ppm ranges, respectively. A baseline correction was applied to each integration in every spectra collected. These integrations were used to calculate the degree of crosslinking as described in chapter 3.¹¹

3.4. Differential scanning calorimetry

BPMEI-salt electrolytes: Solutions were cast on Teflon, dried under argon for 24 hours, and placed under vacuum at room temperature for at least 48 hours. After

drying, 20-30 mg samples were sealed in 40 μ L aluminum pans under argon atmosphere. Thermal data were collected using a Mettler DSC 820 calorimeter under a dry nitrogen purge at heating and cooling rates of 5°C/min. The thermograms were then analyzed using a STAR^e v.6.10 software from Mettler Toledo. Each sample was cycled three times, with the first cycle from room temperature to 150° and then to -150°C. The next two cycles were from -150 to 50°C and back to -150°C. The reported data corresponds to an average of the second heating cycle of at least three different samples.^{9,10}

LP EEI and LP BEI - salt electrolytes: Thermal data were measured with a Mettler DSC 820 calorimeter. Each sample was sealed in a 40 mL aluminum pan and data were collected under a dry nitrogen purge. The samples were cycled three times from -150 to 25°C at a rate of 5°C/min. Data were collected during the heating and cooling phases.⁴

3.5. AC conductivity and impedance spectroscopy

Complex impedance of BPMEI – salt electrolytes: The samples were cast directly onto a 12.5 mm diameter stainless steel electrode in an argon atmosphere. The samples were allowed to dry 24 hours in the glove box and 48 h under vacuum at room temperature before testing. The film thickness was measured using a micrometer built into the conductivity cell. Conductivity measurements were made over the frequency range 0.005-10000 kHz using a

Hewlett-Packard 4192A LF impedance analyzer with Labview 5.1 software (National Instruments). First, the reproducibility of the conductivity data was checked by cycling the sample between room temperature and 80°C at least three times, collecting data at room temperature and 80°C only. Then data were collected in a heating cycle ranging from room temperature to 160°C in 20°C increments. Finally, measurements at room temperature 160°C were repeated. The conductivities were not measured for compositions of 5:1 and above, due to interfacial contact problems between the electrodes and the electrolyte. The impedance plots were curve fitted using commercially available software Solartron Instruments LTD, Levm 7.1v.^{9,10}

Four-probe conductivity measurements: Two different setups were used to measure the conductivity of crosslinked LPEI·HCl based membranes.

Setup A: This setup has been described earlier.¹ Measurements were carried out at room temperature. Samples were allowed to equilibrate for 24 hours before measurements were taken. Measurements were taken in a glass tube with two stopcocks and four platinum wires fed through the top. The four-probe consisted of a longitudinal geometry in which two platinum wires were used to apply current to the ends of a sample. Two more platinum wires were used to measure the voltage drop along the film near the center of the sample. A Teflon-coated clamp was used to compress the sample against the four wires. Typical sample dimensions were 1 cm x 0.1 cm x 0.3 cm.

In order to control the relative humidity inside the glass tube saturated salt solutions were prepared and placed in the interior of the glass tube as constant activity sources.^{12,13} Samples were inserted and the stopcocks were closed to avoid solvent evaporation. A Wavetek sweep generator was used in conjunction with a Keithley Model 175 autoranging multimeter and a Keithley Model 169 multimeter to vary the applied frequency between 100 and 500 kHz, measure the voltage and measure the current, respectively. The impedance was plotted versus the A.C. frequency, and the bulk resistance was taken in the frequency independent impedance range of the plot.¹⁴ Statistical analysis of the error in the ionic conductivity measurements was not done. In general, measurements were repeated once. Reported data were not greater than a half order of magnitude off from the initial measurement.

Setup B: The conductivity of each sample was determined under a constant flow of nitrogen (ca. 80 sccm) using an in-plane conductivity test system by BekkTeck, model BT512. The system consists of a pair of Poco Graphite Blocks with a precision, machined serpentine flow-pattern, and a pair of gold plated connectors fastened with aluminum end plates with gas inputs and outputs, a thermocouple well and two cartridge heaters to allow temperature control, as well as a poly(tetrafluoroethylene) insert that supports a sample with longitudinal geometry. The insert includes four platinum wires evenly spaced across the sample. The testing system allows control of the temperature of the sample, as well as the flow rate and temperature of the gas used. The equipment is coupled to a dew

point saturator to control the relative humidity inside the conductivity cell. Typical sample dimensions were 2.5 cm x 0.06 cm x 0.5 cm. The temperature range was between 30°C and 130°C. A Keithley 2400 Source meter was used to measure current and voltage across the platinum electrodes in a similar fashion to setup A. BektTech LabView VIs software was used to automate tests as well as data acquisition.

3.6. MEA preparation and fuel cell tests: See chapter 5.

References

- (1) Erickson, M. J. Ph. D. Dissertation, The University of Oklahoma, 2004.
- (2) York, S.; Frech, R.; Snow, A.; Glatzhofer, D. *Electrochim. Acta* 2001, *46*, 1533-1537.
- (3) Saegusa, T.; Ikeda, H.; Fujii, H. *Macromolecules* 1972, *5*, 108.
- (4) Frech, R.; Giffin, G. A.; Yopez Castillo, F.; Glatzhofer, D. T.; Eisenblatter, J. *Electrochim. Acta* 2005, *50*, 3963-3968.
- (5) Sanders, R. A.; Snow, A. G.; Frech, R.; Glatzhofer, D. T. *Electrochim. Acta* 2003, *48*, 2247-2253.
- (6) Tanaka, R.; Koike, M.; Tsutsui, T.; Tanaka, T. *J. Polym. Sci. Polym. Lett.* 1978, *16*, 13-16.
- (7) Glatzhofer, D. T.; Erickson, M. J.; Frech, R.; Yopez, F.; Furneaux, J. E. *Solid State Ionics* 2005, *176*, 2861-2865.
- (8) Tanaka, R.; Ueoka, I.; Takaki, Y.; Kataoka, K.; Saito, S. *Macromolecules* 1983, *16*, 849-853.
- (9) Rocher, N. M. Ph.D. Dissertation, University of Oklahoma, 2006.
- (10) Rocher, N. M.; Yopez Castillo, F.; Frech, R.; Glatzhofer, D. T. *to be submitted for publication.*

- (11) Giffin, G. A.; Yopez Castillo, F.; Frech, R.; Glatzhofer, D. T.; Burba, C. M. *Polymer* 2009, *50*, 171-176.
- (12) Greenspan, L. *J. Res. NBS A: Phys. Chem.* 1977, *81A*, 89-96.
- (13) Wexler, A. In *CRC Handbook of Chemistry and Physics*; CRC Press: Boca Raton, 2004.
- (14) Cahan, B. D.; Wainright, J. S. *J. Electrochem. Soc.* 1993, *140*, L185-L186.